NAVAL AIR WARFARE CENTER AIRCRAFT DIVISION
PATUXENT RIVER, MARYLAND

TECHNICAL REPORT

REPORT NO: NAWCADPAX/TR-2012/200

CALCULATION OF IMPEDANCE MATRIX INNER INTEGRAL TO PRESCRIBED PRECISION FOR THE MAGNETIC FIELD INTEGRAL EQUATION

by

John S. Asvestas
Dennis W. Richardson
Oliver E. Allen

19 July 2012

Approved for public release; distribution is unlimited.

DEPARTMENT OF THE NAVY
NAVAL AIR WARFARE CENTER AIRCRAFT DIVISION
PATUXENT RIVER, MARYLAND

CALCULATION OF IMPEDANCE MATRIX INNER INTEGRAL TO PRESCRIBED
PRECISION FOR THE MAGNETIC FIELD INTEGRAL EQUATION

by

John S. Asvestas
Dennis W. Richardson
Oliver E. Allen

RELEASED BY:

_____ 19 Jul 2012
DOUGLAS P. McLAUGHLIN / AIR-4.5.5 / DATE
Head, Radar and Antenna Systems Division
Naval Air Warfare Center Aircraft Division

NAWCADPAX/TR-2012/200

REPORT DOCUMENTATION PAGE		Form Approved OMB No. 0704-0188

Public reporting burden for this collection of information is estimated to average 1 hour per response, including the time for reviewing instructions, searching existing data sources, gathering and maintaining the data needed, and completing and reviewing this collection of information. Send comments regarding this burden estimate or any other aspect of this collection of information, including suggestions for reducing this burden, to Department of Defense, Washington Headquarters Services, Directorate for Information Operations and Reports (0704-0188), 1215 Jefferson Davis Highway, Suite 1204, Arlington, VA 22202-4302. Respondents should be aware that notwithstanding any other provision of law, no person shall be subject to any penalty for failing to comply with a collection of information if it does not display a currently valid OMB control number. **PLEASE DO NOT RETURN YOUR FORM TO THE ABOVE ADDRESS.**

1. REPORT DATE: 12/10/2008 19 July 2012	2. REPORT TYPE Technical Report	3. DATES COVERED
4. TITLE AND SUBTITLE: Calculation of Impedance Matrix Inner Integral to Prescribed Precision for the Magnetic Field Integral Equation		5a. CONTRACT NUMBER
		5b. GRANT NUMBER
		5c. PROGRAM ELEMENT NUMBER
6. AUTHOR(S) John S. Asvestas Dennis W. Richardson Oliver E. Allen		5d. PROJECT NUMBER
		5e. TASK NUMBER
		5f. WORK UNIT NUMBER
7. PERFORMING ORGANIZATION NAME(S) AND ADDRESS(ES) Naval Air Warfare Center Aircraft Division 48110 Shaw Road Patuxent River, Maryland 20670		8. PERFORMING ORGANIZATION REPORT NUMBER NAWCADPAX/TR-2012/200
9. SPONSORING/MONITORING AGENCY NAME(S) AND ADDRESS(ES) Naval Air Systems Command 47123 Buse Road Unit IPT Patuxent River, Maryland 20670-1547		10. SPONSOR/MONITOR'S ACRONYM(S) ILIR
		11. SPONSOR/MONITOR'S REPORT NUMBER(S): N/A

12. DISTRIBUTION/AVAILABILITY STATEMENT

Approved for public release; distribution is unlimited.

13. SUPPLEMENTARY NOTES

14. ABSTRACT

The Method of Moments (MoM) is a powerful computational electromagnetics method for analyzing antennas in situ. In a previous report, we presented a new method for evaluating the inner integral of the impedance matrix element in the traditional Rao-Wilton-Glisson formulation of MoM for the electric field integral equation. In this report, we extend our method to the magnetic field integral equation. We show how, in this case, the inner integral can be written in terms of two scalar integrals, a surface integral over the integration triangle (IT) and a line integral over the boundary of the IT. Just as with the original integral, neither of these integrals can be evaluated analytically. In our method, we bypass this obstacle by replacing the original integrand (modified by a constant phase factor) by its Taylor series and by keeping enough terms to guarantee a number of significant digits in the integration outcome. We have accomplished this for both the surface integral and the line integral. We present a systematic derivation of the formulas for the two integrals and we conduct an extensive testing of our results against quadratures and cubatures.

15. SUBJECT TERMS

Method of Moments (MoM); Rao-Wilton-Glisson

16. SECURITY CLASSIFICATION OF:			17. LIMITATION OF ABSTRACT	18. NUMBER OF PAGES	19a. NAME OF RESPONSIBLE PERSON John S. Asvestas
a. REPORT	b. ABSTRACT	c. THIS PAGE			19b. TELEPHONE NUMBER (include area code)
Unclassified	Unclassified	Unclassified	SAR	109	631-673-8176

Standard Form 298 (Rev. 8-98)
Prescribed by ANSI Std. Z39-18

SUMMARY

The Method of Moments (MoM) is a powerful computational electromagnetics method for analyzing antennas in situ. In a previous report, we presented a new method for evaluating the inner integral of the impedance matrix element in the traditional Rao-Wilton-Glisson formulation of MoM for the electric field integral equation. In this report, we extend our method to the magnetic field integral equation. We show how, in this case, the inner integral can be written in terms of two scalar integrals, a surface integral over the integration triangle (IT) and a line integral over the boundary of the IT. Just as with the original integral, neither of these integrals can be evaluated analytically. In our method, we bypass this obstacle by replacing the original integrand (modified by a constant phase factor) by its Taylor series and by keeping enough terms to guarantee a number of significant digits in the integration outcome. We have accomplished this for both the surface integral and the line integral. We present a systematic derivation of the formulas for the two integrals and we conduct an extensive testing of our results against quadratures and cubatures.

Contents

List of Tables

List of Figures

INTRODUCTION

The Method of Moments (MoM) is one of the principal methods for electromagnetic simulations in the frequency domain. In this method, we express an unknown current density as a linear combination of known functions and the objective of the MoM is to determine the coefficients in this expansion by minimizing the square of the modulus of the residual error. It ultimately leads to a system of linear algebraic equations, the solution of which yields the values of the coefficients of the current density expansion. The elements of the matrix (known as the impedance matrix (IM)) are expressed as double surface integrals over flat, triangular regions of space. In a previous report (reference 1), we computed the inner of these integrals to a prescribed precision for the Electric Field Integral Equation (EFIE). This work appeared also as a paper but in a more condensed form (reference 2). In the present study, we compute the inner integral for the Magnetic Field Integral Equation (MFIE). On both occasions, the object under consideration is a perfect conductor.

Our motivation for including the MFIE in this prescribed-precision analysis is that, usually, the MFIE is combined linearly with the EFIE into one equation so as to eliminate the effect of the internal resonances of the target structure (reference 3, Theorem 4.47). Moreover, the MFIE operator appears also in the pair of integral equations that describe the behavior of penetrable materials, both lossless and lossy. For such materials, the wave number is generally complex.

The motivation for computing the matrix elements to prescribed precision is presented in reference 1 and repeated here. Until recently, the quantities of interest in electromagnetic simulations (for both scattering and radiation problems) were the far electric and magnetic fields. From these, we could compute the radar cross section of a target or the radiation patterns of an antenna. This allowed for a considerable degree of error in computing the elements of the IM in the MoM because of the error smoothing effect of the near- to far-field transformation (integration). Moreover, due to computer hardware limitations, the size of the IM was small enough so that the round-off error did not have a severe effect on the accuracy of the solution.

In recent years, the MoM is being applied to problems where near-field information is needed (e.g., antennas and antenna arrays). This necessitates a more accurate computation of the elements of the IM than when only the far fields are of interest. Additionally, advances in computer hardware allow us to address problems that result in an IM system with millions of unknowns. Thus, the effect of the round-off error becomes more pronounced. Both of these reasons lead us to the conclusion that the more accurate the representation of the IM is, the better the quality of the solution. A third observation we made recently is the following. In computing the interior fields due to a slit on a perfectly conducting enclosure, we noticed that the result was corrupted by numerical noise. To verify this, we considered a hollow cube with perfectly conducting walls under the exterior influence of a plane, electromagnetic wave. We computed the surface current density using MoM, and used the result to compute the fields inside the cavity. The fields inside the cavity should ideally be equal to zero since the walls of the cavity are perfectly conducting. We found that the fields inside reached as high as a tenth of the amplitude of the incident field when operating the MoM in its default mode. We had to increase the number of unknowns seventy-fold before we could get the interior field's amplitude to be a hundredth of that of the exterior field (24 dB down, to be precise). The increase in number of

unknowns was due to the increase of the grid density. This results in a more accurate calculation of the impedance matrix elements since the region of integration becomes smaller for each element and, hence, the variation of the integrand over it is smaller. The alternative to an extremely fine grid and the attendant expense in time and hardware is to be able to use a standard grid (the side of a triangle less or equal to a tenth of a wavelength) and use the present method to calculate the inner integral to a specified number of significant digits (SD). This is the central theme of the present study: the computation of the inner surface integral of the IM element to prescribed precision for the MFIE.

In Section 1, we apply to the MFIE the MoM in the manner of Rao-Wilton-Glisson (RWG) (reference 4). We then proceed to show that the inner surface integral of the IM can be written in terms of a surface integral over the integration triangle (IT) and a line integral around the IT's boundary. Both of these integrals are scalar. In the line integral, we have as integrand the free-space Green's function while, in the surface integral, the normal derivative of the same function. The approach we employ to calculate these integrals to a prescribed precision is analogous to that in reference 1: we approximate each of the two integrands using Taylor's Theorem with a Remainder (reference 5). This theorem allows us to approximate the integrand (that we do not know how to integrate analytically) by a polynomial that we can integrate analytically. The degree of approximation, *i.e.*, the number of SD to which the approximation is accurate is known and, hence, so is that of the integration. The result of this evaluation is given in terms of elementary transcendental functions for which there exist robust computational algorithms.

In Section 2, we deal with the surface integral and show that it can be computed using a three-term iteration that has as its starting point the solid-angle integral. It also involves a known term that is related to the integral of the Green's function over the IT and which we have computed in reference 1 by converting it to a line integral. We summarize the results from reference 1 in Section 5. In Section 3, we turn to the evaluation of the line integral and analyze it in quite the same way we analyzed the integral of the Green's function over the IT in reference 1. In Section 4, we discuss two formulas for computing the solid angle integral. In Section 6, we validate our formulas using the Gauss-Kronrod quadrature (GKQ) (reference 6) as it appears in Matlab (reference 7) for the line integral and the cubatures from reference 1 for the surface integral.

In conclusion, we have extended our work on calculating the inner integral of the IM element to prescribed precision to the MFIE. We mention that the algorithms we developed are not for all observation points (OP) but, rather, for those close to the IT. We hope that, in a subsequent report, we will carry the same analysis as in Part II of reference 1 to determine the spherical region about the IT's centroid where it is necessary and/or advantageous to use the present method, and, outside of which it is preferable to use the GKQ for the line integral and cubatures for the surface integral.

We know of no other method that calculates the inner integral of the IM element for MFIE to a prescribed precision.

SECTION 1: THE MAGNETIC FIELD INTEGRAL EQUATION

The MFIE (also known as Maue's integral equation) for a closed and bounded perfectly conducting surface S is (reference 8, pp. 354-355)

$$\frac{1}{2}\mathbf{J}^t(\mathbf{r}') = \mathbf{J}^{inc}(\mathbf{r}') - \hat{n}' \times \int_S \mathbf{J}^t(\mathbf{r}) \times \nabla g(\mathbf{r},\mathbf{r}')\, dS\,, \quad \mathbf{r}' \in S \tag{1.1}$$

where $\hat{n}'$ is the exterior unit normal on S and

$$g(\mathbf{r},\mathbf{r}') = -\frac{e^{-ik|\mathbf{r}-\mathbf{r}'|}}{4\pi|\mathbf{r}-\mathbf{r}'|}\,, \quad k = \omega\sqrt{\varepsilon_0\mu_0} \tag{1.2}$$

with $\mathbf{r}$ the integration point and $\mathbf{r}'$ the observation point

$$\mathbf{r} = x\hat{x} + y\hat{y} + z\hat{z}\,, \quad \mathbf{r}' = x'\hat{x} + y'\hat{y} + h\hat{z}\,. \tag{1.3}$$

The unknown and known linear current densities are defined by

$$\mathbf{J}^t(\mathbf{r}') = \hat{n}' \times \mathbf{H}^t(\mathbf{r}')\,, \quad \mathbf{J}^{inc}(\mathbf{r}') = \hat{n}' \times \mathbf{H}^{inc}(\mathbf{r}') \tag{1.4}$$

respectively, where $\mathbf{H}^t$ and $\mathbf{H}^{inc}$ are the total (unknown) and incident (known) magnetic fields. A harmonic time dependence $\exp(i\omega t)$ is suppressed throughout.

To the integral equation in (1.1), we now apply the RWG (reference 4) formulation of the MoM. This is a well-known procedure and, hence, we provide only a brief outline. The scatterer's surface is converted to one made up of flat triangles. The total number of edges is N. We consider the edge as a directed-line segment and we define identical basis and test functions

$$\mathbf{f}_n(\mathbf{r}) = \begin{cases} \dfrac{l_n}{2A_n^+}\boldsymbol{\rho}_n^+\,, & \mathbf{r} \in T_n^+ \\[2ex] \dfrac{l_n}{2A_n^-}\boldsymbol{\rho}_n^-\,, & \mathbf{r} \in T_n^- \\[2ex] \mathbf{0}\,, & \text{elsewhere} \end{cases} \tag{1.5}$$

where l_n is the length of the edge and A_n^+ (A_n^-) is the area of the triangle attached to the edge and positively (negatively) oriented with respect to the normal. The vectors $\boldsymbol{\rho}_n^+$ and $\boldsymbol{\rho}_n^-$ lie on the two triangles, the first emanating from the corner opposite to the side under consideration and the second terminating there.

We expand the unknown current density in terms of the basis functions

$$\mathbf{J}^t(\mathbf{r}) = \sum_{n=1}^{N} a_n \mathbf{f}_n(\mathbf{r}) \tag{1.6}$$

and substitute in the integral equation (1.1)

$$\frac{1}{2}\sum_{n=1}^{N} a_n \mathbf{f}_n(\mathbf{r}') = \mathbf{J}^{inc}(\mathbf{r}') - \hat{n}' \times \sum_{n=1}^{N} a_n \int_{T_n} \mathbf{f}_n(\mathbf{r}) \times \nabla g(\mathbf{r},\mathbf{r}') dS, \quad \mathbf{r}' \in S \tag{1.7}$$

where

$$T_n = T_n^+ \cup T_n^-. \tag{1.8}$$

We test this equation by taking the dot product with $\mathbf{f}_m(\mathbf{r}')$ and integrating over S

$$\frac{1}{2}\sum_{n=1}^{N} a_n \int_{T_m} \mathbf{f}_m(\mathbf{r}') \cdot \mathbf{f}_n(\mathbf{r}') dS' = \int_{T_m} \mathbf{f}_m(\mathbf{r}') \cdot \mathbf{J}^{inc}(\mathbf{r}') dS'$$

$$-\sum_{n=1}^{N} a_n \int_{T_m} \mathbf{f}_m(\mathbf{r}') \cdot \left\{ \hat{n}' \times \int_{T_n} \mathbf{f}_n(\mathbf{r}) \times \nabla g(\mathbf{r},\mathbf{r}') dS \right\} dS', \quad m = 1,2,...,N. \tag{1.9}$$

The only values of n in the first integral in this expression that contribute are those for which $\mathbf{f}_n$ has a domain in common with $\mathbf{f}_m$. Using standard vector identities for the last integral, we can write this expression in the form

$$\frac{1}{2}\sum_{n=1}^{N} a_n \int_{T_m} \mathbf{f}_m(\mathbf{r}') \cdot \mathbf{f}_n(\mathbf{r}') dS' = \int_{T_m} \mathbf{f}_m(\mathbf{r}') \cdot \mathbf{J}^{inc}(\mathbf{r}') dS'$$

$$-\sum_{n=1}^{N} a_n \int_{T_m} \left\{ [\mathbf{f}_m(\mathbf{r}') \times \hat{n}'] \cdot \int_{T_n} \mathbf{f}_n(\mathbf{r}) \times \nabla g(\mathbf{r},\mathbf{r}') dS \right\} dS', \quad m = 1,2,...,N. \tag{1.10}$$

We are interested in the accurate calculation of the integral

$$\mathbf{I}_n(\mathbf{r}') = \int_{T_n} \mathbf{f}_n(\mathbf{r}) \times \nabla g(\mathbf{r},\mathbf{r}') dS. \tag{1.11}$$

For simplicity, we consider a single triangle T, as shown in Figure 1.1, and define

$$\mathbf{I}^{(l)}(\mathbf{r}') = \int_{T} \mathbf{f}^{(l)}(\mathbf{r}) \times \nabla g(\mathbf{r},\mathbf{r}') dS, \quad \mathbf{f}^{(l)}(\mathbf{r}) = \mathbf{r} - \mathbf{r}_l, \quad l = 1,2,3. \tag{1.12}$$

The function $\mathbf{f}^{(l)}$ is proportional to a basis function. The superscript refers to a corner of *T*. Coordinates are centered at the centroid of the triangle with the *z*-axis perpendicular to the triangle.
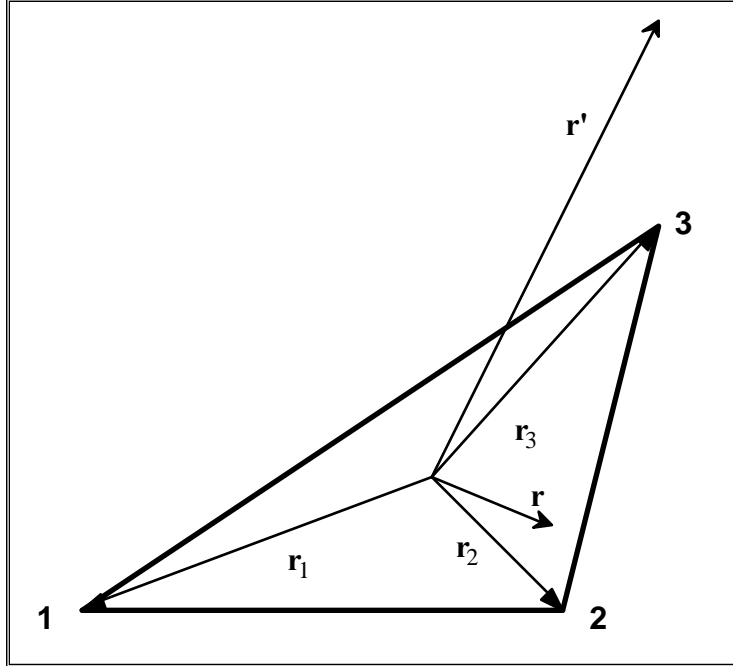
Figure 1.1: The Integration Triangle

The integral in (1.12) is the one we are interested in computing to a prescribed number of significant digits. To this end, we transform it to a form that we can evaluate. We write

$$\mathbf{A}(\mathbf{r},\mathbf{r}') = (\mathbf{r}-\mathbf{r}_l) \times \nabla g(\mathbf{r},\mathbf{r}') = (\mathbf{r}-\mathbf{r}') \times \nabla g(\mathbf{r},\mathbf{r}') + (\mathbf{r}'-\mathbf{r}_l) \times \nabla g(\mathbf{r},\mathbf{r}')$$

$$= (\mathbf{r}-\mathbf{r}') \times \nabla g(\mathbf{r},\mathbf{r}') + (\mathbf{r}'-\mathbf{r}_l) \times \left[\nabla_S g(\mathbf{r},\mathbf{r}') + \hat{z}\frac{\partial g(\mathbf{r},\mathbf{r}')}{\partial z} \right] \qquad (1.13)$$

where the subscript *S* denotes the surface gradient. From (1.2)

$$\nabla g(\mathbf{r},\mathbf{r}') = \frac{\partial g(\mathbf{r},\mathbf{r}')}{\partial |\mathbf{r}-\mathbf{r}'|} \nabla |\mathbf{r}-\mathbf{r}'| = \frac{\partial g(\mathbf{r},\mathbf{r}')}{\partial |\mathbf{r}-\mathbf{r}'|} \frac{\mathbf{r}-\mathbf{r}'}{|\mathbf{r}-\mathbf{r}'|} \qquad (1.14)$$

and, thus, the first of the two terms in (1.15) is equal to zero. We can then write

$$\mathbf{A}(\mathbf{r},\mathbf{r}') = (\mathbf{r}'-\mathbf{r}_l) \times \left[\nabla_S g(\mathbf{r},\mathbf{r}') + \hat{z}\frac{\partial g(\mathbf{r},\mathbf{r}')}{\partial z} \right]. \qquad (1.15)$$

From (1.12) we can then write

$$\mathbf{I}^{(l)}(\mathbf{r}') = \int_T (\mathbf{r} - \mathbf{r}_l) \times \nabla g(\mathbf{r},\mathbf{r}') dS = (\mathbf{r}' - \mathbf{r}_l) \times \left\{ \int_T \nabla_S g(\mathbf{r},\mathbf{r}') dS + \hat{z} \int_T \frac{\partial g(\mathbf{r},\mathbf{r}')}{\partial z} dS \right\}$$

$$= (\mathbf{r}' - \mathbf{r}_l) \times \int_{\partial T} \hat{v} g(\mathbf{r},\mathbf{r}') ds - \hat{z} \times (\mathbf{r}' - \mathbf{r}_l) \int_T \frac{\partial g(\mathbf{r},\mathbf{r}')}{\partial z} dS \tag{1.16}$$

where $\hat{v}$ the exterior unit normal to the side of the triangle (lying in the triangle's plane) and ∂T is the triangle's boundary. We have also used Identity 43 on p. 503 of reference 8 in transforming the first surface integral into a line integral. We deal with the remaining surface integral in the next section.

We have thus expressed the surface integral in (1.12) in terms of a line integral and a surface integral. This is the principal result. We concentrate next on the case where $\mathbf{r}'$ is a point in the triangle's interior. In this case, the first term in (1.16) is a vector that has only a z-component. When that vector is dotted into the vector $\mathbf{f}_m(\mathbf{r}') \times \hat{n}'$ in (1.10) the result is zero since the latter is transverse to this direction. In order to evaluate the contribution of the second term in (1.16), we move the OP to the position

$$\mathbf{r}' = \mathbf{r}' + \varepsilon \hat{z}, \quad \varepsilon > 0; \quad \mathbf{r}' \in T \tag{1.17}$$

we evaluate the integral and then let ε go to zero. For the integral, we write

$$\int_T \frac{\partial g(\mathbf{r},\mathbf{r}')}{\partial z} dS = -\frac{1}{4\pi} \left\{ \int_{T_m^+} \frac{\partial}{\partial z} |\mathbf{r} - \varepsilon \hat{z}|^{-1} dS + \int_{T_m^+} \frac{\partial}{\partial z} \left[\frac{e^{-ik|\mathbf{r} - \varepsilon \hat{z}|} - 1}{|\mathbf{r} - \varepsilon \hat{z}|} \right] dS \right\} = -\frac{1}{4\pi} \{ J_1(\mathbf{r}') + J_2(\mathbf{r}') \}.$$

$$\tag{1.18}$$

The first of these integrals, J_1, is the integral that measures the solid angle subtended by the triangle at the point $\mathbf{r}'$ (see Appendix C). As $\varepsilon \to 0$, this integral goes to 2π

$$J_1(\mathbf{r}') = 2\pi. \tag{1.19}$$

This contribution, however, has already been accounted for in the derivation of the MFIE (1.1). Thus, we must omit it here or we will have a double count.

For the remaining integral in (1.18), we let

$$R = |\mathbf{r} - \varepsilon \hat{z}| \tag{1.20}$$

and write

$$J_2(\mathbf{r}') = \int_T \frac{\partial}{\partial z}\left[\frac{e^{-ikR}-1}{R}\right]dS = \int_{D_0} \frac{\partial}{\partial z}\left[\frac{e^{-ikR}-1}{R}\right]dS + \int_{T-D_0} \frac{\partial}{\partial z}\left[\frac{e^{-ikR}-1}{R}\right]dS \qquad (1.21)$$

where D_0 is a solid disk with center at the origin and radius ρ_0. The radius is small enough so that the entire disk lies within the triangle. The second of these integrals is over the region bounded by the triangle's perimeter and the disk's circumference; thus, this integral is not singular when $\varepsilon = 0$ and, since its integrand is equal to zero when $\varepsilon = 0$, the integral itself is equal to zero. For the first integral, we write

$$\frac{\partial}{\partial z}\left[\frac{e^{-ikR}-1}{R}\right] = \frac{\partial}{\partial R}\left[\frac{e^{-ikR}-1}{R}\right]\left(\frac{-\varepsilon}{R}\right) = \left(\frac{-\varepsilon}{R}\right)\frac{-ikRe^{-ikR}-\left(e^{-ikR}-1\right)}{R^2}$$

$$= \varepsilon\frac{ike^{-ikR}}{R^2} - i\frac{\varepsilon}{R^2}ke^{-ikR/2}\frac{\sin\left(kR/2\right)}{kR/2} \qquad (1.22)$$

from which we get that

$$\left|\frac{\partial}{\partial z}\left[\frac{e^{-ikR}-1}{R}\right]\right| \le \varepsilon\frac{2k}{R^2}. \qquad (1.23)$$

Thus,

$$\left|\int_{D_0} \frac{\partial}{\partial z}\left[\frac{e^{-ikR}-1}{R}\right]dS\right| \le 4\pi k\varepsilon \int_0^{\rho_0} \frac{\rho d\rho}{\rho^2+\varepsilon^2} = 2\pi k\varepsilon\left[\ln\left(\rho_0^2+\varepsilon^2\right)-2\ln\left(\varepsilon\right)\right]\xrightarrow[\varepsilon\to 0]{} 0. \qquad (1.24)$$

Thus, (1.21) is equal to zero in the limit. From this result and (1.21), we have for the limit of (1.18) that

$$\int_T \frac{\partial g(\mathbf{r},\mathbf{r}')}{\partial z}dS = -\frac{1}{2}, \quad \mathbf{r}' \in T. \qquad (1.25)$$

As we pointed out above, this contribution has already been accounted for in the derivation of (1.1). *For computational purposes, this integral should be set equal to zero whenever the OP is in the interior of the triangle. Consequently, the entire term in (1.16) should be set equal to zero in such a case*

$$\mathbf{I}^{(l)}(\mathbf{r}') = \int_T (\mathbf{r}-\mathbf{r}_l)\times\nabla g(\mathbf{r},\mathbf{r}')dS = \mathbf{0}, \quad \mathbf{r}' \in T. \qquad (1.26)$$

We close this section by noting that an alternate testing of (1.7) leads to the same inner integral as the one above. We show this in Appendix A.

SECTION 2: REMAINING SURFACE INTEGRAL

For the last integral in (1.16), and for all $\mathbf{r}' \notin T$ (in fact, not in the triangle's plane), we write

$$F(\mathbf{r}') = \int_T \frac{\partial g(\mathbf{r},\mathbf{r}')}{\partial z} dS = -\frac{1}{4\pi} \int_T \frac{\partial}{\partial z}\left(\frac{e^{-ikR}}{R}\right) dS = -\frac{e^{-ikr'}}{4\pi} \int_T \frac{\partial}{\partial z}\left(\frac{e^{-ik(R-r')}}{R}\right) dS$$

$$= -\frac{e^{-ikr'}}{4\pi} \int_T \frac{\partial}{\partial z}\left\{\frac{\cos\left[k(R-r')\right] - i\sin\left[k(R-r')\right]}{R}\right\} dS$$

$$= -\frac{e^{-ikr'}}{4\pi} \sum_{n=0}^{N_c-1} \frac{(-1)^n k^{2n}}{(2n)!} \int_T \frac{\partial}{\partial z}\left\{\frac{(R-r')^{2n}}{R}\right\} dS + \frac{ie^{-ikr'}}{4\pi} \sum_{n=0}^{N_s-1} \frac{(-1)^n k^{2n+1}}{(2n+1)!} \int_T \frac{\partial}{\partial z}\left\{\frac{(R-r')^{2n+1}}{R}\right\} dS . \quad (2.1)$$

Here we assume that $\mathbf{r}' \notin T$ for then, by agreement, we set F equal to zero. F is also (legitimately) zero whenever the OP is in the triangle's plane and exterior to the triangle. We normalize all distances with respect to wavelength (see also reference 1, p. 5) and write

$$F(\mathbf{r}') = -\frac{e^{-i2\pi r'}}{4\pi} \sum_{n=0}^{N_c-1} \frac{(-1)^n (2\pi)^{2n}}{(2n)!} \int_T \frac{\partial}{\partial z}\left\{\frac{(R-r')^{2n}}{R}\right\} dS$$

$$+ \frac{ie^{-i2\pi r'}}{4\pi} \sum_{n=0}^{N_s-1} \frac{(-1)^n (2\pi)^{2n+1}}{(2n+1)!} \int_T \frac{\partial}{\partial z}\left\{\frac{(R-r')^{2n+1}}{R}\right\} dS \qquad (2.2)$$

with distance measured in wavelengths.

We define

$$P_n(\mathbf{r}') = \int_T \frac{\partial}{\partial z}\left\{\frac{(R-r')^n}{R}\right\} dS , \quad n = 0,1,2,... \qquad (2.3)$$

and

$$Q_n(\mathbf{r}') = (n+1)\int_T \frac{(R-r')^n}{R} dS , \quad n = 0,1,2,... \qquad (2.4)$$

then

$$P_{n+1}(\mathbf{r}') = \int_T \frac{\partial}{\partial z}\left\{\frac{(R-r')^{n+1}}{R}\right\} dS = \int_T \frac{\partial}{\partial z}\left\{(R-r')^n \left(\frac{R-r'}{R}\right)\right\} dS$$

$$= \int_T \frac{\partial(R-r')^n}{\partial z} dS - r'P_n(\mathbf{r}') = -nz'\int_T \frac{(R-r')^{n-1}}{R} dS - r'P_n(\mathbf{r}') \qquad (2.5)$$

from which we get that

$$P_1(\mathbf{r}') = -r' P_0(\mathbf{r}')$$ (2.6)

and

$$P_{n+2}(\mathbf{r}') = -z' Q_n(\mathbf{r}') - r' P_{n+1}(\mathbf{r}'), \quad n = 0,1,2,...$$ (2.7)

This iteration converges for $r' < 1$. Since, however, Q_n is computed also, then the OP must be interior to a sphere centered at the centroid and radius of one-half of a wavelength (reference 1, Section 3). We also note that (2.4) has been thoroughly studied and evaluated in (reference 1, Section 2 and Appendix A). It remains then to evaluate (2.3) for $n = 0$. We will do that in Section 4.

While performing verification and validation work on (2.2), we noticed that, when the point z' is over the triangle and tending to zero, the imaginary part of F does not tend to zero as it should but to a finite albeit small number. We traced the cause of the problem to the fact that, in the final stage, we subtract two almost equal numbers. We modified the algorithm for this case, and we present the details in Appendix B. We summarize the result as follows.
For a point over a triangle, if either

$$z' < \frac{\sqrt{5 \cdot 10^{-M}}}{2\pi}$$ (2.8)

or

$$z' < \frac{\sqrt{10\varepsilon}}{2\pi}$$ (2.9)

then

$$\text{Im}\{F(\mathbf{r}')\} = z' \sum_{n=0}^{N-2} \frac{(-1)^n (n+1)(2\pi)^{2n+2}}{(2n+3)!} \int_T \rho^{2n} dS .$$ (2.10)

Above, M is the number of significant digits desired and ε is the machine epsilon. The latter is given in Table B.1 for different precisions. Moreover,

$$N = \max(N_c, N_s)$$ (2.11)

with N_c and N_s obtained from (3.14) and (3.12), respectively.

We proceed in the next section with the evaluation of the first integral in (1.16).

10

SECTION 3: NUMERICAL CONSIDERATIONS FOR LINE INTEGRAL IN (1.16)

In this section, we evaluate the integral in (1.16)

$$\mathbf{I}_1^{(l)}(\mathbf{r}') = (\mathbf{r}' - \mathbf{r}_l) \times \int_{\partial T} \hat{v}\, g(\mathbf{r}, \mathbf{r}')\, ds = (\mathbf{r}' - \mathbf{r}_l) \times \sum_{j=1}^{3} \hat{v}_j \int_{s_j} g(\mathbf{r}, \mathbf{r}')\, ds \tag{3.1}$$

where $\hat{v}_j$ is the exterior unit normal on the j-th side of the triangle, lying in the triangle's plane, and s_j is the j-th side and, also, its length. We can also write this result in terms of its component in the triangle's plane and one along the z-direction

$$\mathbf{I}_1^{(l)}(\mathbf{r}') = (\boldsymbol{\rho}' + z'\hat{z} - \mathbf{r}_l) \times \sum_{j=1}^{3} \hat{v}_j \int_{s_j} g(\mathbf{r}, \mathbf{r}')\, ds$$

$$= (\boldsymbol{\rho}' - \mathbf{r}_l) \times \sum_{j=1}^{3} \hat{v}_j \int_{s_j} g(\mathbf{r}, \mathbf{r}')\, ds + z'\hat{z} \times \sum_{j=1}^{3} \hat{v}_j \int_{s_j} g(\mathbf{r}, \mathbf{r}')\, ds$$

$$= -\hat{z}(\boldsymbol{\rho}' - \mathbf{r}_l) \cdot \sum_{j=1}^{3} \hat{t}_j \int_{s_j} g(\mathbf{r}, \mathbf{r}')\, ds + z' \sum_{j=1}^{3} \hat{t}_j \int_{s_j} g(\mathbf{r}, \mathbf{r}')\, ds \tag{3.2}$$

where $\hat{t}_j$ is the unit tangent to the j-side of the triangle, given by

$$\hat{t}_j = \hat{z} \times \hat{v}_j \tag{3.3}$$

and

$$\boldsymbol{\rho}' = x'\hat{x} + y'\hat{y} \tag{3.4}$$

is the projection of the observation point onto the xy-plane.

We consider the integral

$$\int_{s_j} \frac{e^{-ik|\mathbf{r}-\mathbf{r}'|}}{|\mathbf{r}-\mathbf{r}'|}\, ds = e^{-ikr'} \int_{s_j} \frac{e^{-ik(R-r')}}{R}\, ds = e^{-i2\pi r'} \int_{s_j} \frac{e^{-i2\pi(R-r')}}{R}\, ds = e^{-i2\pi r'}\, I(\mathbf{r}', j) \tag{3.5}$$

where, in the last integral all distances are measured in wavelengths. The multiplication and division by the exponential is justified below. We re-write the integral as

$$I(\mathbf{r}', j) = \int_{s_j} \frac{\cos\left[2\pi(R-r')\right] - i\sin\left[2\pi(R-r')\right]}{R}\, ds\ . \tag{3.6}$$

In evaluating this integral, we follow the procedure in reference 1. We can show that the argument of the trigonometric functions is bounded. The centroid of a triangle divides each median in a 2:1 ratio. The longer of the two parts is the distance from the centroid to the vertex of the median. Thus, the largest distance from the centroid to a point on the triangle is equal to two thirds the longest of the three medians. However, a median is shorter than the longer of the two adjacent sides; thus, the longest distance from the centroid to the triangle's perimeter is less than two thirds the length of the triangle's longest side. We combine this with the fact that the side of a triangle (in this case that formed by the observation, integration and centroid points) is always greater than the difference of the other two sides to obtain the bound

$$\left| R - r' \right| \le r < \frac{2}{3} l_{\text{max}} \tag{3.7}$$

where l_{max} is the length of the longest side of the triangle. Though this is not a strict bound, it is one that holds for all observation points; thus, no matter how far away the observation point is from the integration triangle, the number of terms in the expansion will be the same as for a point near the triangle. Moreover, for an actual grid, we can search among all triangles for the longest side and use that value in (3.7). In this way, we do not have to test all triangles separately, conserving a lot of compute time. Had the exponential factor not been inserted in (3.5), we would need more and more terms in the expansion as the observation point receded from the triangle.

We proceed now to expand (3.6) in a Maclaurin series and keep the first N terms

$$I_{N_c,N_s}(\mathbf{r}',j) = \sum_{n=0}^{N_c-1} \frac{(-1)^n (2\pi)^{2n}}{(2n)!} \int_{s_j} \frac{(R-r')^{2n}}{R} \, ds - i \sum_{n=0}^{N_s-1} \frac{(-1)^n (2\pi)^{2n+1}}{(2n+1)!} \int_{s_j} \frac{(R-r')^{2n+1}}{R} \, ds \tag{3.8}$$

In determining the number of terms N, we use Taylor's Theorem with a Remainder (reference 5, p. 113). If we require a number M of correct significant digits, then we proceed as follows to determine the number of terms. The series for the sine is

$$\frac{\sin\left[2\pi(R-r')\right]}{2\pi(R-r')} = \sum_{n=0}^{N-1} \frac{(-1)^n \left[2\pi(R-r')\right]^{2n}}{(2n+1)!} + R_s\left(N, 2\pi(R-r')\right) \tag{3.9}$$

where R_s is the remainder of the series and is bounded by the first omitted term

$$\left| R_s\left(N, 2\pi(R-r')\right) \right| \le \frac{\left[2\pi \left| R-r' \right|_{\text{max}}\right]^{2N}}{(2N+1)!} < \frac{\left(\frac{4\pi}{3} l_{\text{max}}\right)^{2N}}{(2N+1)!}. \tag{3.10}$$

12

We can then write for the relative error

$$\frac{\left|\frac{\sin\left[2\pi\left(R-r'\right)\right]}{2\pi\left(R-r'\right)}-\sum_{n=0}^{N-1}\frac{\left(-1\right)^{n}\left[2\pi\left(R-r'\right)\right]^{2n}}{\left(2n+1\right)!}\right|}{\left|\frac{\sin\left[2\pi\left(R-r'\right)\right]}{2\pi\left(R-r'\right)}\right|}$$

$$=\frac{\left|R_{s}\left(N,2\pi\left(R-r'\right)\right)\right|}{\left|\frac{\sin\left[2\pi\left(R-r'\right)\right]}{2\pi\left(R-r'\right)}\right|}<\frac{\left(\frac{4\pi}{3}l_{max}\right)^{2N}}{\left(2N+1\right)!\left|\frac{\sin\left[2\pi\left|R-r'\right|_{max}\right]}{2\pi\left|R-r'\right|_{max}}\right|}\leq\frac{\left(\frac{4\pi}{3}l_{max}\right)^{2N}}{\left(2N+1\right)!\left|\frac{\sin\left(\frac{4\pi}{3}l_{max}\right)}{\frac{4\pi}{3}l_{max}}\right|}. \qquad (3.11)$$

The number of terms is determined by requiring that the relative error is smaller than 5 divided by the number 10 raised to the number of significant digits M plus one, or

$$\frac{\left(\frac{4\pi}{3}l_{max}\right)^{2N}}{\left(2N+1\right)!}<5\cdot10^{-M-1}\left|\frac{\sin\left(\frac{4\pi}{3}l_{max}\right)}{\frac{4\pi}{3}l_{max}}\right|. \qquad (3.12)$$

Once the triangle's dimensions are known, we can solve this expression for N.

In this discussion, we have assumed that the argument of the sine function is small; in practice, the longest side of a triangle does not exceed one tenth of a wavelength and, hence, the largest argument is approximately equal to $0.4\pi/3$ of a radian or 24 deg. This means that the trigonometric functions in the original integrals hardly exhibit an oscillatory behavior.

For the cosine we have

$$\frac{\left|\cos\left[2\pi\left(R-r'\right)\right]-\sum_{n=0}^{N-1}\frac{\left(-1\right)^{n}\left[2\pi\left(R-r'\right)\right]^{2n}}{\left(2n\right)!}\right|}{\left|\cos\left[2\pi\left(R-r'\right)\right]\right|}\leq\frac{\frac{\left[2\pi\left(R-r'\right)\right]^{2N}}{\left(2N\right)!}}{\left|\cos\left[2\pi\left(R-r'\right)_{max}\right]\right|}\leq\frac{\left(\frac{4}{3}\pi l_{max}\right)^{2N}}{\left(2N\right)!\left|\cos\left(\frac{4}{3}\pi l_{max}\right)\right|} \qquad (3.13)$$

and the test is

$$\frac{\left(\frac{4}{3}\pi l_{\max}\right)^{2N}}{(2N)!} < 5 \cdot 10^{-M-1} \cos\left(\frac{4}{3}\pi l_{\max}\right). \tag{3.14}$$

As an example, in Table 3.1 we give the number of terms in the sine and cosine expansions that are required to guarantee a certain number of significant digits.

Table 3.1: Number of terms that guarantee a given number of SD.
Largest side of triangle less than or equal to a tenth of a wavelength.

No. of SD	Sine	Cosine
4	3	3
5	3	3
6	4	3
7	4	4
8	4	4
9	5	5
10	5	5
11	5	5
12	6	6
13	6	6
14	6	6
15	7	7

We now let

$$J_j^{(n)}(\mathbf{r}') = \int_{s_j} \frac{(R-r')^n}{R} ds \quad , \quad n = 0, 1, 2, \dots \tag{3.15}$$

We can now proceed as with (2.5). We do not see the advantage; however, over the following procedure. We expand the binomial in (3.15) and write

$$J_j^{(0)}(\mathbf{r}') = \int_{s_j} \frac{ds}{R} \tag{3.16}$$

while

$$J_j^{(n)}(\mathbf{r}') = \sum_{m=0}^{n} (-1)^{n+m} \binom{n}{m} r'^{n-m} \int_{s_j} R^{m-1} ds$$

$$= (-1)^n r'^n J_j^{(0)}(\mathbf{r}') + \sum_{m=1}^{n} (-1)^{n+m} \binom{n}{m} r'^{n-m} \int_{s_j} R^{m-1} ds \quad , \quad n = 1, 2, \ldots \tag{3.17}$$

We separate even and odd powers

$$J_j^{(n)}(\mathbf{r}') = (-1)^n r'^n J_j^{(0)}(\mathbf{r}') + (-1)^n \sum_{m=1}^{[n/2]} \binom{n}{2m} r'^{n-2m} \int_{s_j} R^{2m-1} ds$$

$$- (-1)^n \sum_{m=0}^{[(n-1)/2]} \binom{n}{2m+1} r'^{n-2m-1} \int_{s_j} R^{2m} ds \tag{3.18}$$

In order to evaluate these integrals, we introduce the following notation (see Figures 3.1 and 3.2)

$$\mathbf{r} = \mathbf{r}_{j+1} + s\hat{t}_j , \quad j = 1, 2, 3 \tag{3.19}$$

with the indices running cyclically. We also write

$$\mathbf{r}' = x'\hat{x} + y'\hat{y} + h\hat{z} = \boldsymbol{\rho}' + h\hat{z}, \quad \mathbf{r}_l = x_l \hat{x} + y_l \hat{y} \tag{3.20}$$

and

$$\mathbf{a}_{j+1} = \mathbf{r}_{j+1} - \boldsymbol{\rho}', \quad \tau = s + \hat{t}_j \cdot \mathbf{a}_{j+1}, \quad A_j = \left| \hat{t}_j \times \left(\hat{t}_j \times \mathbf{a}_{j+1} \right) \right|, \quad \varpi = |\mathbf{r} - \boldsymbol{\rho}'| = \left| \mathbf{a}_{j+1} + s\hat{t}_j \right|. \tag{3.21}$$

From these we can write

$$\varpi^2 = s^2 + 2\hat{t}_j \cdot \mathbf{a}_{j+1} s + |\mathbf{a}_{j+1}|^2 = \left(s + \hat{t}_j \cdot \mathbf{a}_{j+1} \right)^2 + |\mathbf{a}_{j+1}|^2 - \left(\hat{t}_j \cdot \mathbf{a}_{j+1} \right)^2 = \left(s + \hat{t}_j \cdot \mathbf{a}_{j+1} \right)^2 + A_j^2 = \tau^2 + A_j^2 \tag{3.22}$$

We also define

$$\mathbf{b}_j = \mathbf{r}_j - \mathbf{r}'; \quad B_j = \sqrt{A_j^2 + h^2} , \quad j = 1, 2, 3. \tag{3.23}$$
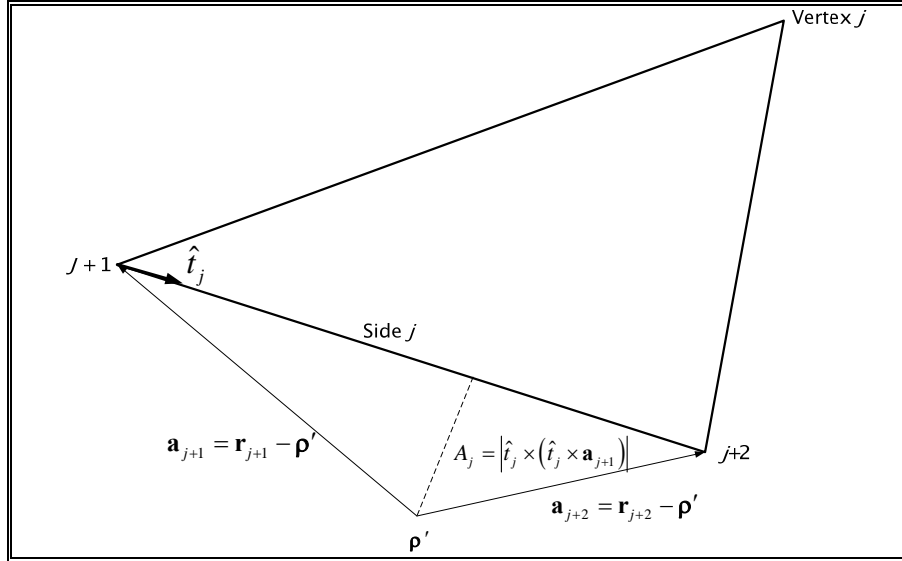
Figure 3.1: Geometrical meaning of the quantities in Equation (3.21).
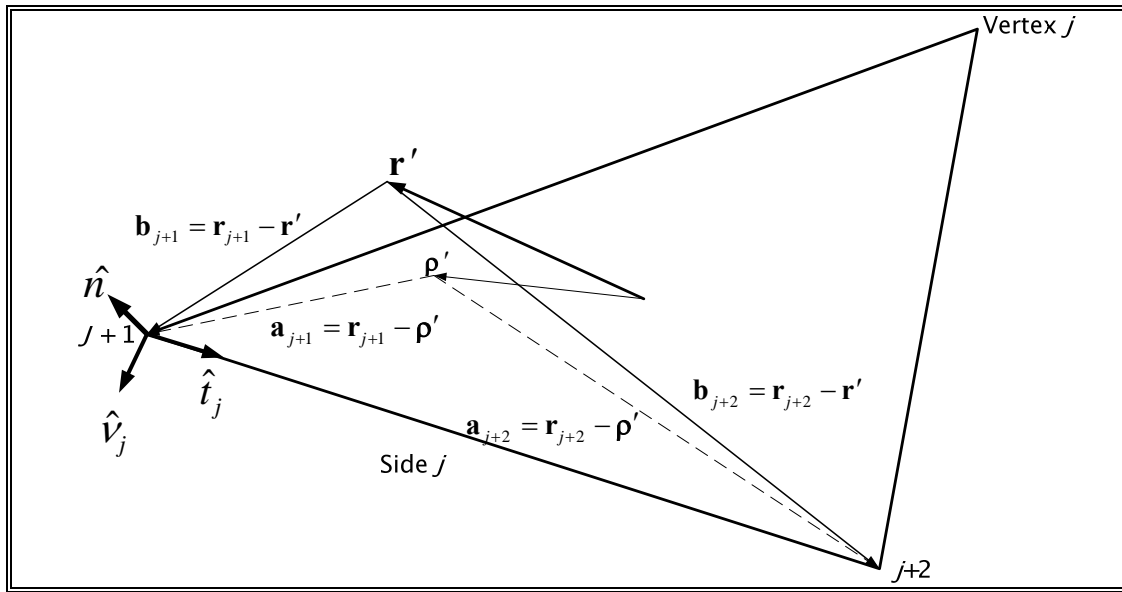
Figure 3.2: Local rectangular coordinates and various vectors.

With these definitions, we have that

$$J_j^{(0)}\left(\mathbf{r}'\right)=\int_{s_j}\frac{ds}{R}=\int_{\hat{t}_j\cdot\mathbf{a}_{j+1}}^{\hat{t}_j\cdot\mathbf{a}_{j+2}}\frac{d\tau}{\sqrt{\tau^2+B_j^{\,2}}}\;.$$

(3.24)

We distinguish three cases. For $\hat{t}_j \cdot \mathbf{b}_{j+2} > \hat{t}_j \cdot \mathbf{b}_{j+1} > 0$, we make the transformation

$$\tau = B_j \tan\theta, \quad d\tau = B_j \sec^2\theta \, d\theta \tag{3.25}$$

and write

$$J_j^{(0)}(\mathbf{r}') = \int_{\arctan(\hat{t}_j \cdot \mathbf{a}_{j+1})}^{\arctan(\hat{t}_j \cdot \mathbf{a}_{j+2})} \sec\theta \, d\theta = \int_{\arctan\left(\frac{\hat{t}_j \cdot \mathbf{a}_{j+1}}{B_j}\right)}^{\arctan\left(\frac{\hat{t}_j \cdot \mathbf{a}_{j+2}}{B_j}\right)} \frac{\sec\theta(\sec\theta + \tan\theta)}{\sec\theta + \tan\theta} \, d\theta$$

$$= \ln|\sec\theta + \tan\theta| \begin{vmatrix} \arctan\left(\dfrac{\hat{t}_j \cdot \mathbf{b}_{j+2}}{B_j}\right) \\ \arctan\left(\dfrac{\hat{t}_j \cdot \mathbf{b}_{j+1}}{B_j}\right) \end{vmatrix} = \ln\left| \frac{\sqrt{1+\left(\dfrac{\hat{t}_j \cdot \mathbf{b}_{j+2}}{B_j}\right)^2} + \dfrac{\hat{t}_j \cdot \mathbf{b}_{j+2}}{B_j}}{\sqrt{1+\left(\dfrac{\hat{t}_j \cdot \mathbf{b}_{j+1}}{B_j}\right)^2} + \dfrac{\hat{t}_j \cdot \mathbf{b}_{j+1}}{B_j}} \right|$$

$$= \ln\left| \frac{\sqrt{B_j^2 + \left(\hat{t}_j \cdot \mathbf{b}_{j+2}\right)^2} + \hat{t}_j \cdot \mathbf{b}_{j+2}}{\sqrt{B_j^2 + \left(\hat{t}_j \cdot \mathbf{b}_{j+1}\right)^2} + \hat{t}_j \cdot \mathbf{b}_{j+1}} \right| = \ln\left(\frac{\left|\mathbf{b}_{j+2}\right| + \hat{t}_j \cdot \mathbf{b}_{j+2}}{\left|\mathbf{b}_{j+1}\right| + \hat{t}_j \cdot \mathbf{b}_{j+1}} \right). \tag{3.26}$$

We examine next the case where $\hat{t}_j \cdot \mathbf{b}_{j+1} < \hat{t}_j \cdot \mathbf{b}_{j+2} < 0$ and write

$$J_j^{(0)}(\mathbf{r}') = \int_{s_j} \frac{ds}{R} = \int_{|\hat{t}_j \cdot \mathbf{a}_{j+2}|}^{|\hat{t}_j \cdot \mathbf{a}_{j+1}|} \frac{d\tau}{\sqrt{\tau^2 + B_j^2}} = \ln|\sec\theta + \tan\theta| \begin{vmatrix} \arctan\dfrac{\left|\hat{t}_j \cdot \mathbf{b}_{j+1}\right|}{B_j} \\ \arctan\dfrac{\left|\hat{t}_j \cdot \mathbf{b}_{j+2}\right|}{B_j} \end{vmatrix}$$

$$= \ln\left| \frac{\sqrt{1+\left(\dfrac{\hat{t}_j \cdot \mathbf{b}_{j+1}}{B_j}\right)^2} + \dfrac{\left|\hat{t}_j \cdot \mathbf{b}_{j+1}\right|}{B_j}}{\sqrt{1+\left(\dfrac{\hat{t}_j \cdot \mathbf{b}_{j+2}}{B_j}\right)^2} + \dfrac{\left|\hat{t}_j \cdot \mathbf{b}_{j+2}\right|}{B_j}} \right| = \ln\left(\frac{\left|\mathbf{b}_{j+1}\right| + \left|\hat{t}_j \cdot \mathbf{b}_{j+1}\right|}{\left|\mathbf{b}_{j+2}\right| + \left|\hat{t}_j \cdot \mathbf{b}_{j+2}\right|} \right). \tag{3.27}$$

For the case

$$\hat{t}_j \cdot \mathbf{b}_{j+1} \leq 0, \quad \hat{t}_j \cdot \mathbf{b}_{j+2} \geq 0 \tag{3.28}$$

we write

$$J_j^{(0)}(\mathbf{r}') = \int\limits_{s_j} \frac{ds}{R} = \int\limits_0^{\left|\hat{t}_j \cdot \mathbf{a}_{j+1}\right|} \frac{d\tau}{\sqrt{\tau^2 + B_j^2}} + \int\limits_0^{\hat{t}_j \cdot \mathbf{a}_{j+2}} \frac{d\tau}{\sqrt{\tau^2 + B_j^2}}$$

$$= \ln\left|\sec\theta + \tan\theta\right| \begin{vmatrix} \arctan\left|\dfrac{\hat{t}_j \cdot \mathbf{b}_{j+1}}{B_j}\right| \\ 0 \end{vmatrix} + \ln\left|\sec\theta + \tan\theta\right| \begin{vmatrix} \arctan\left(\dfrac{\hat{t}_j \cdot \mathbf{b}_{j+2}}{B_j}\right) \\ 0 \end{vmatrix}$$

$$= \ln\left|\sqrt{1 + \left(\frac{\hat{t}_j \cdot \mathbf{b}_{j+1}}{B_j}\right)^2} + \left|\frac{\hat{t}_j \cdot \mathbf{b}_{j+1}}{B_j}\right|\right| + \ln\left|\sqrt{1 + \left(\frac{\hat{t}_j \cdot \mathbf{b}_{j+2}}{B_j}\right)^2} + \frac{\hat{t}_j \cdot \mathbf{b}_{j+2}}{B_j}\right|$$

$$= \ln\left|\frac{\left|\mathbf{b}_{j+1}\right| + \left|\hat{t}_j \cdot \mathbf{b}_{j+1}\right|}{B_j}\right| + \ln\left|\frac{\left|\mathbf{b}_{j+2}\right| + \hat{t}_j \cdot \mathbf{b}_{j+2}}{B_j}\right|. \tag{3.29}$$

We next evaluate the integral

$$K_j^{(1)}(\mathbf{r}') = \int\limits_{s_j} R\,ds \tag{3.30}$$

in each of the above three regions. In the first region ($\hat{t}_j \cdot \mathbf{b}_{j+2} > \hat{t}_j \cdot \mathbf{b}_{j+1} > 0$) we use (3.25) and write

$$K_j^{(1)}(\mathbf{r}') = B_j^2 \int\limits_{\arctan(\hat{t}_j \cdot \mathbf{a}_{j+1})}^{\arctan(\hat{t}_j \cdot \mathbf{a}_{j+2})} \sec^3\theta\,d\theta = B_j^2 \tan\theta\sec\theta \begin{vmatrix} \arctan\left(\dfrac{\hat{t}_j \cdot \mathbf{a}_{j+2}}{B_j}\right) \\ \arctan\left(\dfrac{\hat{t}_j \cdot \mathbf{a}_{j+1}}{B_j}\right) \end{vmatrix} - B_j^2 \int\limits_{\arctan\left(\frac{\hat{t}_j \cdot \mathbf{a}_{j+1}}{B_j}\right)}^{\arctan\left(\frac{\hat{t}_j \cdot \mathbf{a}_{j+2}}{B_j}\right)} \tan^2\theta\sec\theta\,d\theta$$

$$= B_j^2 \left\{ \left(\frac{\hat{t}_j \cdot \mathbf{a}_{j+2}}{B_j}\right)\sqrt{1 + \left(\frac{\hat{t}_j \cdot \mathbf{a}_{j+2}}{B_j}\right)^2} - \left(\frac{\hat{t}_j \cdot \mathbf{a}_{j+1}}{B_j}\right)\sqrt{1 + \left(\frac{\hat{t}_j \cdot \mathbf{a}_{j+1}}{B_j}\right)^2} \right\} - K_j^{(1)}(\mathbf{r}') + B_j^2 \int\limits_{\arctan\left(\frac{\hat{t}_j \cdot \mathbf{a}_{j+1}}{B_j}\right)}^{\arctan\left(\frac{\hat{t}_j \cdot \mathbf{a}_{j+2}}{B_j}\right)} \sec\theta\,d\theta$$

$$= \left(\hat{t}_j \cdot \mathbf{a}_{j+2}\right)\sqrt{B_j^2 + \left(\hat{t}_j \cdot \mathbf{a}_{j+2}\right)^2} - \left(\hat{t}_j \cdot \mathbf{a}_{j+1}\right)\sqrt{B_j^2 + \left(\hat{t}_j \cdot \mathbf{a}_{j+1}\right)^2} - K_j^{(1)}(\mathbf{r}') + B_j^2 \int\limits_{\arctan\left(\frac{\hat{t}_j \cdot \mathbf{a}_{j+1}}{B_j}\right)}^{\arctan\left(\frac{\hat{t}_j \cdot \mathbf{a}_{j+2}}{B_j}\right)} \sec\theta\,d\theta \tag{3.31}$$

or

$$K_j^{(1)}(\mathbf{r}') = \frac{1}{2}\left[\left(\hat{t}_j \cdot \mathbf{b}_{j+2}\right)\left|\mathbf{b}_{j+2}\right| - \left(\hat{t}_j \cdot \mathbf{b}_{j+1}\right)\left|\mathbf{b}_{j+1}\right|\right] + \frac{B_j^2}{2} J_j^{(0)}(\mathbf{r}') \tag{3.32}$$

with $J_j^{(0)}(\mathbf{r}')$ given by (3.26).

In the second region ($\hat{t}_j \cdot \mathbf{b}_{j+1} < \hat{t}_j \cdot \mathbf{b}_{j+2} < 0$)

$$K_j^{(1)}(\mathbf{r}') = \int_{\left|\hat{t}_j \cdot \mathbf{a}_{j+2}\right|}^{\left|\hat{t}_j \cdot \mathbf{a}_{j+1}\right|} \sqrt{\tau^2 + B_j^2}\, d\tau = B_j^2 \int_{\arctan\left(\left|\hat{t}_j \cdot \mathbf{a}_{j+1}\right|\right)}^{\arctan\left(\left|\hat{t}_j \cdot \mathbf{a}_{j+2}\right|\right)} \sec^3\theta\, d\theta$$

$$= \frac{1}{2}\left[\left|\hat{t}_j \cdot \mathbf{b}_{j+1}\right|\left|\mathbf{b}_{j+1}\right| - \left|\hat{t}_j \cdot \mathbf{b}_{j+2}\right|\left|\mathbf{b}_{j+2}\right|\right] + \frac{B_j^2}{2} J_j^{(0)}(\mathbf{r}'). \tag{3.33}$$

In the third region ($\hat{t}_j \cdot \mathbf{b}_{j+1} \le 0$, $\hat{t}_j \cdot \mathbf{b}_{j+2} \ge 0$)

$$K_j^{(1)}(\mathbf{r}') = \int_0^{\left|\hat{t}_j \cdot \mathbf{a}_{j+1}\right|} \sqrt{\tau^2 + B_j^2}\, d\tau + \int_0^{\hat{t}_j \cdot \mathbf{a}_{j+2}} \sqrt{\tau^2 + B_j^2}\, d\tau$$

$$= B_j^2 \tan\theta \sec\theta \left|\arctan\left(\left|\frac{\hat{t}_j \cdot \mathbf{a}_{j+1}}{B_j}\right|\right)\right|_0 - B_j^2 \int_0^{\arctan\left(\left|\frac{\hat{t}_j \cdot \mathbf{a}_{j+1}}{B_j}\right|\right)} \tan^2\theta \sec\theta\, d\theta$$

$$+ B_j^2 \tan\theta \sec\theta \left|\arctan\left(\frac{\hat{t}_j \cdot \mathbf{a}_{j+2}}{B_j}\right)\right|_0 - B_j^2 \int_0^{\arctan\left(\frac{\hat{t}_j \cdot \mathbf{a}_{j+2}}{B_j}\right)} \tan^2\theta \sec\theta\, d\theta$$

$$= B_j^2 \left\{\left|\frac{\hat{t}_j \cdot \mathbf{a}_{j+1}}{B_j}\right|\sqrt{1 + \left(\frac{\hat{t}_j \cdot \mathbf{a}_{j+1}}{B_j}\right)^2} + \left(\frac{\hat{t}_j \cdot \mathbf{a}_{j+2}}{B_j}\right)\sqrt{1 + \left(\frac{\hat{t}_j \cdot \mathbf{a}_{j+2}}{B_j}\right)^2}\right\} - K_j^{(1)}(\mathbf{r}')$$

$$+ B_j^2 \int_0^{\tan^{-1}\left(\left|\frac{\hat{t}_j \cdot \mathbf{a}_{j+1}}{B_j}\right|\right)} \sec\theta\, d\theta + B_j^2 \int_0^{\tan^{-1}\left(\frac{\hat{t}_j \cdot \mathbf{a}_{j+2}}{B_j}\right)} \sec\theta\, d\theta \tag{3.34}$$

or

$$K_j^{(1)}(\mathbf{r}') = \frac{1}{2}\left[\left|\hat{t}_j \cdot \mathbf{b}_{j+1}\right|\left|\mathbf{b}_{j+1}\right| + \left(\hat{t}_j \cdot \mathbf{b}_{j+2}\right)\left|\mathbf{b}_{j+2}\right|\right] + \frac{B_j^2}{2} J_j^{(0)}(\mathbf{r}'). \tag{3.35}$$

We next evaluate the integral in the first sum in (3.18). In the first region

$$K_j^{(2m+1)}(\mathbf{r}') = \int_{s_j} R^{2m+1}\,ds = \int_{\hat{t}_j\cdot\mathbf{a}_{j+1}}^{\hat{t}_j\cdot\mathbf{a}_{j+2}} R^{2m-1}\left(\tau^2 + B_j^2\right)d\tau = \int_{\hat{t}_j\cdot\mathbf{a}_{j+1}}^{\hat{t}_j\cdot\mathbf{a}_{j+2}} \left(\tau^2 + B_j^2\right)^{\frac{2m-1}{2}}\tau^2\,d\tau + B_j^2 K_j^{(2m-1)}(\mathbf{r}')$$

$$= \frac{1}{2m+1}\left(\tau^2 + B_j^2\right)^{\frac{2m+1}{2}}\tau\left|\begin{matrix}\hat{t}_j\cdot\mathbf{a}_{j+2}\\\hat{t}_j\cdot\mathbf{a}_{j+1}\end{matrix}\right. - \frac{1}{2m+1}K_j^{(2m+1)}(\mathbf{r}') + B_j^2 K_j^{(2m-1)}(\mathbf{r}') \qquad (3.36)$$

from which

$$K_j^{(2m+1)}(\mathbf{r}') = \frac{1}{2m+2}\left[\left(\hat{t}_j\cdot\mathbf{a}_{j+2}\right)\left|\mathbf{b}_{j+2}\right|^{2m+1} - \left(\hat{t}_j\cdot\mathbf{a}_{j+1}\right)\left|\mathbf{b}_{j+1}\right|^{2m+1}\right] + \frac{2m+1}{2m+2}B_j^2 K_j^{(2m-1)}(\mathbf{r}'), \quad m=1,2,... \qquad (3.37)$$

Similarly, in the second region

$$K_j^{(2m+1)}(\mathbf{r}') = \frac{1}{2m+2}\left(\left|\hat{t}_j\cdot\mathbf{a}_{j+1}\right|\left|\mathbf{b}_{j+1}\right|^{2m+1} - \left|\hat{t}_j\cdot\mathbf{a}_{j+2}\right|\left|\mathbf{b}_{j+2}\right|^{2m+1}\right) + \frac{2m+1}{2m+2}B_j^2 K_j^{(2m-1)}(\mathbf{r}'), \quad m=1,2,... \qquad (3.38)$$

while in the third region

$$K_j^{(2m+1)}(\mathbf{r}') = \frac{1}{2m+2}\left(\left(\hat{t}_j\cdot\mathbf{a}_{j+2}\right)\left|\mathbf{b}_{j+2}\right|^{2m+1} + \left|\hat{t}_j\cdot\mathbf{a}_{j+1}\right|\left|\mathbf{b}_{j+1}\right|^{2m+1}\right) + \frac{2m+1}{2m+2}B_j^2 K_j^{(2m-1)}(\mathbf{r}'), \quad m=1,2,... \qquad (3.39)$$

For the integral in the second summation in (3.18), we have

$$K_j^{(0)}(\mathbf{r}') = \int_{s_j} ds = s_j \qquad (3.40)$$

for all regions. In the first region

$$K_j^{(2m)}(\mathbf{r}') = \int_{s_j} R^{2m}\,ds = \int_{\hat{t}_j\cdot\mathbf{a}_{j+1}}^{\hat{t}_j\cdot\mathbf{a}_{j+2}} R^{2m-2}\left(\tau^2 + B_j^2\right)d\tau = \int_{\hat{t}_j\cdot\mathbf{a}_{j+1}}^{\hat{t}_j\cdot\mathbf{a}_{j+2}} \left(\tau^2 + B_j^2\right)^{m-1}\tau^2\,d\tau + B_j^2 K_j^{(2m-2)}(\mathbf{r}')$$

$$= \frac{1}{2m}\left(\tau^2 + B_j^2\right)^{m}\tau\left|\begin{matrix}\hat{t}_j\cdot\mathbf{a}_{j+2}\\\hat{t}_j\cdot\mathbf{a}_{j+1}\end{matrix}\right. - \frac{1}{2m}K_j^{(2m)}(\mathbf{r}') + B_j^2 K_j^{(2m-2)}(\mathbf{r}') \qquad (3.41)$$

so that

$$K_j^{(2m)}(\mathbf{r}') = \frac{1}{2m+1}\left[\left(\hat{t}_j\cdot\mathbf{a}_{j+2}\right)\left|\mathbf{b}_{j+2}\right|^{2m} - \left(\hat{t}_j\cdot\mathbf{a}_{j+1}\right)\left|\mathbf{b}_{j+1}\right|^{2m}\right] + \frac{2m}{2m+1}B_j^2 K_j^{(2m-2)}(\mathbf{r}'), \quad m=1,2,... \qquad (3.42)$$

In the second region

$$K_j^{(2m)}(\mathbf{r}') = \frac{1}{2m+1}\left[\left|\hat{t}_j \cdot \mathbf{a}_{j+1}\right|\left|\mathbf{b}_{j+1}\right|^{2m} - \left|\hat{t}_j \cdot \mathbf{a}_{j+2}\right|\left|\mathbf{b}_{j+2}\right|^{2m}\right] + \frac{2m}{2m+1}B_j^{\ 2}K_j^{(2m-2)}(\mathbf{r}'), \quad m=1,2,\dots \tag{3.43}$$

and in the third region

$$K_j^{(2m)}(\mathbf{r}') = \frac{1}{2m+1}\left[\left(\hat{t}_j \cdot \mathbf{a}_{j+2}\right)\left|\mathbf{b}_{j+2}\right|^{2m} + \left|\hat{t}_j \cdot \mathbf{a}_{j+1}\right|\left|\mathbf{b}_{j+1}\right|^{2m}\right] + \frac{2m}{2m+1}B_j^{\ 2}K_j^{(2m-2)}(\mathbf{r}'), \quad m=1,2,\dots \tag{3.44}$$

This concludes the evaluation of the integral in (3.6) by its approximation in (3.8).

SECTION 4: NUMERICAL CONSIDERATIONS: THE SOLID ANGLE INTEGRAL

We turn to (2.3) for $n = 0$

$$P_0(\mathbf{r}') = \int_T \frac{\partial}{\partial z}\left(\frac{1}{R}\right) dS \ . \tag{4.1}$$

As we point out in Appendix C, this expression represents the solid angle subtended by the triangle at an observation point that lies in the half space in which the z-axis points. If it lies in the other half of the space, then (4.1) yields the negative of the solid angle. We thus can write

$$P_0(\mathbf{r}') = \begin{cases} \Omega(\mathbf{r}'), & \mathbf{r}' \cdot \hat{z} > 0 \\ -\Omega(\mathbf{r}'), & \mathbf{r}' \cdot \hat{z} < 0 \end{cases} \tag{4.2}$$

where $\Omega(\mathbf{r}') > 0$ is the measure of solid angle.

For $z' = 0$, and for $\mathbf{r}'$ entirely outside the closure of T, (4.1) is equal to zero, as a simple evaluation shows. If $\mathbf{r}'$ is in the interior of the triangle, then the integral is equal to $\pm 2\pi$ as $\mathbf{r}'$ approaches the triangle. This contribution, however, has been accounted for in the derivation of the MFIE (2.1); in fact, it is the reason for the ½ factor in the left-hand side of it. Thus, for $\mathbf{r}'$ in the interior of the triangle, we must treat the integral in (4.1) as an improper integral, in which case it is equal to zero. This is so because the solid angle of the triangle is 2π and so is the solid angle subtended by the small circle with center the OP. The net solid angle is the difference of the two, which is zero. The case where $\mathbf{r}'$ is a point on the boundary of T does not occur here. We also point out that, for the same reasons, the function F in (2.1) is equal to zero for $z' = 0$. In fact, if we examine the first vector in (1.16), we see that it points in the z-direction so that its dot product with the test function (as in (1.10)) is equal to zero since, in this case, the test function lies on the integration triangle and is orthogonal to the z-axis.

One formula for computing the solid angle subtended by a triangle is reference 9

$$\Omega(\mathbf{r}') = 2\tan^{-1}\left[\frac{\mathbf{b}_1 \cdot (\mathbf{b}_2 \times \mathbf{b}_3)}{b_1 b_2 b_3 + (\mathbf{b}_1 \cdot \mathbf{b}_2)b_3 + (\mathbf{b}_2 \cdot \mathbf{b}_3)b_1 + (\mathbf{b}_3 \cdot \mathbf{b}_1)b_2}\right] \tag{4.3}$$

where the vectors are given by (3.23) and the scalars indicate the magnitude of the vectors. Another formula is given in reference 10 but it requires more operations and is to be used only if we notice numerical instabilities in the above. This formula is

$$\Omega(\mathbf{r}') = 2\sum_{n=1}^{3}\tan^{-1}\left[\frac{\dfrac{\hat{q}\cdot\left(\hat{b}_n\times\hat{b}_{n+1}\right)}{\left|\hat{b}_n\times\hat{b}_{n+1}\right|}\left(\dfrac{1-\hat{b}_n\cdot\hat{b}_{n+1}}{1+\hat{b}_n\cdot\hat{b}_{n+1}}\right)^{1/2}}{1-\hat{q}\cdot\hat{b}_n+\dfrac{\hat{q}\cdot\left[\hat{b}_n\times\left(\hat{b}_n\times\hat{b}_{n+1}\right)\right]}{\left|\hat{b}_n\times\hat{b}_{n+1}\right|}\left(\dfrac{1-\hat{b}_n\cdot\hat{b}_{n+1}}{1+\hat{b}_n\cdot\hat{b}_{n+1}}\right)^{1/2}}\right], \quad q_z\leq 0, \quad \hat{b}_n=\frac{\mathbf{b}_n}{\left|\mathbf{b}_n\right|} \tag{4.4}$$

where $\hat{q}$ is a unit vector with its tail at the OP and such that its extension does not cross the triangle. If it does, then 4π must be added to the result (reference 11).

We point out that the surface integral in (4.1) can be converted to a line integral and the same is true for the integral of the normal derivative of the free-space Green's function (references 11 and 12).

Since (4.3) returns a value of 2π when the OP is a point on the triangle's interior, and this has already been accounted for as explained above, we must also subtract 2π from it to bring it back to zero. From the discussion above, this amounts to setting (4.1) equal to zero whenever the OP is in the same plane as the triangle.

$$\text{SECTION 5: NUMERICAL CONSIDERATIONS: } Q_n(\mathbf{r}') \text{ IN (2.4)}$$

As mentioned at the end of Section 2, $Q_n(\mathbf{r}')$ in (2.4) has been evaluated in (reference 1, Section 2 and Appendix A). We quote here results from that document. The relevant integral appears in (1.21) of reference 1 and, as a line integral, in (1.22). We quote the latter here

$$Q_n(\mathbf{r}') = \sum_{j=1}^{3} \hat{v}_j \cdot \left(\mathbf{r}_{j+1} - \mathbf{\rho}' \right) \int_{s_j} \frac{\left(\sqrt{\rho^2 + h^2} - r' \right)^{n+1} - \left(|h| - r' \right)^{n+1}}{\rho^2} ds \tag{5.1}$$

where the notation is that of Section 3 (Equations (3.19) – (3.23) and Figures 3.1 and 3.2. We further write this as

$$Q_n(\mathbf{r}') = \sum_{j=1}^{3} \hat{v}_j \cdot \left(\mathbf{r}_{j+1} - \mathbf{\rho}' \right) K_{n,j}(\mathbf{r}') \tag{5.2}$$

where

$$K_{n,j}(\mathbf{r}') = \int_{s_j} \frac{\left(\sqrt{\rho^2 + h^2} - r' \right)^{n+1} - \left(|h| - r' \right)^{n+1}}{\rho^2} ds , \quad n = 0, 1, 2, \ldots \tag{5.3}$$

From this

$$K_{0,j} = \int_{s_j} \frac{\sqrt{\rho^2 + h^2} - |h|}{\rho^2} ds \tag{5.4}$$

$$K_{1,j} = s_j - 2r' K_{0,j} \tag{5.5}$$

$$K_{n+1,j} = V_{n-1,j} - 2r' K_{n,j} - \rho'^2 K_{n-1,j} , \quad n = 1, 2, \ldots \tag{5.6}$$

where

$$V_{n,j}(\mathbf{r}') = \int_{s_j} \left(\sqrt{\rho^2 + h^2} - r' \right)^{n+1} ds , \quad n = 0, 1, 2, \ldots \tag{5.7}$$

5.1. RESULTS FOR $V_{n,j}$

We have three distinct regions of space. In the region $\hat{t}_j \cdot \mathbf{b}_{j+2} > \hat{t}_j \cdot \mathbf{b}_{j+1} > 0$, we have from (2.21) of reference 1 that

$$V_{n,j} = \sum_{m=0}^{n+1} \left[\frac{(n+1)!}{m!(n+1-m)!} \right] (-r')^{n+1-m} v_{m,j} , \quad n = 0,1,2,...$$ (5.8)

where

$$v_{0,j} = s_j$$ (5.9)

$$v_{1,j} = \frac{1}{2} \left\{ |\mathbf{b}_{j+2}| (\hat{t}_j \cdot \mathbf{b}_{j+2}) - |\mathbf{b}_{j+1}| (\hat{t}_j \cdot \mathbf{b}_{j+1}) + B_j^2 \ln \left| \frac{|\mathbf{b}_{j+2}| + \hat{t}_j \cdot \mathbf{b}_{j+2}}{|\mathbf{b}_{j+1}| + \hat{t}_j \cdot \mathbf{b}_{j+1}} \right| \right\}$$ (5.10)

and

$$v_{m,j} = \frac{1}{m+1} \left\{ |\mathbf{b}_{j+2}|^m (\hat{t}_j \cdot \mathbf{b}_{j+2}) - |\mathbf{b}_{j+1}|^m (\hat{t}_j \cdot \mathbf{b}_{j+1}) \right\} + \frac{m}{m+1} B_j^2 v_{m-2,j} , \quad m = 2,3,...$$ (5.11)

In the region $\hat{t}_j \cdot \mathbf{b}_{j+1} < \hat{t}_j \cdot \mathbf{b}_{j+2} < 0$, we still have the expansion (5.8) with (5.9) holding, while

$$v_{1,j} = \frac{1}{2} \left\{ |\mathbf{b}_{j+1}| |\hat{t}_j \cdot \mathbf{b}_{j+1}| - |\mathbf{b}_{j+2}| |\hat{t}_j \cdot \mathbf{b}_{j+2}| + B_j^2 \ln \left| \frac{|\mathbf{b}_{j+1}| + |\hat{t}_j \cdot \mathbf{b}_{j+1}|}{|\mathbf{b}_{j+2}| + |\hat{t}_j \cdot \mathbf{b}_{j+2}|} \right| \right\}$$ (5.12)

and

$$v_{m,j} = \frac{1}{m+1} \left\{ |\mathbf{b}_{j+1}|^m |\hat{t}_j \cdot \mathbf{b}_{j+1}| - |\mathbf{b}_{j+2}|^m |\hat{t}_j \cdot \mathbf{b}_{j+2}| \right\} + \frac{m}{m+1} B_j^2 v_{m-2,j} , \quad m = 2,3,...$$ (5.13)

In the region $\hat{t}_j \cdot \mathbf{b}_{j+1} \le 0$, $\hat{t}_j \cdot \mathbf{b}_{j+2} \ge 0$, we still have (5.8) and (5.9), while

$$v_{1,j} = \frac{1}{2} \left\{ |\mathbf{b}_{j+1}| |\hat{t}_j \cdot \mathbf{b}_{j+1}| + |\mathbf{b}_{j+2}| (\hat{t}_j \cdot \mathbf{b}_{j+2}) + B_j^2 \ln \left| \frac{(|\mathbf{b}_{j+1}| + |\hat{t}_j \cdot \mathbf{b}_{j+1}|)(|\mathbf{b}_{j+2}| + \hat{t}_j \cdot \mathbf{b}_{j+2})}{B_j^2} \right| \right\}$$ (5.14)

and

$$v_{m,j} = \frac{1}{m+1} \left\{ |\mathbf{b}_{j+1}|^m |\hat{t}_j \cdot \mathbf{b}_{j+1}| + |\mathbf{b}_{j+2}|^m (\hat{t}_j \cdot \mathbf{b}_{j+2}) \right\} + \frac{m}{m+1} B_j^2 v_{m-2,j} , \quad m = 2,3,...$$ (5.15)

This concludes the evaluation of (5.7). The iteration formulas (5.11), (5.13), and (5.15) do not converge everywhere. In Appendix B of reference 1, we show that, for the iteration to be stable, we need $0 \le B_j < 1$.

5.2. RESULTS OF $K_{0,j}$

In the first region, we have from (2.57) in reference 1 that

$$
K_{0,j} = \ln\left(\frac{|\mathbf{b}_{j+2}| + |\hat{t}_j \cdot \mathbf{b}_{j+2}|}{|\mathbf{b}_{j+1}| + |\hat{t}_j \cdot \mathbf{b}_{j+1}|}\right) + \frac{|h|}{A_j}\left\{\tan^{-1}\left[\frac{|h|\left(|h| + |\mathbf{b}_{j+2}|\right) + A_j^2}{A_j |\hat{t}_j \cdot \mathbf{b}_{j+2}|}\right]\right.
$$

$$
\left. - \tan^{-1}\left[\frac{|h|\left(|h| + |\mathbf{b}_{j+1}|\right) + A_j^2}{A_j |\hat{t}_j \cdot \mathbf{b}_{j+1}|}\right]\right\}, \quad \hat{t}_j \cdot \mathbf{b}_{j+2} > \hat{t}_j \cdot \mathbf{b}_{j+1} > 0. \tag{5.16}
$$

If

$$
A_j < \sqrt{3 \cdot 10^{-M}}\, \frac{|h|\left(|h| + |\mathbf{b}_{j+2}|\right)}{|\hat{t}_j \cdot \mathbf{b}_{j+2}|} \tag{5.17}
$$

with *M* the number of significant digits desired, then we replace (5.16) by

$$
K_{0,j} = \ln\left(\frac{|\mathbf{b}_{j+2}| + |\hat{t}_j \cdot \mathbf{b}_{j+2}|}{|\mathbf{b}_{j+1}| + |\hat{t}_j \cdot \mathbf{b}_{j+1}|}\right) - |h|\left\{\frac{|\hat{t}_j \cdot \mathbf{b}_{j+2}|}{|h|\left(|h| + |\mathbf{b}_{j+2}|\right) + A_j^2} - \frac{|\hat{t}_j \cdot \mathbf{b}_{j+1}|}{|h|\left(|h| + |\mathbf{b}_{j+1}|\right) + A_j^2}\right\}
$$

$$
\hat{t}_j \cdot \mathbf{b}_{j+2} > \hat{t}_j \cdot \mathbf{b}_{j+1} > 0 \tag{5.18}
$$

while, if $h = 0$,

$$
K_{0,j} = \ln\left(\frac{|\mathbf{b}_{j+2}| + |\hat{t}_j \cdot \mathbf{b}_{j+2}|}{|\mathbf{b}_{j+1}| + |\hat{t}_j \cdot \mathbf{b}_{j+1}|}\right), \quad h = 0, \quad \hat{t}_j \cdot \mathbf{b}_{j+2} > \hat{t}_j \cdot \mathbf{b}_{j+1} > 0. \tag{5.19}
$$

Similarly,

$$
K_{0,j} = -\ln\left(\frac{|\mathbf{b}_{j+2}| + |\hat{t}_j \cdot \mathbf{b}_{j+2}|}{|\mathbf{b}_{j+1}| + |\hat{t}_j \cdot \mathbf{b}_{j+1}|}\right) - \frac{|h|}{A_j}\left\{\tan^{-1}\left[\frac{|h|\left(|h| + |\mathbf{b}_{j+2}|\right) + A_j^2}{A_j |\hat{t}_j \cdot \mathbf{b}_{j+2}|}\right]\right.
$$

$$
\left. - \tan^{-1}\left[\frac{|h|\left(|h| + |\mathbf{b}_{j+1}|\right) + A_j^2}{A_j |\hat{t}_j \cdot \mathbf{b}_{j+1}|}\right]\right\}, \quad \hat{t}_j \cdot \mathbf{b}_{j+1} < \hat{t}_j \cdot \mathbf{b}_{j+2} < 0 \tag{5.20}
$$

and, if

$$A_j < \sqrt{3 \cdot 10^{-M}} \, \frac{\left|h\right|\left(\left|h\right| + \left|\mathbf{b}_{j+1}\right|\right)}{\left|\hat{t}_j \cdot \mathbf{b}_{j+1}\right|}$$

(5.21)

then

$$K_{0,j} = -\ln\left(\frac{\left|\mathbf{b}_{j+2}\right| + \left|\hat{t}_j \cdot \mathbf{b}_{j+2}\right|}{\left|\mathbf{b}_{j+1}\right| + \left|\hat{t}_j \cdot \mathbf{b}_{j+1}\right|}\right) + \left|h\right|\left\{\frac{\left|\hat{t}_j \cdot \mathbf{b}_{j+2}\right|}{\left|h\right|\left(\left|h\right| + \left|\mathbf{b}_{j+2}\right|\right) + A_j^{\,2}} - \frac{\left|\hat{t}_j \cdot \mathbf{b}_{j+1}\right|}{\left|h\right|\left(\left|h\right| + \left|\mathbf{b}_{j+1}\right|\right) + A_j^{\,2}}\right\}$$

(5.22)

while, if $h = 0$,

$$K_{0,j} = -\ln\left(\frac{\left|\mathbf{b}_{j+2}\right| + \left|\hat{t}_j \cdot \mathbf{b}_{j+2}\right|}{\left|\mathbf{b}_{j+1}\right| + \left|\hat{t}_j \cdot \mathbf{b}_{j+1}\right|}\right), \quad h = 0, \quad \hat{t}_j \cdot \mathbf{b}_{j+1} < \hat{t}_j \cdot \mathbf{b}_{j+2} < 0.$$

(5.23)

Finally,

$$K_{0,j} = \ln\left[\frac{\left(\left|\mathbf{b}_{j+1}\right| + \left|\hat{t}_j \cdot \mathbf{b}_{j+1}\right|\right)\left(\left|\mathbf{b}_{j+2}\right| + \left|\hat{t}_j \cdot \mathbf{b}_{j+2}\right|\right)}{B_j^{\,2}}\right] - \frac{\left|h\right|}{A_j}\tan^{-1}\left[\frac{\left|\hat{t}_j \cdot \mathbf{b}_{j+1}\right|A_j}{A_j^{\,2} + \left|h\right|\left(\left|\mathbf{b}_{j+1}\right| + \left|h\right|\right)}\right]$$
$$- \frac{\left|h\right|}{A_j}\tan^{-1}\left[\frac{\left|\hat{t}_j \cdot \mathbf{b}_{j+2}\right|A_j}{A_j^{\,2} + \left|h\right|\left(\left|\mathbf{b}_{j+2}\right| + \left|h\right|\right)}\right], \quad \hat{t}_j \cdot \mathbf{b}_{j+1} \le 0, \quad \hat{t}_j \cdot \mathbf{b}_{j+2} \ge 0$$

(5.24)

and, if

$$\frac{\left|\hat{t}_j \cdot \mathbf{b}_{j+1}\right|A_j}{A_j^{\,2} + \left|h\right|\left(\left|\mathbf{b}_{j+1}\right| + \left|h\right|\right)} < 10^{-8}$$

(5.25)

we replace (5.24) by

$$K_{0,j} = \ln\left[\frac{\left(\left|\mathbf{b}_{j+1}\right| + \left|\hat{t}_j \cdot \mathbf{b}_{j+1}\right|\right)\left(\left|\mathbf{b}_{j+2}\right| + \left|\hat{t}_j \cdot \mathbf{b}_{j+2}\right|\right)}{B_j^{\,2}}\right] - \frac{\left|\hat{t}_j \cdot \mathbf{b}_{j+1}\right|\left|h\right|}{A_j^{\,2} + \left|h\right|\left(\left|\mathbf{b}_{j+1}\right| + \left|h\right|\right)}$$
$$- \frac{\left|h\right|}{A_j}\tan^{-1}\left[\frac{\left|\hat{t}_j \cdot \mathbf{b}_{j+2}\right|A_j}{A_j^{\,2} + \left|h\right|\left(\left|\mathbf{b}_{j+2}\right| + \left|h\right|\right)}\right], \quad \hat{t}_j \cdot \mathbf{b}_{j+1} \le 0, \quad \hat{t}_j \cdot \mathbf{b}_{j+2} \ge 0$$

(5.26)

while, if

$$\frac{\left|\hat{t}_j \cdot \mathbf{b}_{j+2}\right| A_j}{A_j^2 + |h|\left(\left|\mathbf{b}_{j+2}\right| + |h|\right)} < 10^{-8} \tag{5.27}$$

then we replace (5.24) by

$$K_{0,j} = \ln\left[\frac{\left(\left|\mathbf{b}_{j+1}\right| + \left|\hat{t}_j \cdot \mathbf{b}_{j+1}\right|\right)\left(\left|\mathbf{b}_{j+2}\right| + \left|\hat{t}_j \cdot \mathbf{b}_{j+2}\right|\right)}{B_j^2}\right] - \frac{|h|}{A_j}\tan^{-1}\left[\frac{\left|\hat{t}_j \cdot \mathbf{b}_{j+1}\right| A_j}{A_j^2 + |h|\left(\left|\mathbf{b}_{j+1}\right| + |h|\right)}\right]$$
$$- \frac{\left|\hat{t}_j \cdot \mathbf{b}_{j+2}\right| |h|}{A_j^2 + |h|\left(\left|\mathbf{b}_{j+2}\right| + |h|\right)}, \quad \hat{t}_j \cdot \mathbf{b}_{j+1} \le 0, \quad \hat{t}_j \cdot \mathbf{b}_{j+2} \ge 0. \tag{5.28}$$

If both (5.25) and (5.27) obtain, then we replace (5.24) by

$$K_{0,j} = \ln\left[\frac{\left(\left|\mathbf{b}_{j+1}\right| + \left|\hat{t}_j \cdot \mathbf{b}_{j+1}\right|\right)\left(\left|\mathbf{b}_{j+2}\right| + \left|\hat{t}_j \cdot \mathbf{b}_{j+2}\right|\right)}{B_j^2}\right] - \frac{\left|\hat{t}_j \cdot \mathbf{b}_{j+1}\right| |h|}{A_j^2 + |h|\left(\left|\mathbf{b}_{j+1}\right| + |h|\right)}$$
$$- \frac{\left|\hat{t}_j \cdot \mathbf{b}_{j+2}\right| |h|}{A_j^2 + |h|\left(\left|\mathbf{b}_{j+2}\right| + |h|\right)}, \quad \hat{t}_j \cdot \mathbf{b}_{j+1} \le 0, \quad \hat{t}_j \cdot \mathbf{b}_{j+2} \ge 0. \tag{5.29}$$

If $h = 0$, then $A_j \ne 0$ and

$$K_{0,j} = \ln\left[\frac{\left(\left|\mathbf{b}_{j+1}\right| + \left|\hat{t}_j \cdot \mathbf{b}_{j+1}\right|\right)\left(\left|\mathbf{b}_{j+2}\right| + \left|\hat{t}_j \cdot \mathbf{b}_{j+2}\right|\right)}{B_j^2}\right], \quad h = 0, \quad \hat{t}_j \cdot \mathbf{b}_{j+1} \le 0, \quad \hat{t}_j \cdot \mathbf{b}_{j+2} \ge 0. \tag{5.30}$$

The rest of the $K_{n,j}$ can be computed from the iteration formulas (5.5) and (5.6). In Appendix B of reference 1, we show that the iteration formula does not converge for all positions of the observation point. We discuss this issue in the concluding section.

SECTION 6: VALIDATION

In this section, we provide validation for our numerical approach to evaluating the surface and line integrals in (1.16). We begin with the surface integral, given by (2.1)

$$F(\mathbf{r}') = -\frac{1}{4\pi} \int_T \frac{\partial}{\partial z} \left(\frac{e^{-ikR}}{R} \right) dS .$$ (6.1)

We use the Khayat and Wilton test triangle (reference 13), shown in Figure 6.1, and a 10-m wavelength. We choose the 35 OPs displayed in Tables 6.1 – 6.11. All distances are in meters and all calculations are performed in double precision (DP). The number of terms in the expansion of sine and cosine is 8 each, providing 15 SDs of accuracy. The reason for having eight terms rather than seven (as suggested in Table 3.1) is that the hypotenuse of the triangle is longer than a tenth of a wavelength. Of the 35 OPs, 3 are off the triangle's plane. Of the rest, 16 are inside the triangle and 16 outside. From Sections 2 and 4, the result for the surface integral for a point on the plane of the triangle and inside the triangle should be (-0.5 + i0); for a point outside the triangle, it should be (0 + i0). For all the exterior points, we obtained the correct result to 15 SDs, as shown in Table 6.12.

For the interior points, shown in Table 6.13, the results are mixed. For the real part, we get agreement to 15 SDs for 9 out of the 16 outcomes; for the rest, we get agreement to 14 SDs. We attribute this to round-off error rather than failure of the algorithm. For the imaginary part, the agreement is not as good. Although we get numbers of the order of 10 to the negative 17 or 18, these numbers are not close enough to zero, the correct answer. This is because the final stage of the calculation involves the subtraction of two almost identical numbers. For this case, we developed a special formula that is valid when z' is appropriately close to the triangle's surface. It is given by (2.10) and we repeat it here

$$\text{Im}\{F(\mathbf{r}')\} = z' \sum_{n=0}^{N-2} \frac{(-1)^n (n+1)(2\pi)^{2n+2}}{(2n+3)!} \int_T \rho^{2n} dS .$$ (6.2)

We present the derivation of this formula in Appendix B. The integral in (6.2) can be evaluated either analytically or by the GKQ (as implemented in Matlab (reference 7)) when converted to a line integral (see Appendix B) or by cubatures. We provide a typical example of the use of (6.2) in Figure 6.2. We note that (6.2) takes over when the distance from the triangle is less than about 10 to the -8. That two triangles will be so near each other is unlikely to happen in practice. It is prudent, however, to know the limitations of an algorithm and to provide alternatives.
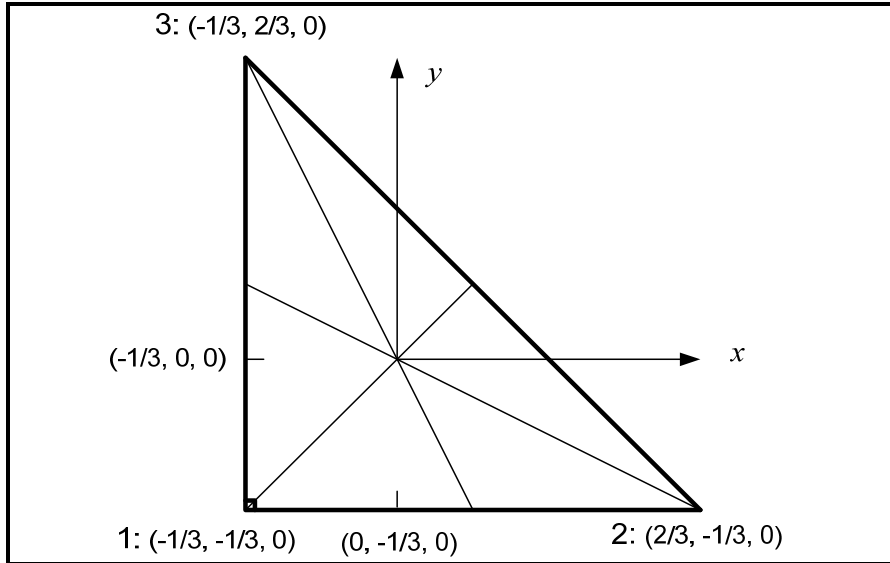
Figure 6.1: Test Triangle

Table 6.1: Points on the $z = 0$ plane and inside the triangle. They lie on the line $y = x$.

Title	Centroid Coordinates
Case 1	(-7/30, -7/30, 0)
Case 2	(-2/15, -2/15, 0)
Case 3	(-1/30, -1/30, 0)
Case 4	(1/15, 1/15, 0)

Table 6.2: Points on the $z = 0$ plane and outside the triangle. They lie on the line $y = x$.

Title	Centroid Coordinates
Case 5	(4/15, 4/15, 0)
Case 6	(11/30, 11/30, 0)
Case 7	(7/15, 7/15, 0)
Case 8	(17/30, 17/30, 0)

Table 6.3: Points above the triangle.

Title	Centroid Coordinates
Case 9	(-7/30, -7/30, 0.1)
Case 10	(-7/30, -7/30, 0.01)
Case 11	(-7/30, -7/30, 0.001)

Table 6.4: Points on the $z = 0$ plane, inside the triangle and along the median of the upper left angle: $(-1/3+10^{-N}/2, 2/3-10^{-N}, 0)$, $N = 1, 2, 3$.

Title	Centroid Coordinates
Case 12	(-1/3+0.1/2, 2/3-0.1, 0)
Case 13	(-1/3+0.01/2, 2/3-0.01, 0)
Case 14	(-1/3+0.001/2, 2/3-0.001, 0)

Table 6.5: Points on the $z = 0$ plane, outside the triangle and along the median of the upper left angle: $(-1/3-10^{-N}/2, 2/3+10^{-N}, 0)$, $N = 1, 2, 3$.

Title	Centroid Coordinates
Case 15	(-1/3-0.1/2, 2/3+0.1, 0)
Case 16	(-1/3-0.01/2, 2/3+0.01, 0)
Case 17	(-1/3-0.001/2, 2/3+0.001, 0)

Table 6.6: Points on the $z = 0$ plane, inside the triangle and along the bisector of the upper left angle: $\left(-\dfrac{1}{3}+10^{-N}, \dfrac{2}{3}-\dfrac{10^{-N}}{\sqrt{2}-1}, 0\right)$, $N = 1, 2, 3$

Title	Centroid Coordinates
Case 18	$\left(-\dfrac{1}{3}+0.1, \dfrac{2}{3}-\dfrac{0.1}{\sqrt{2}-1}, 0\right)$
Case 19	$\left(-\dfrac{1}{3}+0.01, \dfrac{2}{3}-\dfrac{0.01}{\sqrt{2}-1}, 0\right)$
Case 20	$\left(-\dfrac{1}{3}+0.001, \dfrac{2}{3}-\dfrac{0.001}{\sqrt{2}-1}, 0\right)$

Table 6.7: Points on the $z = 0$ plane, outside the triangle and along the bisector of the upper left angle: $\left(-\dfrac{1}{3} - 10^{-N}, \ \dfrac{2}{3} + \dfrac{10^{-N}}{\sqrt{2}-1}, 0 \right)$, $\quad N = 1, 2, 3$

v	Centroid Coordinates
Case 21	$\left(-\dfrac{1}{3} - 0.1, \ \dfrac{2}{3} + \dfrac{0.1}{\sqrt{2}-1}, 0 \right)$
Case 22	$\left(-\dfrac{1}{3} - 0.01, \ \dfrac{2}{3} + \dfrac{0.01}{\sqrt{2}-1}, 0 \right)$
Case 23	$\left(-\dfrac{1}{3} - 0.001, \ \dfrac{2}{3} + \dfrac{0.001}{\sqrt{2}-1}, 0 \right)$

Table 6.8: Points on the $z = 0$ plane, inside the triangle and along the median of the lower right angle: $(2/3 - 10^{-N}, -1/3 + 10^{-N}/2, 0)$, $\quad N = 1, 2, 3$.

Title	Centroid Coordinates
Case 24	(2/3-0.1, -1/3+0.1/2, 0)
Case 25	(2/3-0.01, -1/3+0.01/2, 0)
Case 26	(2/3-0.001, -1/3+0.001/2, 0)

Table 6.9: Points on the $z = 0$ plane, outside the triangle and along the median of the lower right angle: $(2/3 + 10^{-N}, -1/3 - 10^{-N}/2, 0)$, $N = 1, 2, 3$.

Title	Centroid Coordinates
Case 27	(2/3+0.1, -1/3-0.1/2, 0)
Case 28	(2/3+0.01, -1/3-0.01/2, 0)
Case 29	(2/3+0.001, -1/3-0.001/2, 0)

Table 6.10: Points on the $z = 0$ plane, inside the triangle and along the bisector of the lower right angle: $\left(\dfrac{2}{3} - \dfrac{10^{-N}}{\sqrt{2}-1}, -\dfrac{1}{3} + 10^{-N}, 0 \right)$, $N = 1, 2, 3$.

Title	Centroid Coordinates
Case 30	$\left(\dfrac{2}{3} - \dfrac{0.1}{\sqrt{2}-1}, -\dfrac{1}{3} + 0.1, 0 \right)$
Case 31	$\left(\dfrac{2}{3} - \dfrac{0.01}{\sqrt{2}-1}, -\dfrac{1}{3} + 0.01, 0 \right)$
Case 32	$\left(\dfrac{2}{3} - \dfrac{0.001}{\sqrt{2}-1}, -\dfrac{1}{3} + 0.001, 0 \right)$

Table 6.11: Points on the $z = 0$ plane, outside the triangle and along the bisector of the lower right angle: $\left(\dfrac{2}{3} + \dfrac{10^{-N}}{\sqrt{2}-1}, -\dfrac{1}{3} - 10^{-N}, 0 \right)$, $N = 1, 2, 3$.

Title	Centroid Coordinates
Case 33	$\left(\dfrac{2}{3} + \dfrac{0.1}{\sqrt{2}-1}, -\dfrac{1}{3} - 0.1, 0 \right)$
Case 34	$\left(\dfrac{2}{3} + \dfrac{0.01}{\sqrt{2}-1}, -\dfrac{1}{3} - 0.01, 0 \right)$
Case 35	$\left(\dfrac{2}{3} + \dfrac{0.001}{\sqrt{2}-1}, -\dfrac{1}{3} - 0.001, 0 \right)$

Table 6.12: Results for the surface integral (6.1) for points on the triangle's plane but outside the triangle. Algorithms yield exact answer.

		RE{INTG_2}	IM{INTG_2}
Case 5		0.000000000000000E+00	0.000000000000000E+00
Case 6		0.000000000000000E+00	0.000000000000000E+00
Case 7		0.000000000000000E+00	0.000000000000000E+00
Case 8		0.000000000000000E+00	0.000000000000000E+00
Case 15		0.000000000000000E+00	0.000000000000000E+00
Case 16		0.000000000000000E+00	0.000000000000000E+00
Case 17		0.000000000000000E+00	0.000000000000000E+00
Case 21		0.000000000000000E+00	0.000000000000000E+00
Case 22		0.000000000000000E+00	0.000000000000000E+00
Case 23		0.000000000000000E+00	0.000000000000000E+00
Case 27		0.000000000000000E+00	0.000000000000000E+00
Case 28		0.000000000000000E+00	0.000000000000000E+00
Case 29		0.000000000000000E+00	0.000000000000000E+00
Case 33		0.000000000000000E+00	0.000000000000000E+00
Case 34		0.000000000000000E+00	0.000000000000000E+00
Case 35		0.000000000000000E+00	0.000000000000000E+00

Table 6.13: Results for the surface integral (6.1) for points on the triangle's plane and inside the triangle.

		RE{INTG_2}	IM{INTG_2}
Case 1		-5.00000000000000E-01	2.71592644207618E-17
Case 2		-4.99999999999999E-01	-1.12418212759590E-17
Case 3		-5.00000000000000E-01	-1.07573184301296E-18
Case 4		-5.00000000000000E-01	-5.62091063797953E-18
Case 12		-4.99999999999999E-01	-2.31341638554094E-17
Case 13		-4.99999999999999E-01	-1.01101852584273E-17
Case 14		-5.00000000000000E-01	-1.09368894149475E-17
Case 18		-5.00000000000000E-01	-2.60750622482763E-17
Case 19		-5.00000000000000E-01	-6.23551774450725E-17
Case 20		-4.99999999999999E-01	-7.38206154191067E-17
Case 24		-4.99999999999999E-01	-2.31341638554094E-17
Case 25		-4.99999999999999E-01	-1.01101852584273E-17
Case 26		-5.00000000000000E-01	-1.09368894149475E-17
Case 30		-5.00000000000000E-01	-2.60750622482763E-17
Case 31		-5.00000000000000E-01	-6.23551774450725E-17
Case 32		-4.99999999999999E-01	-7.38206154191067E-17

Comparison of imaginary part of surface integral for old (in black) and new (in blue) algorithm

Distance from triangle (λ)

| 1.E-26 | 1.E-23 | 1.E-20 | 1.E-17 | 1.E-14 | 1.E-11 | 1.E-08 | 1.E-05 | 1.E-02 |

$$x' = y' = -\,7/30 \text{ m}$$

Imaginary part of surface integral

1.E-01
1.E-04
1.E-07
1.E-10
1.E-13
1.E-16
1.E-19
1.E-22
1.E-25
1.E-28
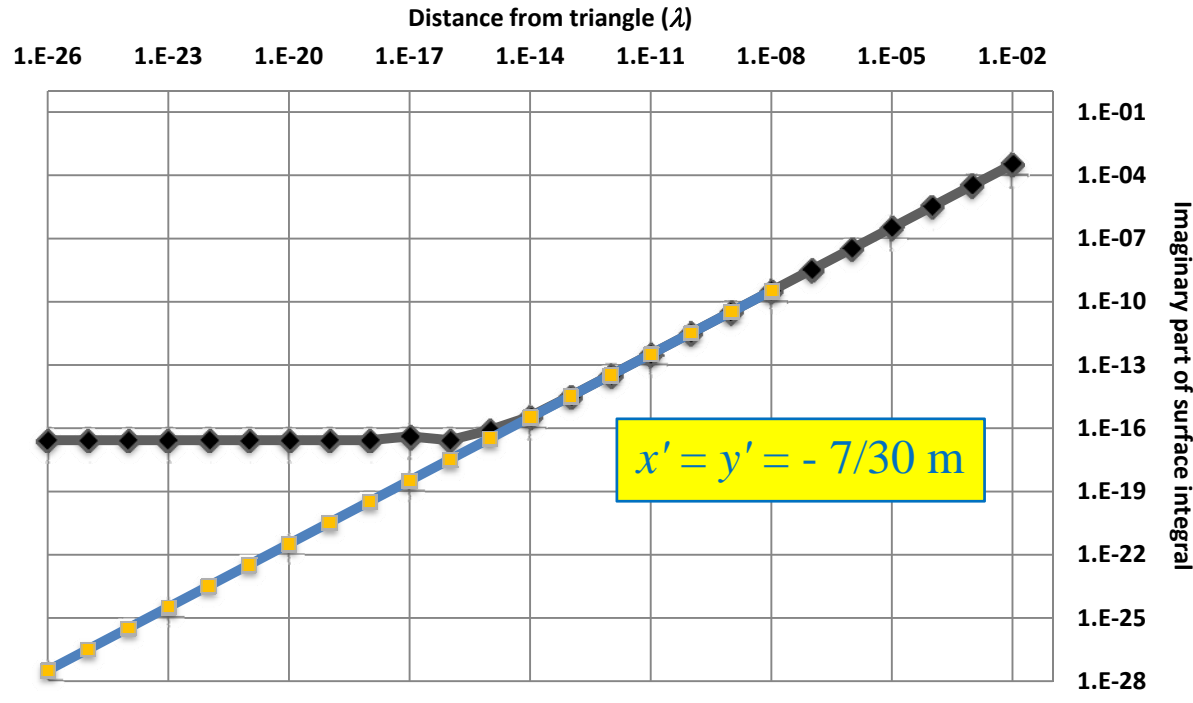
Figure 6.2: Comparison of imaginary part of surface integral from old (6.1) and new (6.2) algorithm. Distance is measured in wavelengths.

We proceed next to a closer examination of the surface integral. Since its calculation depends on an iteration formula that has as a starting point at the solid-angle integral, we test the sensitivity of the initial term. To this end, we use (4.2) with each of expressions (4.3) and (4.4). We refer to them as Formula 1 and Formula 2. Clearly, Formula 1 is more economical than Formula 2. We used this formula to compute (6.1) above; thus, it is well behaved for OPs in the triangle's plane, both inside and outside the triangle. We proceed to check this formula for OPs near one of the triangle's sides. We include here Formula 2 as a check on Formula 1. We test these formulas using the points of Table 6.14. These points lie on the triangle's plane and are approached through values of z' that are also given in Table 6.14. The first point (Case 36) is the same as for Case 1. The next two are the vertices of the base of the triangle. Case 39 is the middle point of the hypotenuse while Case 40 is a point along the bisector of the right angle, and just outside the triangle. As a reminder, the OP is not allowed to lie on the sides or vertices of the IT; thus, for z' equal to zero, cases 36-38 are here to test the solid-angle formulas since we know the outcome at these points when z' is equal to zero. The question of how close the OP can be to a side is one that depends on wavelength. We do not anticipate situations where the distance will be less than a millionth of a wavelength (1 $\mu\lambda$) and we set this number as the lower limit. For the 10-m wavelength we are using, this distance is 10 μm.

Table 6.14: Points in triangle's plane for testing Formulas 1 and 2.
The values of z' are 5, 1, 10^{-2}, 10^{-4}, 10^{-6}, and 0.

Title	Centroid Coordinates
Case 36	(-7/30, -7/30)
Case 37	(-1/3, -1/3)
Case 38	(2/3, -1/3)
Case 39	(1/6, 1/6)
Case 40	(1/5, 1/5)

We perform the calculations for the points in Table 6.14 in single and double precision and exhibit the results in Table 6.15. We discuss each case separately. In Case 36, the OP approaches a point in the interior of the triangle. All DP results but the first agree to 15 SDs. The first pair agrees to 14 SDs. The single precision (SP) results for Formula 1 are better than those of Formula 2. All four results are exact when z' is zero.

In Case 37, the OP approaches the 90-deg corner of the triangle. The correct result at the corner point is 0.25. None of formulas gives this result. In fact, Formula 1 sees the corner point as being outside the triangle while Formula 2 sees it inside the triangle. This may explain the diverging results in DP as that point is approached. We also see that Formula 1 is much better behaved in SP than Formula 2.

In Case 38, the OP approaches the lower-right corner of the triangle. The correct answer at the corner point is 0.125. Both formulas see this point as being outside the triangle and give the wrong result (zero). For the rest of the OPs, there is perfect agreement between the two formulas in DP except when z' is equal to 5 m, in which case the agreement is to 14 SDs. The SP results are good except for one occasion for Formula 2.

In Case 39, the OP approaches the midpoint of the hypotenuse. At that point, the correct answer is 0.5. Clearly, in DP both formulas see this point outside the triangle. In SP, Formula 1 sees it inside while Formula 2 sees it outside. The SP results are not very good in general, while the DP results provide from 10 to 15 SDs.

In Case 40, the OP approaches a point in the triangle's plane but slightly outside the triangle. Both formulas give the exact result when z' becomes zero. In DP, there is agreement to at least 14 SDs. In SP, they mostly provide correct answers to six SDs.

The conclusion we can draw from these runs is that DP should be used when possible and that Formula 1 performs respectably provide the OP is not very close over a side of the triangle. In Appendix D, we present a more detailed comparison when z' is zero or very close to it.

Table 6.15: Results for Formulas 1 and 2 for the OPs in Table 6.14 in SP and DP.
Numbers in DP occupy two rows. Numbers in grey background differ from
one another. Numbers in SP in red do not provide 7 SD according to the DP results.

Case 36	z'	5.00E+00	1.00E+00	1.00E-02	1.00E-04	1.00E-06	0.00E+00
SP	Formula 1	3.141805E-03	6.106466E-02	9.416611E-01	9.994146E-01	9.999941E-01	1.000000E+00
	Formula 2	3.141849E-03	6.106465E-02	9.416611E-01	9.994146E-01	9.999941E-01	1.000000E+00
DP	Formula 1	3.1418053817 4860E-03	6.106466233674 18E-02	9.416610540466 21E-01	9.994146187948 04E-01	9.999941461859 44E-01	1.000000000000 00E+00
	Formula 2	3.1418053817 4867E-03	6.106466233674 18E-02	9.416610540466 21E-01	9.994146187948 04E-01	9.999941461859 44E-01	1.000000000000 00E+00

Case 37	z'	5.00E+00	1.00E+00	1.00E-02	1.00E-04	1.00E-06	0.00E+00
SP	Formula 1	3.120885E-03	5.408673E-02	2.468172E-01	2.499682E-01	2.499997E-01	0.000000E+00
	Formula 2	3.120894E-03	5.408673E-02	2.468187E-01	2.499841E-01	2.499998E-01	1.000000E+00
DP	Formula 1	3.1208851602 7894E-03	5.408672398469 63E-02	2.468171663621 87E-01	2.499681690116 46E-01	2.499996816901 13E-01	0.000000000000 00E+00
	Formula 2	3.1208851602 7894E-03	5.408672398469 63E-02	2.468171663621 92E-01	2.499681690116 24E-01	2.499996816759 64E-01	1.000000000000 00E+00

Case 38	z'	5.00E+00	1.00E+00	1.00E-02	1.00E-04	1.00E-06	0.00E+00
SP	Formula 1	3.061427E-03	4.166667E-02	1.238747E-01	1.249887E-01	1.249999E-01	0.000000E+00
	Formula 2	3.061440E-03	4.166667E-02	1.238747E-01	1.249887E-01	1.249999E-01	0.000000E+00
DP	Formula 1	3.0614270888 5004E-03	4.166666666666 66E-02	1.238746514932 54E-01	1.249887460460 94E-01	1.249998874604 60E-01	0.000000000000 00E+00
	Formula 2	3.0614270888 5008E-03	4.166666666666 66E-02	1.238746514932 54E-01	1.249887460460 94E-01	1.249998874604 60E-01	0.000000000000 00E+00

Case 39	z'	5.00E+00	1.00E+00	1.00E-02	1.00E-04	1.00E-06	0.00E+00
SP	Formula 1	3.151634E-03	6.409422E-02	4.909984E-01	5.000723E-01	5.094833E-01	1.000000E+00
	Formula 2	3.151670E-03	6.409420E-02	4.909987E-01	4.999069E-01	4.999820E-01	0.000000E+00
DP	Formula 1	3.1516345252 0085E-03	6.409421684897 49E-02	4.909983369786 01E-01	4.999099683697 99E-01	4.999990997276 50E-01	0.000000000000 00E+00
	Formula 2	3.1516345252 0092E-03	6.409421684897 49E-02	4.909983369786 00E-01	4.999099683698 99E-01	4.999990996872 48E-01	0.000000000000 00E+00

Case 40	z'	5.00E+00	1.00E+00	1.00E-02	1.00E-04	1.00E-06	0.00E+00
SP	Formula 1	3.147065E-03	6.223706E-02	5.823865E-02	5.922366E-04	5.922377E-06	0.000000E+00
	Formula 2	3.147028E-03	6.223706E-02	5.823865E-02	5.922369E-04	5.922379E-06	0.000000E+00
DP	Formula 1	3.1470641589 7432E-03	6.223706005980 60E-02	5.823863498580 16E-02	5.922367555002 76E-04	5.922377670355 95E-06	0.000000000000 00E+00
	Formula 2	3.1470641589 7428E-03	6.223706005980 60E-02	5.823863498580 16E-02	5.922367555002 75E-04	5.922377670355 95E-06	0.000000000000 00E+00

Now that we chose Formula 1 (Equations (4.2) and (4.3)) as the starting term in the iteration scheme of Section 4, we proceed to compute (6.1), the surface integral of interest, for the points of Table 6.14 except for z' equal to zero. The reason for excluding this point is that we have tested interior and exterior points in the triangle's plane above and that points on the triangle's boundary are not allowed. In its place, we display the value 4.5. In Table 6.16, we display the convergence of our algorithm for Case 36. The tables for the rest of the cases are presented in Appendix E so as not to clutter the main body of the report.

We note that on 1 occasion in this table (and 1 each in Tables E.2 and E.3, a total of 3 occasions out of 60) our formula fails to predict the number of terms in the expansions of Section 4 correctly. In these 3 instances, and for the real part of the integral, 9 terms are required; still, the predicted 8 terms yield 14 SD. We hesitate to change our formula since, as can be seen from the tables, it is a rather conservative one.

Table 6.16: Convergence of our algorithm for the surface integral for the OP of Case 36, Table 6.14. Convergence is to 15 SD and as a function of the number of terms in the trigonometric sums in (2.2). The entries in light green are the first one for which our formula has stabilized to 15 SD.

z' =	5.000		4.500	
	REAL{F(r')}	IMAG{F(r')}	REAL{F(r')}	IMAG{F(r')}
15 SD, Nc=Ns=4	1.63858509704585E-03	4.93439511546236E-03	2.28919850402077E-04	5.82159533394148E-03
15 SD, Nc=Ns=5	1.63858509704592E-03	4.93439511546241E-03	2.28919850402091E-04	5.82159533394151E-03
15 SD, Nc=Ns=6	1.63858509704589E-03	4.93439511546239E-03	2.28919850402082E-04	5.82159533394150E-03
15 SD, Nc=Ns=7	1.63858509704590E-03	4.93439511546240E-03	2.28919850402084E-04	5.82159533394150E-03
15 SD, Nc=Ns=8	1.63858509704589E-03	4.93439511546239E-03	2.28919850402084E-04	5.82159533394150E-03
15 SD, Nc=Ns=9	1.63858509704590E-03	4.93439511546239E-03	2.28919850402084E-04	5.82159533394150E-03
15 SD, Nc=Ns=10	1.63858509704590E-03	4.93439511546239E-03	2.28919850402084E-04	5.82159533394150E-03
15 SD, Nc=Ns=11	1.63858509704590E-03	4.93439511546239E-03	2.28919850402084E-04	5.82159533394150E-03
15 SD, Nc=Ns=12	1.63858509704590E-03	4.93439511546239E-03	2.28919850402084E-04	5.82159533394150E-03
z' =	1.000		0.010	
	REAL{F(r')}	IMAG{F(r')}	REAL{F(r')}	IMAG{F(r')}
15 SD, Nc=Ns=4	-3.68605050811883E-02	3.13416887059356E-03	-4.71122428585698E-01	3.26142239362246E-05
15 SD, Nc=Ns=5	-3.68605050809884E-02	3.13416887043198E-03	-4.71122428617225E-01	3.26142297742437E-05
15 SD, Nc=Ns=6	-3.68605050809884E-02	3.13416887043203E-03	-4.71122428617212E-01	3.26142297717191E-05
15 SD, Nc=Ns=7	-3.68605050809884E-02	3.13416887043203E-03	-4.71122428617212E-01	3.26142297717191E-05
15 SD, Nc=Ns=8	-3.68605050809884E-02	3.13416887043203E-03	-4.71122428617212E-01	3.26142297717191E-05
15 SD, Nc=Ns=9	-3.68605050809884E-02	3.13416887043203E-03	-4.71122428617212E-01	3.26142297717191E-05
15 SD, Nc=Ns=10	-3.68605050809884E-02	3.13416887043203E-03	-4.71122428617212E-01	3.26142297717191E-05
15 SD, Nc=Ns=11	-3.68605050809884E-02	3.13416887043203E-03	-4.71122428617212E-01	3.26142297717191E-05
15 SD, Nc=Ns=12	-3.68605050809884E-02	3.13416887043203E-03	-4.71122428617212E-01	3.26142297717191E-05
z' =	0.0001		0.000001	
	REAL{F(r')}	IMAG{F(r')}	REAL{F(r')}	IMAG{F(r')}
15 SD, Nc=Ns=4	-4.99710323212000E-01	3.26135850866057E-07	-4.99997103199681E-01	3.25367732468421E-09
15 SD, Nc=Ns=5	-4.99710323253529E-01	3.26143592140251E-07	-4.99997103241321E-01	3.26143966793828E-09
15 SD, Nc=Ns=6	-4.99710323253509E-01	3.26143588367667E-07	-4.99997103241301E-01	3.26143589320174E-09
15 SD, Nc=Ns=7	-4.99710323253509E-01	3.26143588367667E-07	-4.99997103241301E-01	3.26143589320174E-09
15 SD, Nc=Ns=8	-4.99710323253509E-01	3.26143588367667E-07	-4.99997103241301E-01	3.26143589320174E-09
15 SD, Nc=Ns=9	-4.99710323253509E-01	3.26143588367667E-07	-4.99997103241301E-01	3.26143589320174E-09
15 SD, Nc=Ns=10	-4.99710323253509E-01	3.26143588367667E-07	-4.99997103241301E-01	3.26143589320174E-09
15 SD, Nc=Ns=11	-4.99710323253509E-01	3.26143588367667E-07	-4.99997103241301E-01	3.26143589320174E-09
15 SD, Nc=Ns=12	-4.99710323253509E-01	3.26143588367667E-07	-4.99997103241301E-01	3.26143589320174E-09

We compare next the values of the surface integral for the five points of Table 6.14. In Tables 6.17.a – 6.17.c, we display the results for Case 36. In the first row of each table we display the values of z' in meters. In the second row, we present the required number of terms in (2.2) of Section 2 to obtain 15 SD (8 terms each for the sine and the cosine). We follow that by a Riemann sum of the integral that involves 10,000 points, not a very economical method especially since it does not provide the required 15 SD. We present the cubature results after the Riemann sum, first for the real part of the integral and, next, for the imaginary part. In Appendix F, we present the methodology we used to compute the integral using cubatures. Although this procedure is not necessary when the OP is as far as half a wavelength from the IT, it is absolutely necessary when the OP is near the IT. The methodology is not new (see, for example, reference 14). The way, however, we computed the integral of the static Green's function is ours. This is a time-consuming way to compute using cubatures but it is used here for the single purpose of comparing with our method since we do not have any other data available. We see that, with a 28-point cubature, we get agreement to 14 SD for the real part of the integral. For the imaginary part, we get 15 SD with a 54-point cubature for the 5.0 case and as many SD for the 4.5 case but with a 28-point cubature. We note that we get 14 SD for either case with a 21-point cubature. The terms highlighted in green are the lowest-point cubature terms for which we get the maximum number of SD to agree with our result.

We remark that, for both cases in Table 6.17.a, we could have gotten the same number of SD by applying the cubatures directly to the integrals. This is because the OP is sufficiently far away from the IT. This is no longer true for the next four cases shown in Tables 6.18 and 6.19. Here, we have to use the methodology of Appendix F to increase the number of SD.

The three tables are summarized in Figure 6.3 where we display the maximum number of SD obtained using cubatures as a function of distance from the triangle. The remaining four cases in Table 6.14 are similar to Case 36. For completeness, the data are provided in Appendix G and the relevant graphs in Figures 6.4 to 6.7. From Table 6.14 (and the discussion following it), Case 36 involves an OP whose projection is an interior point of the triangle. In the next two cases, the OPs project to the lower corners of the triangle, while, in Case 39, to the midpoint of the hypotenuse. In Case 40, the OP projects to a point just outside the triangle. Thus, in the first four cases, the OP approaches a singular point while in the fifth it approaches a regular point that is near a singular point.

For the first four cases, we see that the imaginary part (which is computed using a cubature only) has a quasi-linear behavior and that it loses SD as the OP approaches the IT. At the same time, the order of the cubature that provides the greatest number of SD increases. In the case of the real part (involving two integrals that are evaluated analytically and one through cubature), the result is a U-shaped graph; thus, in the approach of the OP to the IT, we have a good number of SD when far away, we lose a few along the way, and we recover them as we get close to the IT. For the last case (where the OP projects to a point outside the triangle), the behavior of the real part is essentially the same as before. The imaginary part, however, quickly settles to 13 SD and does not fall below that level.

It is clear from the above discussion that we put more trust in the results of our method and much less in those provided by cubatures. The reasons for it are the following. When z' is large (greater than a tenth of a wavelength), we get 15-SD agreement between our results and those provided by cubatures. When z' is less than that, the cubature results fail to settle down as the cubature order increases. Our results derive from analytical formulas. The only way that they can be correct on one occasion and wrong on another is for them to be unstable for certain values of the parameters/arguments. As we discussed earlier, we detected such instability in the imaginary part and corrected for it. We note, however, that this instability occurs for values of z' smaller than the ones we have used. Until fresh numbers appear from another source, we will consider our expressions as providing correct answers to the requested number of SD.

Table 6.17.a: Comparison of our results for the surface integral of Case 36 with those obtained through a Riemann sum and cubatures.

z' =		5.0	4.5
15 SD, Nc=Ns=8			
MFIE METHOD	REAL{F(r')}	1.63858509704589E-03	2.28919850402084E-04
	IMAG{F(r')}	4.93439511546239E-03	5.82159533394150E-03
RIEMANN SUM	REAL{F(r')}	1.63858509715993E-03	2.28919850599920E-04
N = 10,000	IMAG{F(r')}	4.93439511516726E-03	5.82159533362721E-03
CUBATURE DIM	SD	RE{F(r')}	
21		1.63858509704539E-03	2.28919850400982E-04
28	14, 14	1.63858509704591E-03	2.28919850402085E-04
36		1.63858509704591E-03	2.28919850402083E-04
45		1.63858509704592E-03	2.28919850402088E-04
46		1.63858509704591E-03	2.28919850402085E-04
54		1.63858509704591E-03	2.28919850402080E-04
55		1.63858509704591E-03	2.28919850402085E-04
66		1.63858509704591E-03	2.28919850402083E-04
78		1.63858509704591E-03	2.28919850402088E-04
85		1.63858509704591E-03	2.28919850402088E-04
91		1.63858509704591E-03	2.28919850402090E-04
105		1.63858509704591E-03	2.28919850402083E-04
120		1.63858509704591E-03	2.28919850402087E-04
126		1.63858509704591E-03	2.28919850402087E-04
CUBATURE DIM	SD	IM{F(r')}	
21		4.93439511546240E-03	5.82159533394151E-03
28	15	4.93439511546240E-03	5.82159533394150E-03
36		4.93439511546240E-03	5.82159533394150E-03
45		4.93439511546241E-03	5.82159533394152E-03
46		4.93439511546240E-03	5.82159533394150E-03
54	15	4.93439511546239E-03	5.82159533394150E-03
55		4.93439511546240E-03	5.82159533394150E-03
66		4.93439511546239E-03	5.82159533394150E-03
78		4.93439511546240E-03	5.82159533394150E-03
85		4.93439511546240E-03	5.82159533394151E-03
91		4.93439511546240E-03	5.82159533394150E-03
105		4.93439511546239E-03	5.82159533394150E-03
120		4.93439511546240E-03	5.82159533394150E-03
126		4.93439511546240E-03	5.82159533394150E-03

Table 6.17.b: Comparison of our results for the surface integral of Case 36 with those obtained through a Riemann sum and cubatures.

z' =		1.0E+00	1.0E-02
15 SD, Nc=Ns=8			
MFIE METHOD	REAL{F(r')}	-3.68605050809884E-02	-4.71122428617212E-01
	IMAG{F(r')}	3.13416887043203E-03	3.26142297717191E-05
RIEMANN SUM	REAL{F(r')}	-3.68605050787650E-02	-4.71122428619231E-01
N = 10,000	IMAG{F(r')}	3.13416887030680E-03	3.26142297704777E-05
CUBATURE DIM	**SD**	**RE{F(r')}**	
21		-3.68605051035008E-02	-4.71122424239280E-01
28		-3.68605050827459E-02	-4.71122429698403E-01
36		-3.68605050810431E-02	-4.71122430974795E-01
45		-3.68605050809920E-02	-4.71122429253321E-01
46		-3.68605050809830E-02	-4.71122428783164E-01
54		-3.68605050809892E-02	-4.71122428079805E-01
55		-3.68605050809885E-02	-4.71122427827648E-01
66		-3.68605050809885E-02	-4.71122427958889E-01
78	15	-3.68605050809884E-02	-4.71122429539633E-01
85		-3.68605050809884E-02	-4.71122429631584E-01
91		-3.68605050809884E-02	-4.71122429294459E-01
105	10	-3.68605050809884E-02	-4.71122428577606E-01
120		-3.68605050809884E-02	-4.71122428452062E-01
126		-3.68605050809884E-02	-4.71122428824172E-01
CUBATURE DIM	**SD**	**IM{F(r')}**	
21		3.13416887043204E-03	3.26142297717566E-05
28		3.13416887043204E-03	3.26142297717564E-05
36	15	3.13416887043203E-03	3.26142297717573E-05
45	11	3.13416887043204E-03	3.26142297717561E-05
46		3.13416887043203E-03	3.26142297717565E-05
54		3.13416887043203E-03	3.26142297717563E-05
55		3.13416887043204E-03	3.26142297717566E-05
66		3.13416887043203E-03	3.26142297717565E-05
78		3.13416887043204E-03	3.26142297717561E-05
85		3.13416887043204E-03	3.26142297717577E-05
91		3.13416887043204E-03	3.26142297717573E-05
105		3.13416887043203E-03	3.26142297717570E-05
120		3.13416887043204E-03	3.26142297717566E-05
126		3.13416887043203E-03	3.26142297717564E-05

Table 6.17.c: Comparison of our results for the surface integral of Case 36 with those obtained through a Riemann sum and cubatures.

z' =		1.0E-04	1.0E-06
15 SD, Nc=Ns=8			
MFIE METHOD	REAL{F(r')}	-4.99710323253509E-01	-4.99997103241301E-01
	IMAG{F(r')}	3.26143588367667E-07	3.26143589320174E-09
RIEMANN SUM	REAL{F(r')}	-4.99710323252418E-01	-4.99997103238861E-01
N = 10,000	IMAG{F(r')}	3.26143588335231E-07	3.26143588464211E-09
CUBATURE DIM	SD	RE{F(r')}	
21		-4.99710323208003E-01	-4.99997103240846E-01
28		-4.99710323263749E-01	-4.99997103241403E-01
36		-4.99710323279561E-01	-4.99997103241561E-01
45		-4.99710323261100E-01	-4.99997103241377E-01
46		-4.99710323254762E-01	-4.99997103241313E-01
54		-4.99710323247283E-01	-4.99997103241238E-01
55		-4.99710323244832E-01	-4.99997103241214E-01
66		-4.99710323246108E-01	-4.99997103241227E-01
78		-4.99710323264184E-01	-4.99997103241407E-01
85		-4.99710323265882E-01	-4.99997103241424E-01
91		-4.99710323263249E-01	-4.99997103241398E-01
105	12, 12	-4.99710323253062E-01	-4.99997103241296E-01
120		-4.99710323251477E-01	-4.99997103241280E-01
126		-4.99710323255807E-01	-4.99997103241324E-01
CUBATURE DIM	SD	IM{F(r')}	
21		3.26143588348151E-07	3.26143588477216E-09
28		3.26143588348152E-07	3.26143588477219E-09
36		3.26143588348140E-07	3.26143588477203E-09
45		3.26143588348144E-07	3.26143588477210E-09
46		3.26143588348154E-07	3.26143588477214E-09
54		3.26143588348150E-07	3.26143588477214E-09
55		3.26143588348151E-07	3.26143588477214E-09
66		3.26143588348151E-07	3.26143588477215E-09
78	10	3.26143588348163E-07	3.26143588477196E-09
85		3.26143588348147E-07	3.26143588477194E-09
91	8	3.26143588348247E-07	3.26143588477247E-09
105		3.26143588348149E-07	3.26143588477214E-09
120		3.26143588348154E-07	3.26143588477216E-09
126		3.26143588348148E-07	3.26143588477210E-09
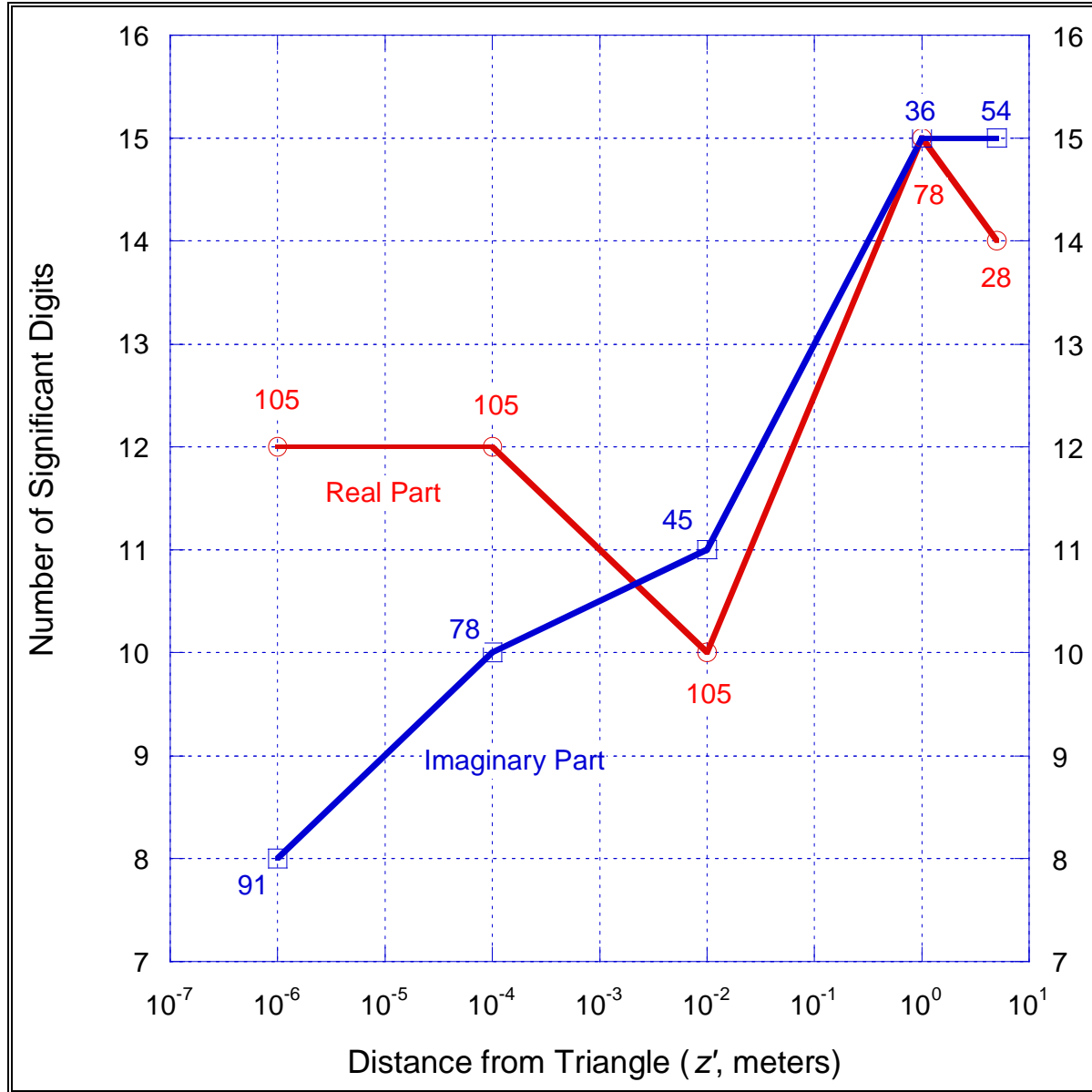
Figure 6.3: Case 36 for surface integral: maximum number of SD obtained using cubatures as a function of distance from IT. A number attached to a calculation point (z', w) gives the size of the smallest cubature that provides w SD at the point z'.
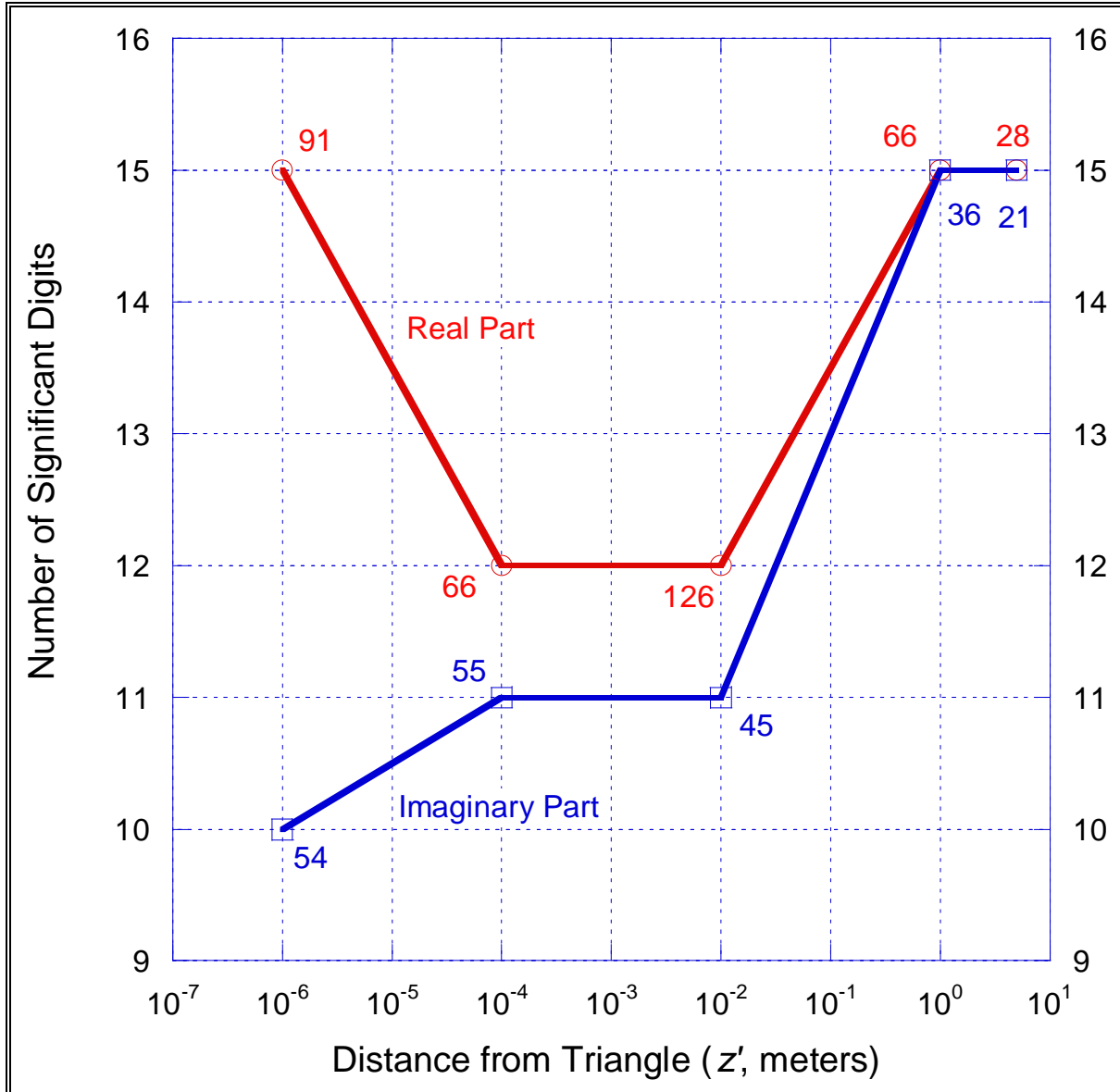
Figure 6.4: Case 37 for surface integral: maximum number of SD obtained using cubatures as a function of distance from IT. A number attached to a calculation point (z', w) gives the size of the smallest cubature that provides w SD at the point z'.
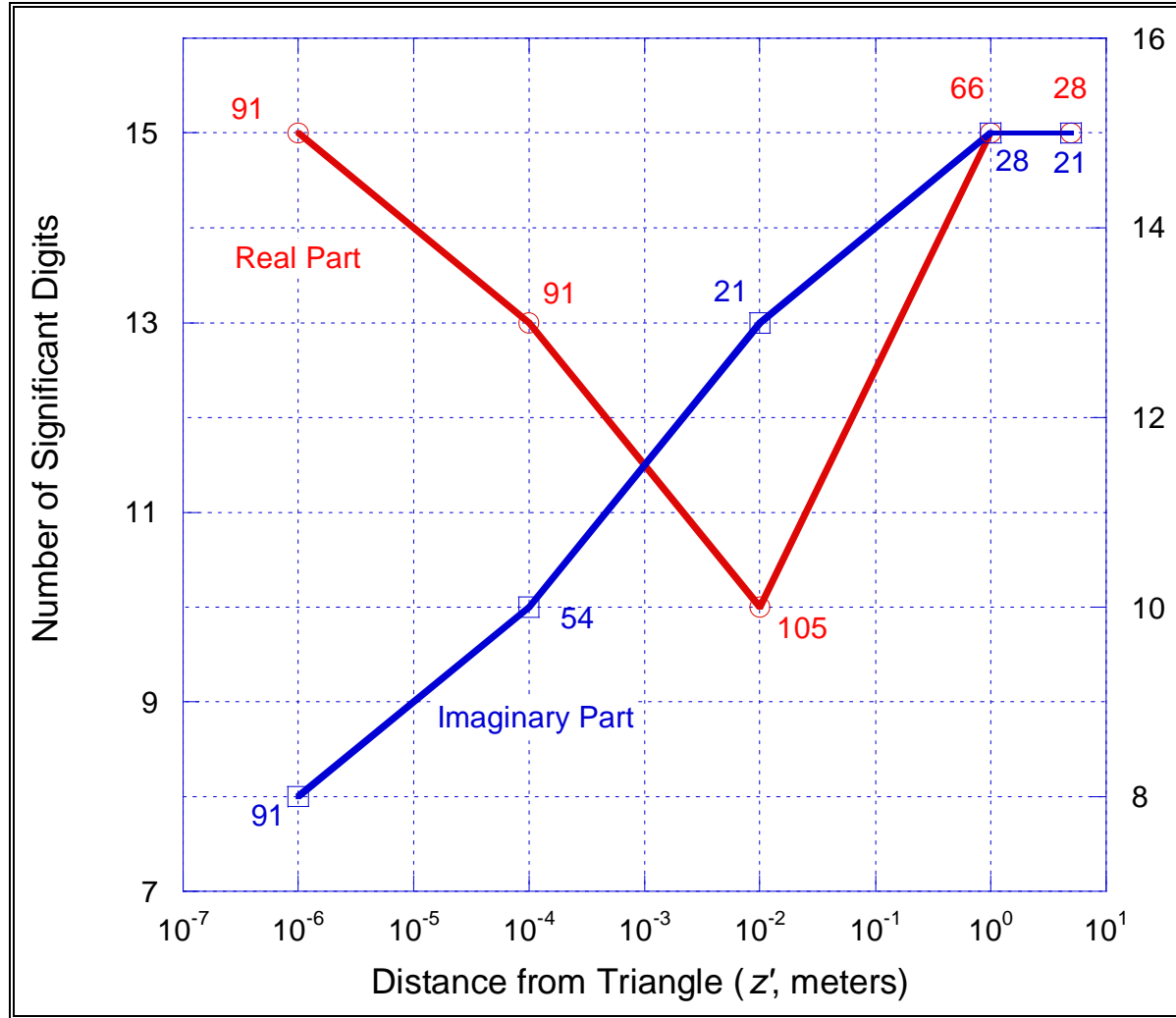
Figure 6.5: Case 38 for surface integral: maximum number of SD obtained using cubatures as a function of distance from IT. A number attached to a calculation point (z', w) gives the size of the smallest cubature that provides w SD at the point z'.
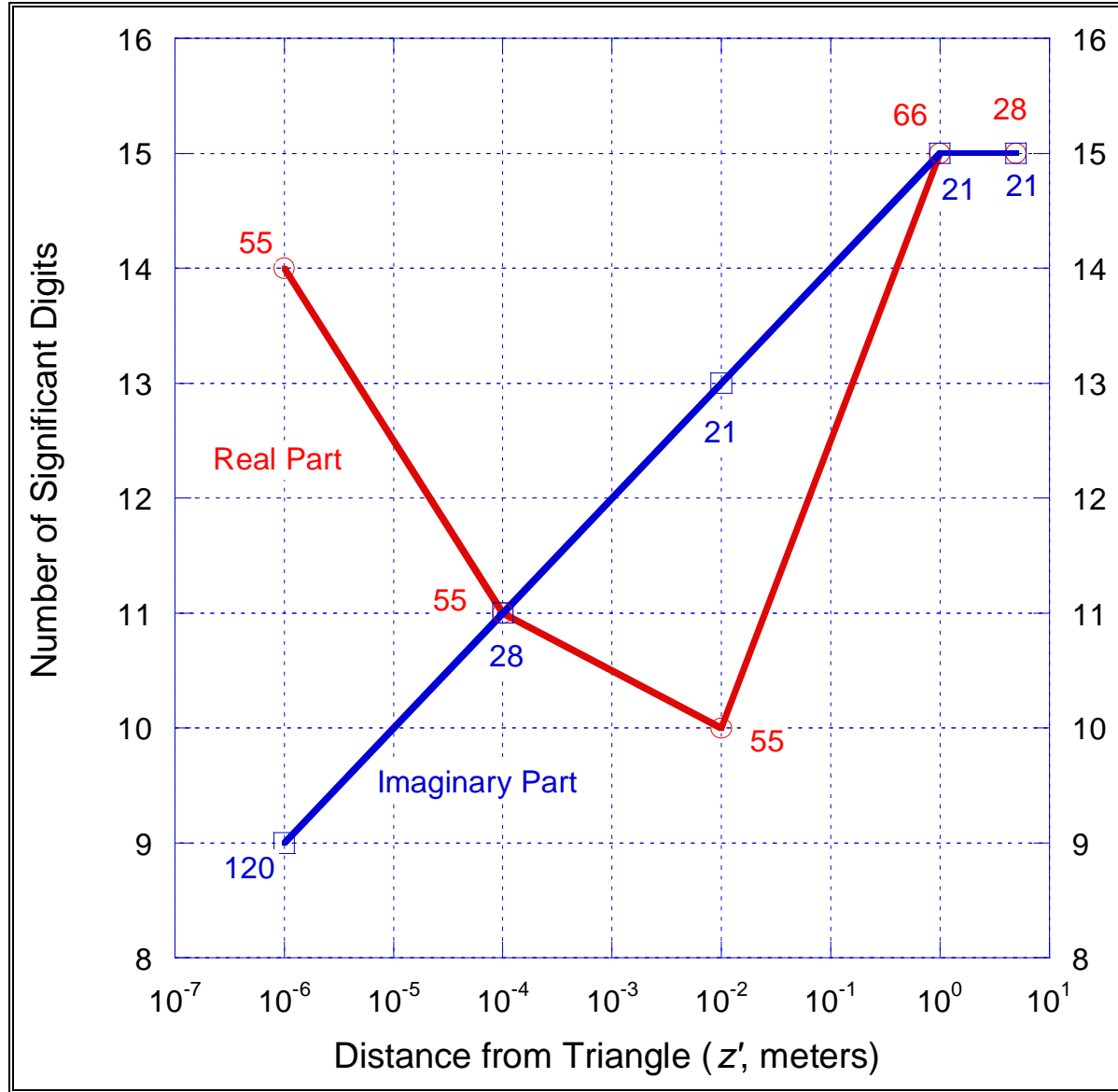
Figure 6.6: Case 39 for surface integral: maximum number of SD obtained using cubatures as a function of distance from IT. A number attached to a calculation point (z', w) gives the size of the smallest cubature that provides w SD at the point z'.
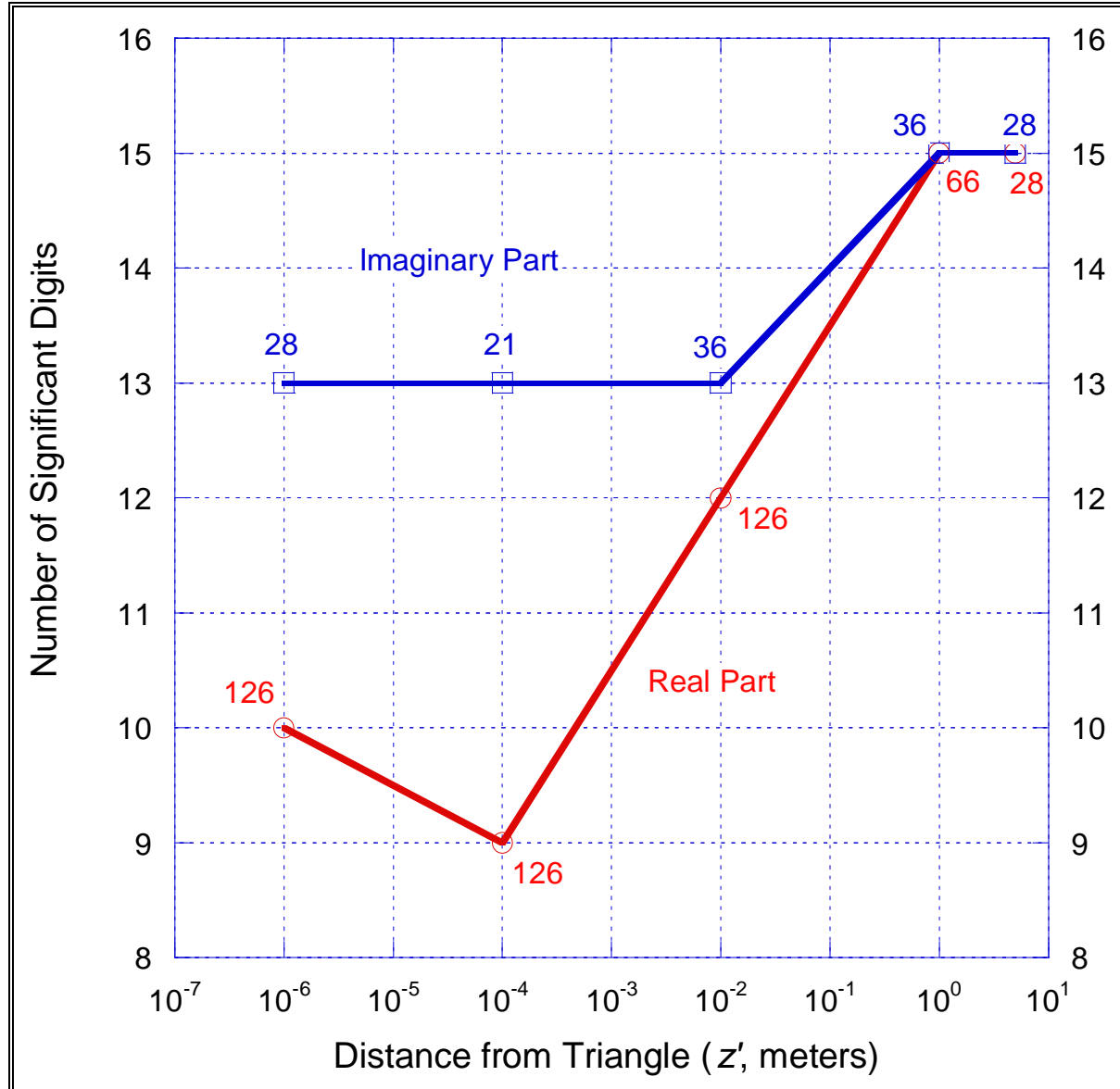
Figure 6.7: Case 40 for surface integral: maximum number of SD obtained using cubatures as a function of distance from IT. A number attached to a calculation point (z', w) gives the size of the smallest cubature that provides w SD at the point z'.

We turn now to the evaluation of the line integral. The exact form of this integral is given by the left-hand side of (3.5) and repeated here

$$L(\mathbf{r}', j) = \int_{s_j} \frac{e^{-ik|\mathbf{r}-\mathbf{r}'|}}{|\mathbf{r}-\mathbf{r}'|} \, ds, \quad j = 1, 2, 3 \tag{6.3}$$

where s_j stands for one of the sides of the triangle. We compare each side separately. The number of a side is the same as the number of the vertex opposite that side. The comparison in this case

is with Matlab's GKQ algorithm. We set the relative tolerance in this subroutine to its minimum, $2.22*10^{-14}$. The numbers we obtained using our method (and requiring 15 SD) agree with those of the GKQ algorithm to at least 14 SD. We present part of these results in Table 6.18.

Table 6.18: Evaluation of line integral in (6.3) and comparison with Matlab's GKQ.

		RE{INTG_1}	IM{INTG_1}	MATLAB QUADGK ALGORITHM	
CASE 1	SIDE 1	1.90582350126434E+00	-8.60420498191187E-01	1.90582350126434E+00	-8.60420498191187E-01
	SIDE 2	3.69035907422533E+00	-6.17945178406258E-01	3.69035907422534E+00	-6.17945178406258E-01
	SIDE 3	3.69035907422533E+00	-6.17945178406258E-01	3.69035907422534E+00	-6.17945178406258E-01
		RE{INTG_1}	IM{INTG_1}	MATLAB QUADGK ALGORITHM	
CASE 5	SIDE 1	4.51600791903947E+00	-8.77728566109124E-01	4.51600791903947E+00	-8.77728566109124E-01
	SIDE 2	1.37627563290081E+00	-6.09751108502621E-01	1.37627563290082E+00	-6.09751108502621E-01
	SIDE 3	1.37627563290081E+00	-6.09751108502621E-01	1.37627563290082E+00	-6.09751108502621E-01
		RE{INTG_1}	IM{INTG_1}	MATLAB QUADGK ALGORITHM	
CASE 11	SIDE 1	1.90582086366456E+00	-8.60420440840094E-01	1.90582086366456E+00	-8.60420440840094E-01
	SIDE 2	3.69027366103930E+00	-6.17945137475203E-01	3.69027366103930E+00	-6.17945137475203E-01
	SIDE 3	3.69027366103930E+00	-6.17945137475203E-01	3.69027366103930E+00	-6.17945137475203E-01
		RE{INTG_1}	IM{INTG_1}	MATLAB QUADGK ALGORITHM	
CASE 14	SIDE 1	1.06141588860891E+01	-8.50594455858452E-01	1.06141588860895E+01	-8.50594455858453E-01
	SIDE 2	9.63978848276054E+00	-6.14740566007970E-01	9.63978848276057E+00	-6.14740566007970E-01
	SIDE 3	6.65841995235531E-01	-5.74796541407303E-01	6.65841995235532E-01	-5.74796541407304E-01
		RE{INTG_1}	IM{INTG_1}	MATLAB QUADGK ALGORITHM	
CASE 17	SIDE 1	6.97821202303442E+00	-8.50425853556906E-01	6.97821202303448E+00	-8.50425853556907E-01
	SIDE 2	6.75413585870779E+00	-6.14659499455112E-01	6.75413585870781E+00	-6.14659499455112E-01
	SIDE 3	6.63760055152963E-01	-5.74600762567182E-01	6.63760055152964E-01	-5.74600762567182E-01
		RE{INTG_1}	IM{INTG_1}	MATLAB QUADGK ALGORITHM	
CASE 20	SIDE 1	9.37027630463920E+00	-8.50701732371761E-01	9.37027630463922E+00	-8.50701732371761E-01
	SIDE 2	9.11674874498877E+00	-6.14797666248879E-01	9.11674874498878E+00	-6.14797666248879E-01
	SIDE 3	6.67242696421228E-01	-5.74926715022366E-01	6.67242696421228E-01	-5.74926715022366E-01
		RE{INTG_1}	IM{INTG_1}	MATLAB QUADGK ALGORITHM	
CASE 23	SIDE 1	6.14264876010087E+00	-8.50317969612828E-01	6.14264876010089E+00	-8.50317969612829E-01
	SIDE 2	5.89087476299632E+00	-6.14601954320508E-01	5.89087476299633E+00	-6.14601954320508E-01
	SIDE 3	6.62366864094923E-01	-5.74470195405343E-01	6.62366864094923E-01	-5.74470195405343E-01
		RE{INTG_1}	IM{INTG_1}	MATLAB QUADGK ALGORITHM	
CASE 26	SIDE 1	1.06141588860894E+01	-8.50594455858452E-01	1.06141588860894E+01	-8.50594455858453E-01
	SIDE 2	6.65841995235531E-01	-5.74796541407303E-01	6.65841995235532E-01	-5.74796541407304E-01
	SIDE 3	9.63978848276054E+00	-6.14740566007970E-01	9.63978848276057E+00	-6.14740566007970E-01
		RE{INTG_1}	IM{INTG_1}	MATLAB QUADGK ALGORITHM	
CASE 29	SIDE 1	6.97821202303442E+00	-8.50425853556906E-01	6.97821202303446E+00	-8.50425853556907E-01
	SIDE 2	6.63760055152963E-01	-5.74600762567182E-01	6.63760055152964E-01	-5.74600762567182E-01
	SIDE 3	6.75413585870779E+00	-6.14659499455112E-01	6.75413585870781E+00	-6.14659499455112E-01
		RE{INTG_1}	IM{INTG_1}	MATLAB QUADGK ALGORITHM	
CASE 32	SIDE 1	9.37027630463920E+00	-8.50701732371761E-01	9.37027630463922E+00	-8.50701732371761E-01
	SIDE 2	6.67242696421228E-01	-5.74926715022366E-01	6.67242696421228E-01	-5.74926715022366E-01
	SIDE 3	9.11674874498877E+00	-6.14797666248879E-01	9.11674874498878E+00	-6.14797666248879E-01
		RE{INTG_1}	IM{INTG_1}	MATLAB QUADGK ALGORITHM	
CASE 35	SIDE 1	6.14264876010087E+00	-8.50317969612828E-01	6.14264876010089E+00	-8.50317969612829E-01
	SIDE 2	6.62366864094923E-01	-5.74470195405343E-01	6.62366864094923E-01	-5.74470195405343E-01
	SIDE 3	5.89087476299632E+00	-6.14601954320508E-01	5.89087476299633E+00	-6.14601954320508E-01

We also compute according to Table 6.14 but for the z' values we use for the surface integral, as in Table 6.16. We note here that if the OP were exactly on the boundary, *i.e.*, z' were equal to zero, the line integral in question would not exist. Fortunately, the OP cannot be on the boundary; however, if it is near enough, it may create problems for any quadrature used to evaluate the integral. We demonstrate this in Table 6.19 with Case 38. In this case, the OP is right above the right-lower corner. We see that, in the approach to the corner, the GKQ starts losing SD. This is true for the real part of the integral, the one that is singular. Sides 1 and 3

(hypotenuse and base, respectively) have this corner in common. While for Side 2 we get 14 SD at the 10^{-6} value, for the other two sides 12 for the real part but 15 for the imaginary. For completeness, we present the rest of the cases in Appendix H.

Table 6.19: The line integral of (6.3) for an OP above the lower right-hand corner of the triangle.

Casae	38	PRESENT METHOD		MATLAB G-K QUADRATURE	
z'	SIDE	RE{INTG_1}	IM{INTG_1}	RE{INTG_1}	IM{INTG_1}
5.0	S 1	-2.78778877123972E-01	1.14280517687205E-02	-2.78778877123972E-01	1.14280517687205E-02
	S 2	-1.94184778869090E-01	1.60631223094381E-02	-1.94184778869090E-01	1.60631223094381E-02
	S 3	-1.98613359322592E-01	4.11400306068688E-03	-1.98613359322592E-01	4.11400306068682E-03
1.0	S 1	8.11487798461838E-01	-7.94679252600586E-01	8.11487798461838E-01	-7.94679252600586E-01
	S 2	3.80119469546867E-01	-5.36269065701851E-01	3.80119469546868E-01	-5.36269065701851E-01
	S 3	6.64800195907522E-01	-5.74698696029768E-01	6.64800195907522E-01	-5.74698696029768E-01
0.01	S 1	5.45383286748471E+00	-8.50504527263624E-01	5.45383286748472E+00	-8.50504527263625E-01
	S 2	6.64757229191059E-01	-5.74694775231700E-01	6.64757229191059E-01	-5.74694775231700E-01
	S 3	5.20119889335351E+00	-6.14696002448062E-01	5.20119889335352E+00	-6.14696002448062E-01
1.E-04	S 1	1.00590502389874E+01	-8.50510221982515E-01	1.00590502389879E+01	-8.50510221982516E-01
	S 2	6.64800191610610E-01	-5.74698695637687E-01	6.64800191610610E-01	-5.74698695637687E-01
	S 3	9.80640081789547E+00	-6.14700082256520E-01	9.80640081789576E+00	-6.14700082256520E-01
1.E-06	S 1	1.46642204342387E+01	-8.50510222551989E-01	1.46642204342812E+01	-8.50510222551989E-01
	S 2	6.64800195907092E-01	-5.74698696029728E-01	6.64800195907093E-01	-5.74698696029729E-01
	S 3	1.44115710116020E+01	-6.14700082664502E-01	1.44115710116311E+01	-6.14700082664502E-01

SUMMARY AND CONCLUSIONS

We have considered the problem of computing the inner integral of the MFIE to a prescribed precision. This integral is given by (1.12). In evaluating this integral, our aim has been to take the greatest advantage possible of the results we obtained in reference 1. In Section 1, we re-write the integral as a line integral over the boundary of the integration triangle and a remaining surface integral over the triangle. In Section 3, we use the same techniques as in reference 1 to evaluate the line integral to prescribed precision. In Section 2, we show that the remaining surface integral can be written in such a way as to have to evaluate a solid-angle integral and one that we have already evaluated in reference 1. In Section 4, we give an explicit formula for measuring solid angle. It may be the most compact formula for the purpose. In Section 5, we quote results from reference 1 regarding the remaining integral in Section 2. In Section 6, we provide a thorough validation of our results.

The principal equations are the following. The integral under consideration is given by (1.12). It is re-written as two integrals in (1.16). The surface integral in (1.16) is written in terms of a Maclaurin-series expansion in (2.2). The integrals in this expansion are given by the iteration formulas (2.6) – (2.7), as well as the integral (2.4). Results for the latter are given in Section 5, as quoted from reference 1. The initial iterate is the solid angle integral, an explicit formula for which is given in Section 4. The line integral in (1.16) is evaluated in Section 3. The key integral is given by (3.6). It is expanded in a Maclaurin series in (3.8) and evaluated iteratively.

The iterative formulas that we use in this report do not converge for all values of the OP. In reference 1 we showed that the two formulas in Section 5, namely, (5.4) – (5.6) and (5.9) – (5.11) (and two other, similar sets further down) converge for the OP being within half-a-wavelength from the triangle's centroid. Using the approach of Appendix B in reference 1, we can show that (2.7) converges for observation points within a wavelength from the centroid. For the iteration formulas (3.37) and (3.42), we reach the same conclusion. Thus, if the observation point is within half-a wavelength from the centroid, our scheme converges. Unfortunately, time did not permit us to determine where we should use our method and where we should be using quadratures and cubatures, as we did in Part II of reference 1. This part remains to be done. Although the task of accomplishing this is straightforward, it is a time-consuming one. There remains also the outer integral, in the present case, the first of the iterated integrals in (1.10). This integral is over the observation triangle and involves a basis function and the inner integral, the one we evaluated in this report. The outer integral (in our approach) can only be evaluated numerically. It would be interesting to conduct a study as in Part II of reference 1 to see what size cubatures are required. for a specified accuracy.

In this report and in reference 1, we considered the case of perfect conductors. When other materials are present, then a pair of integral equations is required to determine the unknown electric and magnetic current densities. These equations involve the same kernels that appear in the EFIE and the MFIE. If the materials are lossless, then the present analysis and that in reference 1 apply directly. If they are lossy, then the wavenumber becomes complex and results not only in an oscillatory motion, as we have encountered to this point, but also in an exponentially decaying factor. The latter can also be replaced by its Taylor-series expansion,

multiplying the sine and cosine expansions. The analysis from this point on would proceed as in the present report and reference 1.

REFERENCES

1. J. S. Asvestas, S. Yankovich and O. E. Allen, "Calculation of impedance matrix inner integral to prescribed precision", NAWCAD Patuxent River Report No. NAWCADPAX/TR-2008/227, of Dec 2008.

2. J. S. Asvestas, S. Yankovich and O. E. Allen, "Calculation of impedance matrix inner integral to prescribed precision", *IEEE Trans Antennas Propagat*, Vol. 58, No. 2, pp. 479-487.

3. D. Colton and R. Kress, *Integral Equation Methods in Scattering Theory*. New York: John Wiley & Sons, 1983.

4. S. M. Rao, D. R. Wilton, and A. W. Glisson, "Electromagnetic Scattering by surfaces of arbitrary shape", *IEEE Trans. Antennas Propagat.,* Vol. AP-30, No. 3, pp. 409-418, 1982.

5. T. M. Apostol, *Mathematical Analysis*, 2nd ed. Reading, MA: Addison Wesley, 1974.

6. P. J. Davis and P. Rabinowitz, *Methods of Numerical Integration*. Orlando: Academic Press, 1984.

7. http://www.mathworks.com/help/techdoc/ref/quadgk.html

8. J. Van Bladel, *Electromagnetic Fields*. New York: McGraw-Hill, 1964.

9. A. Van Oosterom and J. Strackee, "The solid angle of a plane triangle", *IEEE Trans Biomed Eng*, Vol. BME-30, No. 2, pp. 125-126, 1983.

10. J. S. Asvestas and D. C. Englund, "Computing the solid angle subtended by a planar figure", *Optical Eng*, Vol. 33, No. 12, pp. 4055-4059, 1994.

11. J. S. Asvestas, "Line integrals and physical optics. Part I. The transformation of the solid angle surface integral to a line integral", *J. Opt. Soc. Amer. A*, Vol. 2, pp. 891-895, 1985.

12. J. S. Asvestas, "Line integrals and physical optics. Part II. The conversion of the Kirchhoff surface integral to a line integral", *J. Opt. Soc. Amer. A*, Vol. 2, pp. 896-902, 1985.

13. M. A. Khayat and D. R. Wilton, "Numerical evaluation of singular and near-singular potential integrals", *IEEE Trans. Antennas Propagat.,* Vol. 53, No. 10, pp. 3180-3190, 2005.

14. P. Ylä-Oijala and M. Taskinen, "Calculation of CFIE Impedance Matrix Elements with RWG and *n* x RWG Functions", *IEEE Trans. Antennas Propagat.,* Vol. 51, No. 8, pp. 1837-1846, 2003.

15. http://en.wikipedia.org/wiki/Machine_epsilon

ACRONYMS

EFIE	Electric Field Integral Equation
GKQ	Gauss-Kronrod Quadrature.
IM	Impedance Matrix
IT	Integration Triangle
MFIE	Magnetic Field Integral Equation
MoM	Method of Moments
OP	Observation Point
RWG	Rao-Wilton-Glisson

<div align="center">

APPENDIX A
ANOTHER TESTING OF MFIE

</div>

In this Appendix, we test (1.7) using $\hat{n}' \times \mathbf{f}_m(\mathbf{r}')$ as the testing function. We thus have

$$\frac{1}{2}\sum_{n=1}^{N} a_n \int_{T_m} \left[\hat{n}' \times \mathbf{f}_m(\mathbf{r}')\right] \cdot \mathbf{f}_n(\mathbf{r}') dS' = \int_{T_m} \left[\hat{n}' \times \mathbf{f}_m(\mathbf{r}')\right] \cdot \mathbf{J}^{inc}(\mathbf{r}') dS'$$

$$-\sum_{n=1}^{N} a_n \int_{T_m} dS' \left[\hat{n}' \times \mathbf{f}_m(\mathbf{r}')\right] \cdot \hat{n}' \times \int_{T_n} dS \mathbf{f}_n(\mathbf{r}) \times \nabla g(\mathbf{r}, \mathbf{r}') \ , \quad \mathbf{r}' \in T_m \ , \quad m = 1, 2, 3, ..., N \ . \tag{A.1}$$

Using well-known vector identities, we can re-write this as

$$\frac{1}{2}\sum_{n=1}^{N} a_n \int_{T_m} \hat{n}' \cdot \left[\mathbf{f}_m(\mathbf{r}') \times \mathbf{f}_n(\mathbf{r}')\right] dS' = \int_{T_m} \hat{n}' \cdot \left[\mathbf{f}_m(\mathbf{r}') \times \mathbf{J}^{inc}(\mathbf{r}')\right] dS'$$

$$-\sum_{n=1}^{N} a_n \int_{T_m} dS' \mathbf{f}_m(\mathbf{r}') \cdot \int_{T_n} dS \mathbf{f}_n(\mathbf{r}) \times \nabla g(\mathbf{r}, \mathbf{r}') \ , \quad \mathbf{r}' \in T_m \ , \quad m = 1, 2, 3, ..., N \ . \tag{A.2}$$

The integral of interest is the same as in (1.11).

THIS PAGE INTENTIONALLY LEFT BLANK

APPENDIX B
IMAGINARY PART OF SURFACE INTEGRAL FOR OBSERVATION POINTS PROJECTING ONTO THE INTEGRATION TRIANGLE AND IN CLOSE PROXIMITY TO IT

In (2.2), we consider the case where the OP is above the triangle and in close proximity to it. The imaginary part of the integral is given by

$$\text{Im}\{F(\mathbf{r}')\} = -\frac{1}{4\pi}\text{Im}\left\{\int_T \frac{\partial}{\partial z}\left(\frac{e^{-i2\pi R}}{R}\right)dS\right\} = \frac{1}{4\pi}\int_T \frac{\partial}{\partial z}\left[\frac{\sin(2\pi R)}{R}\right]dS.$$

(B.1)

We perform the indicated differentiation

$$\text{Im}\{F(\mathbf{r}')\} = -\frac{z'}{4\pi}\int_T \frac{2\pi R\cos(2\pi R) - \sin(2\pi R)}{R^3}dS$$

$$= \frac{z'}{4\pi}\int_T \frac{2\pi R[1-\cos(2\pi R)] + [\sin(2\pi R) - 2\pi R]}{R^3}dS$$

$$= \frac{z'}{2}\int_T \frac{1-\cos(2\pi R)}{R^2}dS - \frac{z'}{4\pi}\int_T \frac{2\pi R - \sin(2\pi R)}{R^3}dS$$

(B.2)

where

$$R = \sqrt{(x-x')^2 + (y-y')^2 + z'^2} = \sqrt{\rho^2 + z'^2}, \quad z' \neq 0, \quad \rho = \sqrt{(x-x')^2 + (y-y')^2}.$$

(B.3)

We expand the trigonometric function according to the number of SDs we require and write

$$\text{Im}\{F(\mathbf{r}')\} = \frac{z'}{2}\sum_{n=1}^{N_c-1}\frac{(-1)^{n+1}(2\pi)^n}{(2n)!}\int_T R^{2(n-1)}dS - \frac{z'}{2}\sum_{n=1}^{N_s-1}\frac{(-1)^{n+1}(2\pi)^{2n}}{(2n+1)!}\int_T R^{2(n-1)}dS.$$

(B.4)

We let

$$N = \max(N_c, N_s)$$

(B.5)

and redefine (B.4) as

$$\text{Im}\{F(\mathbf{r}')\} = \frac{z'}{2}\sum_{n=1}^{N-1}\frac{(-1)^{n+1}(2\pi)^{2n}}{(2n)!}\int_T R^{2(n-1)}dS - \frac{z'}{2}\sum_{n=1}^{N-1}\frac{(-1)^{n+1}(2\pi)^{2n}}{(2n+1)!}\int_T R^{2(n-1)}dS$$

$$= \frac{z'}{2}\sum_{n=1}^{N-1}(-1)^{n+1}(2\pi)^{2n}\left[\frac{1}{(2n)!} - \frac{1}{(2n+1)!}\right]\int_T R^{2(n-1)}dS = z'\sum_{n=1}^{N-1}\frac{(-1)^{n+1}(n)(2\pi)^{2n}}{(2n+1)!}\int_T R^{2(n-1)}dS$$

$$= z' \sum_{n=0}^{N-2} \frac{(-1)^n (n+1)(2\pi)^{2n+2}}{(2n+3)!} \int_T R^{2n} dS .$$

(B.6)

We use (B.3) to re-write this as

$$\mathrm{Im}\{F(\mathbf{r}')\} = z' \sum_{n=0}^{N-2} \frac{(-1)^n (n+1)(2\pi)^{2n+2}}{(2n+3)!} \int_T \left(\rho^2 + z'^2\right)^n dS .$$

(B.7)

We expand the binomial

$$\mathrm{Im}\{F(\mathbf{r}')\} = z' \sum_{n=0}^{N-2} \frac{(-1)^n (n+1)(2\pi)^{2n+2}}{(2n+3)!} \sum_{m=0}^{n} \binom{n}{m} z'^{2m} \int_T \rho^{2(n-m)} dS$$

(B.8)

and collect terms in powers of z'

$$\mathrm{Im}\{F(\mathbf{r}')\} = z' \sum_{n=0}^{N-2} \frac{(-1)^n (n+1)(2\pi)^{2n+2}}{(2n+3)!} \int_T \rho^{2n} dS$$

$$+ z'^3 \sum_{n=1}^{N-2} \frac{(-1)^n (n+1)(2\pi)^{2n+2}}{(2n+3)!} \binom{n}{1} \int_T \rho^{2(n-1)} dS$$

$$+ z'^5 \sum_{n=2}^{N-2} \frac{(-1)^n (n+1)(2\pi)^{2n+2}}{(2n+3)!} \binom{n}{2} \int_T \rho^{2(n-2)} dS$$

$$\vdots$$

$$+ z'^{2(N-3)+1} \sum_{n=N-3}^{N-2} \frac{(-1)^n (n+1)(2\pi)^{2n+2}}{(2n+3)!} \sum_{m=0}^{n} \binom{n}{N-3} \int_T \rho^{2(n-N+3)} dS$$

$$+ z'^{2(N-2)+1} \frac{(-1)^N (N-1)(2\pi)^{2n+2}}{(2N-1)!} \int_T dS .$$

(B.9)

Alternatively, we can re-arrange (B.8) in terms of equal powers of ρ to obtain

$$\mathrm{Im}\{F(\mathbf{r}')\} = z'(2\pi)^2 \left[\int_T dS\right] \sum_{n=0}^{N-2} \frac{(-1)^n (n+1)(2\pi z')^{2n}}{(2n+3)!}$$

$$+ z'(2\pi)^2 \left[\int_T \rho^2 dS\right] \sum_{n=1}^{N-2} \frac{(-1)^n (n+1)(2\pi z')^{2n}}{(2n+3)!} \binom{n}{n-1} z'^{-2}$$

$$+ z'(2\pi)^2 \int_T \rho^4 dS \sum_{n=2}^{N-2} \frac{(-1)^n (n+1)(2\pi z')^{2n}}{(2n+3)!} \binom{n}{n-2} z'^{-4}$$

$$\vdots$$

$$+z'(2\pi)^2\left[\int_T \rho^{2(N-3)}dS\right]\sum_{n=N-3}^{N-2}\frac{(-1)^n(n+1)(2\pi z')^{2n}}{(2n+3)!}\binom{n}{N-3}z'^{-2(N-3)}$$

$$+z'(2\pi)^2\left[\int_T \rho^{2(N-2)}dS\right]\frac{(-1)^N(N-1)(2\pi z')^{2(N-2)}}{(2N-1)!}.\tag{B.10}$$

Shifting indices, we get

$$\text{Im}\{F(\mathbf{r}')\}=z'(2\pi)^2\left[\int_T dS\right]\sum_{n=0}^{N-2}\frac{(-1)^n(n+1)(2\pi z')^{2n}}{(2n+3)!}$$

$$-z'(2\pi)^4\left[\int_T \rho^2 dS\right]\sum_{n=0}^{N-3}\frac{(-1)^n(n+2)(n+1)(2\pi z')^{2n}}{(2n+5)!}$$

$$+z'(2\pi)^6\int_T \rho^4 dS\sum_{n=0}^{N-4}\frac{(-1)^n(n+3)(n+2)(n+1)(2\pi z')^{2n}}{2(2n+7)!}$$

$$\vdots$$

$$-z'(2\pi)^2\left[\int_T \rho^{2(N-3)}dS\right]\sum_{n=0}^{1}\frac{(-1)^{n+N}(n+N-2)(2\pi z')^{2n}}{(2n+2N-3)!}\binom{n+N-3}{N-3}$$

$$+z'(2\pi)^2\left[\int_T \rho^{2(N-2)}dS\right]\frac{(-1)^N(N-1)(2\pi)^{2(N-2)}}{(2N-1)!}.\tag{B.11}$$

Making the leading term in each sum equal to one, we get

$$\text{Im}\{F(\mathbf{r}')\}=\frac{z'(2\pi)^2}{3!}\left[\int_T dS\right]\sum_{n=0}^{N-2}\frac{(-1)^n\,3!(n+1)(2\pi z')^{2n}}{(2n+3)!}$$

$$-\frac{z'2(2\pi)^4}{5!}\left[\int_T \rho^2 dS\right]\sum_{n=0}^{N-3}\frac{(-1)^n\,5!(n+2)(n+1)(2\pi z')^{2n}}{2(2n+5)!}$$

$$+\frac{z'3(2\pi)^6}{7!}\int_T \rho^4 dS\sum_{n=0}^{N-4}\frac{(-1)^n\,7!(n+3)(n+2)(n+1)(2\pi z')^{2n}}{3!(2n+7)!}$$

$$\vdots$$

$$-\frac{z'(N-2)(2\pi)^2}{(2N-3)!}\left[\int_T \rho^{2(N-3)}dS\right]\sum_{n=0}^{1}\frac{(-1)^{n+N}(2N-3)!(n+N-2)(2\pi z')^{2n}}{(N-2)(2n+2N-3)!}\binom{n+N-3}{N-3}$$

$$+z'(2\pi)^2\left[\int_T \rho^{2(N-2)}dS\right]\frac{(-1)^N(N-1)(2\pi)^{2(N-2)}}{(2N-1)!}.\tag{B.12}$$

APPENDIX B

The leading term in each sum is equal to one. The general term of the first sum is greater than the general term of the second sum, which is greater than that of the third sum, and so on. Thus, if we set the second term of the first sum to be less than 0.5×10^{-M} or less than the machine epsilon, then we only need retain the first term in each sum. For each case we get

$$\frac{(2\pi z')^2}{10} < 0.5 \cdot 10^{-M} \quad \Rightarrow \quad z' < \frac{\sqrt{5 \cdot 10^{-M}}}{2\pi} \tag{B.13}$$

and

$$\frac{(2\pi z')^2}{10} < \varepsilon \quad \Rightarrow \quad z' < \frac{\sqrt{10\varepsilon}}{2\pi}. \tag{B.14}$$

From (reference 15), we have obtained Table 1 that presents the IEEE 754-2008 standard and gives the value of machine epsilon in the last column. For values of z' as in (B.13) or (B.14), we can replace the sums in (B.12) by one (their leading term). This corresponds to using only the first term in (B.9)

$$\text{Im}\{F(\mathbf{r}')\} = z' \sum_{n=0}^{N-2} \frac{(-1)^n (n+1)(2\pi)^{2n+2}}{(2n+3)!} \int_T \rho^{2n} dS. \tag{B.15}$$

Table B.1: Machine epsilon for IEEE 754-2008 standard.

IEEE 754 - 2008	Common Name	Base b	*Fractional* digits p	Machine Epsilon $b^{-p}/2$	Value
binary16	half precision	2	10	2^{-11}	4.88e-04
binary32	single precision	2	23	2^{-24}	5.96e-08
binary64	double precision	2	52	2^{-53}	1.11e-16
binary128	quad(ruple) precision	2	112	2^{-113}	9.63e-35

We turn to the evaluation of the integrals in (B.15). The integrands are polynomials in x and y of degree $2n$. Hence, we can find an appropriate cubature that integrates them exactly. Alternatively, and since

$$\frac{1}{2(n+1)} \nabla \cdot (\mathbf{\rho}\rho^{2n}) = \frac{1}{2(n+1)} \left[\mathbf{\rho} \cdot \nabla \rho^{2n} + \rho^{2n} \nabla \cdot \mathbf{\rho} \right] \tag{B.16}$$

$$= \frac{1}{2(n+1)} \left[2n\mathbf{\rho} \cdot \hat{\rho}\rho^{2n-1} + 2\rho^{2n} \right] = \rho^{2n} \tag{B.17}$$

we can use the divergence theorem in two dimensions to write

$$\int_T \rho^{2n} dS = \frac{1}{2(n+1)} \int_T \nabla \cdot \left(\rho \rho^{2n} \right) dS = \frac{1}{2(n+1)} \int_{\partial T} \left(\hat{v} \cdot \rho \right) \rho^{2n} ds \tag{B.18}$$

with $\hat{v}$ the exterior unit normal vector to the triangle's side. The line integrals can be evaluated to machine precision using a GKQ. These integrals can also be evaluated analytically. Using Figure 3.2 and the definitions in that section, we first write

$$\int_{\partial T} \left(\hat{v} \cdot \rho \right) \rho^{2n} ds = \sum_{j=1}^{3} \hat{v}_j \cdot \int_{s_j} \rho \rho^{2n} ds \tag{B.19}$$

and then evaluate

$$\hat{v}_j \cdot \int_{s_j} \rho \rho^{2n} ds = \hat{v}_j \cdot \int_0^{s_j} \left(\mathbf{a}_{j+1} + \hat{t}_j s \right) \left\{ \left| \mathbf{a}_{j+1} \right|^2 + 2\hat{t}_j \cdot \mathbf{a}_{j+1} s + s^2 \right\}^n ds \tag{B.20}$$

$$= \left(\hat{v}_j \cdot \mathbf{a}_{j+1} \right) \int_0^{s_j} \left\{ \left| \mathbf{a}_{j+1} \right|^2 + 2\hat{t}_j \cdot \mathbf{a}_{j+1} s + s^2 \right\}^n ds = \left(\hat{v}_j \cdot \mathbf{a}_{j+1} \right) \int_0^{s_j} \left\{ \left(s + \hat{t}_j \cdot \mathbf{a}_{j+1} \right)^2 + \left| \mathbf{a}_{j+1} \right|^2 - \left(\hat{t}_j \cdot \mathbf{a}_{j+1} \right)^2 \right\}^n ds$$

$$= \left(\hat{v}_j \cdot \mathbf{a}_{j+1} \right) \int_{\hat{t}_j \cdot \mathbf{a}_{j+1}}^{s_j + \hat{t}_j \cdot \mathbf{a}_{j+2}} \left\{ \tau^2 + \left(\hat{v}_j \cdot \mathbf{a}_{j+1} \right)^2 \right\}^n ds = \left(\hat{v}_j \cdot \mathbf{a}_{j+1} \right) \sum_{m=0}^{n} \binom{n}{m} \left(\hat{v}_j \cdot \mathbf{a}_{j+1} \right)^{2(n-m)} \int_{\hat{t}_j \cdot \mathbf{a}_{j+1}}^{s_j + \hat{t}_j \cdot \mathbf{a}_{j+2}} \tau^{2m} ds$$

$$= \left(\hat{v}_j \cdot \mathbf{a}_{j+1} \right) \sum_{m=0}^{n} \binom{n}{m} \frac{\left(\hat{v}_j \cdot \mathbf{a}_{j+1} \right)^{2(n-m)}}{2m+1} \left[\left(s_j + \hat{t}_j \cdot \mathbf{a}_{j+2} \right)^{2m+1} - \left(\hat{t}_j \cdot \mathbf{a}_{j+1} \right)^{2m+1} \right]. \tag{B.21}$$

THIS PAGE INTENTIONALLY LEFT BLANK

APPENDIX C
ON THE SOLID-ANGLE SUBTENDED BY A PLANAR FIGURE AT A POINT IN SPACE

We consider a planar surface T and a point in space. The point is off the surface and we call it the OP. From this point, we draw a straight line to a point on the boundary of T and we let the boundary point go once around the boundary. This action generates a cone-like surface whose apex is the OP and base is the planar surface T. With center the OP, we draw a sphere of unit radius. We call T_S the region of the sphere that the cone-like structure intercepts. The surface area of T_S is the solid angle value subtended by T at the OP and is a positive quantity between 0 and 4π steradians. The mathematical formula for it is

$$\Omega = -\int_{T_S} \frac{\partial}{\partial r}\left(\frac{1}{r}\right)\Big|_{r=1} r^2 \sin\theta \, d\theta \, d\varphi = \int_{T_S} \sin\theta \, d\theta \, d\varphi = A(T_S) \tag{C.1}$$

where $A(T_S)$ stands for the area of T_S. The second integral is valid for any radius of the sphere that is less than the minimum distance between the OP and the boundary. By the divergence theorem, we can write (C.1) as

$$\Omega(\mathbf{r}';T) = \int_T \hat{n}\cdot\nabla\left(\frac{1}{R}\right) dS \tag{C.2}$$

where R is the distance from the OP to a point of T and $\hat{n}$ is the unit normal vector on T pointing into the region bounded by T, T_S, and the lateral surface of the cone; thus, $\hat{n}$ has a positive component in the direction of the OP. The integral in (C.2) can be used for any position of the OP. If the OP is reflected into the half-space away from which the normal is pointing, then the result will be the negative of the solid angle. To make things clear, if T lies on the xy-plane and $\hat{n}$ points in the *z-direction, then*

$$\Omega\left(\mathbf{r}_i';T\right) = \int_T \hat{z}\cdot\nabla\left(\frac{1}{\left|\mathbf{r}-\mathbf{r}_i'\right|}\right) dS = -\int_T \hat{z}\cdot\nabla\left(\frac{1}{\left|\mathbf{r}-\mathbf{r}'\right|}\right) dS, \quad z' > 0 \tag{C.3}$$

where $\mathbf{r}_i'$ is the image of $\mathbf{r}'$ about the xy-plane and $\mathbf{r}' = x'\hat{x} + y'\hat{y} + z'\hat{z}$.

THIS PAGE INTENTIONALLY LEFT BLANK

APPENDIX D
COMPARISON OF TWO SOLID-ANGLE FORMULAS FOR POINTS NEAR AND
ON A TRIANGLE'S BOUNDARY

We consider here the triangle of Figure 6.1 and the OPs of Table 6.14 when z' is equal to zero or very close to it. At these OPs, we compute the normalized solid angle Formula 1 (given by (4.1) and (4.2)) and Formula 2 (given by (4.1) and (4.3)). We display the results in Table D.1 for three values of z': 10^{-18}, 10^{-20} and 0 m. We display both SP and DP results. We discuss first the DP results.

Case 36 represents a point in the interior of the triangle and we see that both formulas provide the correct result when z' is equal to zero. The results for z' equal to 10^{-18} and 10^{-20} are also correct to DP.

Case 40 represents a point in the exterior of the triangle and both formulas agree for all three values of z'.

Case 37 represents the left vertex of the base of the triangle. In the approach to it, both formulas provide the correct answer to DP accuracy. When z' is equal to zero, however, Formula 1 treats the point as if it were exterior to the triangle, while Formula 2 sees it inside the triangle. The correct answer is 0.25.

Case 38 represents the right vertex of the base of the triangle. In the approach to it, both formulas provide the correct answer to DP accuracy. When z' is equal to zero, however, both formulas see a point outside the triangle. The correct answer is 0.125.

Case 39 represents the middle point of the hypotenuse. For all three values of z', Formula 1 sees a point exterior to the triangle. For the first two values of z', Formula 2 provides the correct value (both numbers are close to 0.5) but fails when z' is equal to zero and views the point as an exterior point.

What is happening in the last three cases? The coordinates of the vertex in Case 37 are (-1/3, -1/3, 0). When the number 1/3 is rounded off in DP, it becomes a smaller number than it actually is; thus, the point (-1/3, -1/3, 0) in Figure 6.1 will move to the right and up, landing inside the triangle. For reasons, we cannot explain, both formulas see the desired position (-1/3, -1/3, 0) when z' is different from zero but Formula 1 sees an exterior point when z' is equal to zero, while Formula 2 sees an interior point. Since in the computer the point is an interior point, we may claim that Formula 2 gives a better answer than Formula 1 when z' is zero.

The coordinates of the vertex for Case 38 are (2/3, -1/3, 0). When 2/3 is rounded off, it becomes larger while 1/3 becomes smaller; thus, the point are (2/3, -1/3, 0) moves to the right and up in Figure 6.1, landing outside the triangle. This is what both formulas see for z' equal to zero and provide the correct result. For z' different from zero, they see Vertex 2 in Figure 1.

The coordinates of the point in Case 39 are (1/6, 1/6, 0). When 1/6 is rounded off, it becomes larger; thus, the midpoint of the hypotenuse moves to the right and up, landing outside the triangle. This is what Formula 1 sees, while Formula 2 sees the original point for z' different from zero and the shifted point for z' equal to zero.

Turning to SP, we see that, in Cases 36 – 38, SP provides the same kind of result as DP, with Formula 2 performing slightly better than Formula 1. In Case 39, Formula 1 behaves as for DP, while Formula 2 provides the correct answer for points of the triangle but only to four SDs. In Case 40, both formulas behave as in DP but, for points off the triangle, they both provide only six SDs. In general, we would advise avoiding SP calculations for the solid angle.

Table D.1: Normalized solid angle values for the OPs of Table 6.14

			9	10	0
	Case 36		9	10	0
		z'	1.00E-18	1.00E-20	0.00E+00
SP	Formula 1		1.000000E+00	1.000000E+00	1.000000E+00
	Formula 2		1.000000E+00	1.000000E+00	1.000000E+00
DP	Formula 1		1.00000000000000E+00	1.00000000000000E+00	1.00000000000000E+00
	Formula 2		1.00000000000000E+00	1.00000000000000E+00	1.00000000000000E+00
	Case 37		9	10	
		z'	1.00E-18	1.00E-20	0.00E+00
SP	Formula 1		2.500000E-01	2.500004E-01	0.000000E+00
	Formula 2		2.500000E-01	2.500000E-01	1.000000E+00
DP	Formula 1		2.50000000000000E-01	2.50000000000000E-01	0.00000000000000E+00
	Formula 2		2.50000000000000E-01	2.50000000000000E-01	1.00000000000000E+00
	Case 38		9	10	
		z'	1.00E-18	1.00E-20	0.00E+00
SP	Formula 1		1.250000E-01	1.250003E-01	0.000000E+00
	Formula 2		1.250000E-01	1.250000E-01	0.000000E+00
DP	Formula 1		1.25000000000000E-01	1.25000000000000E-01	0.00000000000000E+00
	Formula 2		1.25000000000000E-01	1.25000000000000E-01	0.00000000000000E+00
	Case 39		9	10	
		z'	1.00E-18	1.00E-20	0.00E+00
SP	Formula 1		1.000000E+00	1.000000E+00	1.000000E+00
	Formula 2		4.999827E-01	4.999827E-01	0.000000E+00
DP	Formula 1		5.73354097941042E-03	5.73416107719460E-05	0.00000000000000E+00
	Formula 2		4.99999998758519E-01	4.99999998758519E-01	0.00000000000000E+00
	Case 40		9	10	
		z'	1.00E-18	1.00E-20	0.00E+00
SP	Formula 1		5.922377E-18	5.922376E-20	0.000000E+00
	Formula 2		5.922380E-18	5.922379E-20	0.000000E+00
DP	Formula 1		5.92237767136760E-18	5.92237767136760E-20	0.00000000000000E+00
	Formula 2		5.92237767136760E-18	5.92237767136760E-20	0.00000000000000E+00

THIS PAGE INTENTIONALLY LEFT BLANK

APPENDIX E
CONVERGENCE OF FORMULA (2.2) FOR THE SURFACE INTEGRAL

In this Appendix, we present results as in Table 6.16 for the remaining cases in Table 6.14. In Table E.1, we display the convergence of our algorithm for the surface integral for the OP of Case 37, Table 6.14. Convergence is to 15 SD and as a function of the number of terms in the trigonometric sums in (2.2). The entries in light green are the first ones for which our formula has stabilized to 15 SD. The OP is above the right-angle corner of the IT.

In Table E.2, we display the convergence of our algorithm for the surface integral for the OP of Case 38, Table 6.14. Convergence is to 15 SD and as a function of the number of terms in the trigonometric sums in (2.2). The entries in light green are the first one for which our formula has stabilized to 15 SD. The OP is above the lower right-hand corner of the IT.

In Table E.3, we display the convergence of our algorithm for the surface integral for the OP of Case 39, Table 6.14. Convergence is to 15 SD and as a function of the number of terms in the trigonometric sums in (2.2). The entries in light green are the first one for which our formula has stabilized to 15 SD. The OP is above the midpoint of the hypotenuse of the IT.

In Table E.4, we display the convergence of our algorithm for the surface integral for the OP of Case 40, Table 6.14. Convergence is to 15 SD and as a function of the number of terms in the trigonometric sums in (2.2). The entries in light green are the first one for which our formula has stabilized to 15 SD. The OP approaches a point in the triangle's plane but slightly outside the IT.

Table E.1: Convergence of our algorithm for Case 37.

z′ =	5.000		4.500	
	REAL{F(r')}	IMAG{F(r')}	REAL{F(r')}	IMAG{F(r')}
15 SD, Nc=Ns=4	1.66229178654614E-03	4.90079446997064E-03	2.67743268334130E-04	5.78612816705256E-03
15 SD, Nc=Ns=5	1.66229178654613E-03	4.90079446997063E-03	2.67743268334127E-04	5.78612816705257E-03
15 SD, Nc=Ns=6	1.66229178654613E-03	4.90079446997064E-03	2.67743268334123E-04	5.78612816705257E-03
15 SD, Nc=Ns=7	1.66229178654613E-03	4.90079446997064E-03	2.67743268334125E-04	5.78612816705257E-03
15 SD, Nc=Ns=8	1.66229178654613E-03	4.90079446997064E-03	2.67743268334125E-04	5.78612816705257E-03
15 SD, Nc=Ns=9	1.66229178654613E-03	4.90079446997064E-03	2.67743268334125E-04	5.78612816705257E-03
15 SD, Nc=Ns=10	1.66229178654613E-03	4.90079446997064E-03	2.67743268334125E-04	5.78612816705257E-03
15 SD, Nc=Ns=11	1.66229178654613E-03	4.90079446997064E-03	2.67743268334125E-04	5.78612816705257E-03
15 SD, Nc=Ns=12	1.66229178654613E-03	4.90079446997064E-03	2.67743268334125E-04	5.78612816705257E-03
z′ =	1.000		0.010	
	REAL{F(r')}	IMAG{F(r')}	REAL{F(r')}	IMAG{F(r')}
15 SD, Nc=Ns=4	-3.30414650310833E-02	3.11999935023589E-03	-1.23597765705000E-01	3.24684202112266E-05
15 SD, Nc=Ns=5	-3.30414650308276E-02	3.11999935001453E-03	-1.23597765854258E-01	3.24684605349130E-05
15 SD, Nc=Ns=6	-3.30414650308277E-02	3.11999935001460E-03	-1.23597765854119E-01	3.24684604964339E-05
15 SD, Nc=Ns=7	-3.30414650308277E-02	3.11999935001460E-03	-1.23597765854119E-01	3.24684604964614E-05
15 SD, Nc=Ns=8	-3.30414650308277E-02	3.11999935001460E-03	-1.23597765854119E-01	3.24684604964614E-05
15 SD, Nc=Ns=9	-3.30414650308277E-02	3.11999935001460E-03	-1.23597765854119E-01	3.24684604964614E-05
15 SD, Nc=Ns=10	-3.30414650308277E-02	3.11999935001460E-03	-1.23597765854119E-01	3.24684604964614E-05
15 SD, Nc=Ns=11	-3.30414650308277E-02	3.11999935001460E-03	-1.23597765854119E-01	3.24684604964614E-05
15 SD, Nc=Ns=12	-3.30414650308277E-02	3.11999935001460E-03	-1.23597765854119E-01	3.24684604964614E-05
z′ =	0.0001		0.000001	
	REAL{F(r')}	IMAG{F(r')}	REAL{F(r')}	IMAG{F(r')}
15 SD, Nc=Ns=4	-1.24986000435264E-01	3.24638198652974E-07	-1.24999859824252E-01	3.19908567264832E-09
15 SD, Nc=Ns=5	-1.24986000612371E-01	3.24685938990200E-07	-1.24999859824252E-01	3.19908567264832E-09
15 SD, Nc=Ns=6	-1.24986000612198E-01	3.24685891449776E-07	-1.24999860001661E-01	3.24690652364757E-09
15 SD, Nc=Ns=7	-1.24986000612199E-01	3.24685891484467E-07	-1.24999860001488E-01	3.24685888125090E-09
15 SD, Nc=Ns=8	-1.24986000612199E-01	3.24685891484467E-07	-1.24999860001488E-01	3.24685891594534E-09
15 SD, Nc=Ns=9	-1.24986000612199E-01	3.24685891484467E-07	-1.24999860001488E-01	3.24685891594534E-09
15 SD, Nc=Ns=10	-1.24986000612199E-01	3.24685891484467E-07	-1.24999860001488E-01	3.24685891594534E-09
15 SD, Nc=Ns=11	-1.24986000612199E-01	3.24685891484467E-07	-1.24999860001488E-01	3.24685891594534E-09
15 SD, Nc=Ns=12	-1.24986000612199E-01	3.24685891484467E-07	-1.24999860001488E-01	3.24685891594534E-09

Table E.2: Convergence of our algorithm for Case 38.

z' =	5.000		4.500	
	REAL{F(r')}	IMAG{F(r')}	REAL{F(r')}	IMAG{F(r')}
15 SD, Nc=Ns=4	1.72890617968269E-03	4.80316359879893E-03	3.77040226833441E-04	5.68301993259905E-03
15 SD, Nc=Ns=5	1.72890617968236E-03	4.80316359879895E-03	3.77040226832750E-04	5.68301993259891E-03
15 SD, Nc=Ns=6	1.72890617968236E-03	4.80316359879895E-03	3.77040226832730E-04	5.68301993259888E-03
15 SD, Nc=Ns=7	1.72890617968236E-03	4.80316359879895E-03	3.77040226832735E-04	5.68301993259889E-03
15 SD, Nc=Ns=8	1.72890617968236E-03	4.80316359879895E-03	3.77040226832734E-04	5.68301993259889E-03
15 SD, Nc=Ns=9	1.72890617968236E-03	4.80316359879895E-03	3.77040226832735E-04	5.68301993259889E-03
15 SD, Nc=Ns=10	1.72890617968236E-03	4.80316359879895E-03	3.77040226832735E-04	5.68301993259889E-03
15 SD, Nc=Ns=11	1.72890617968236E-03	4.80316359879895E-03	3.77040226832735E-04	5.68301993259889E-03
15 SD, Nc=Ns=12	1.72890617968236E-03	4.80316359879895E-03	3.77040226832735E-04	5.68301993259889E-03
z' =	1.000		0.010	
	REAL{F(r')}	IMAG{F(r')}	REAL{F(r')}	IMAG{F(r')}
15 SD, Nc=Ns=4	-2.61083307157073E-02	3.07874207729961E-03	-6.20687139259531E-02	3.20426950357757E-05
15 SD, Nc=Ns=5	-2.61083307127430E-02	3.07874207412868E-03	-6.20687168746579E-02	3.20440013915789E-05
15 SD, Nc=Ns=6	-2.61083307127456E-02	3.07874207413142E-03	-6.20687168676938E-02	3.20439982283057E-05
15 SD, Nc=Ns=7	-2.61083307127456E-02	3.07874207413142E-03	-6.20687168677051E-02	3.20439982334936E-05
15 SD, Nc=Ns=8	-2.61083307127456E-02	3.07874207413142E-03	-6.20687168677050E-02	3.20439982334867E-05
15 SD, Nc=Ns=9	-2.61083307127456E-02	3.07874207413142E-03	-6.20687168677050E-02	3.20439982334867E-05
15 SD, Nc=Ns=10	-2.61083307127456E-02	3.07874207413142E-03	-6.20687168677050E-02	3.20439982334867E-05
15 SD, Nc=Ns=11	-2.61083307127456E-02	3.07874207413142E-03	-6.20687168677050E-02	3.20439982334867E-05
15 SD, Nc=Ns=12	-2.61083307127456E-02	3.07874207413142E-03	-6.20687168677050E-02	3.20439982334867E-05
z' =	0.0001		0.000001	
	REAL{F(r')}	IMAG{F(r')}	REAL{F(r')}	IMAG{F(r')}
15 SD, Nc=Ns=4	-6.24956958255921E-02	3.18993899829706E-07	-6.24999537153430E-02	1.75553548874080E-09
15 SD, Nc=Ns=5	-6.24956991069065E-02	3.20444859397371E-07	-6.24999570001650E-02	3.20801988734267E-09
15 SD, Nc=Ns=6	-6.24956990989495E-02	3.20441250759051E-07	-6.24999569921975E-02	3.20440649164474E-09
15 SD, Nc=Ns=7	-6.24956990989627E-02	3.20441256837172E-07	-6.24999569922107E-02	3.20441258052063E-09
15 SD, Nc=Ns=8	-6.24956990989627E-02	3.20441256830233E-07	-6.24999569922107E-02	3.20441257358174E-09
15 SD, Nc=Ns=9	-6.24956990989627E-02	3.20441256830233E-07	-6.24999569922107E-02	3.20441257358174E-09
15 SD, Nc=Ns=10	-6.24956990989627E-02	3.20441256830233E-07	-6.24999569922107E-02	3.20441257358174E-09
15 SD, Nc=Ns=11	-6.24956990989627E-02	3.20441256830233E-07	-6.24999569922107E-02	3.20441257358174E-09
15 SD, Nc=Ns=12	-6.24956990989627E-02	3.20441256830233E-07	-6.24999569922107E-02	3.20441257358174E-09

Table E.3: Convergence of our algorithm for Case 39.

z' =	5.000		4.500	
	REAL{F(r')}	IMAG{F(r')}	REAL{F(r')}	IMAG{F(r')}
15 SD, Nc=Ns=4	1.62745189256200E-03	4.95019906577087E-03	2.10686757212165E-04	5.83827756766792E-03
15 SD, Nc=Ns=5	1.62745189256203E-03	4.95019906577090E-03	2.10686757212217E-04	5.83827756766799E-03
15 SD, Nc=Ns=6	1.62745189256201E-03	4.95019906577089E-03	2.10686757212195E-04	5.83827756766797E-03
15 SD, Nc=Ns=7	1.62745189256202E-03	4.95019906577089E-03	2.10686757212200E-04	5.83827756766797E-03
15 SD, Nc=Ns=8	1.62745189256202E-03	4.95019906577089E-03	2.10686757212199E-04	5.83827756766797E-03
15 SD, Nc=Ns=9	1.62745189256202E-03	4.95019906577089E-03	2.10686757212200E-04	5.83827756766797E-03
15 SD, Nc=Ns=10	1.62745189256202E-03	4.95019906577089E-03	2.10686757212200E-04	5.83827756766797E-03
15 SD, Nc=Ns=11	1.62745189256202E-03	4.95019906577089E-03	2.10686757212200E-04	5.83827756766797E-03
15 SD, Nc=Ns=12	1.62745189256202E-03	4.95019906577089E-03	2.10686757212200E-04	5.83827756766797E-03

z' =	1.000		0.010	
	REAL{F(r')}	IMAG{F(r')}	REAL{F(r')}	IMAG{F(r')}
15 SD, Nc=Ns=4	-3.85251154820082E-02	3.14083404792880E-03	-2.45768216011015E-01	3.26827981196468E-05
15 SD, Nc=Ns=5	-3.85251154819883E-02	3.14083404791340E-03	-2.45768216011319E-01	3.26827981281253E-05
15 SD, Nc=Ns=6	-3.85251154819883E-02	3.14083404791340E-03	-2.45768216011319E-01	3.26827981281800E-05
15 SD, Nc=Ns=7	-3.85251154819883E-02	3.14083404791340E-03	-2.45768216011319E-01	3.26827981281800E-05
15 SD, Nc=Ns=8	-3.85251154819883E-02	3.14083404791340E-03	-2.45768216011319E-01	3.26827981281800E-05
15 SD, Nc=Ns=9	-3.85251154819883E-02	3.14083404791340E-03	-2.45768216011319E-01	3.26827981281800E-05
15 SD, Nc=Ns=10	-3.85251154819883E-02	3.14083404791340E-03	-2.45768216011319E-01	3.26827981281800E-05
15 SD, Nc=Ns=11	-3.85251154819883E-02	3.14083404791340E-03	-2.45768216011319E-01	3.26827981281800E-05
15 SD, Nc=Ns=12	-3.85251154819883E-02	3.14083404791340E-03	-2.45768216011319E-01	3.26827981281800E-05

z' =	0.0001		0.000001	
	REAL{F(r')}	IMAG{F(r')}	REAL{F(r')}	IMAG{F(r')}
15 SD, Nc=Ns=4	-2.49957723082499E-01	3.26829087442671E-07	-2.49999577236076E-01	3.26810445913695E-09
15 SD, Nc=Ns=5	-2.49957723083909E-01	3.26829273902691E-07	-2.49999577237499E-01	3.26829278735652E-09
15 SD, Nc=Ns=6	-2.49957723083909E-01	3.26829273854127E-07	-2.49999577237499E-01	3.26829273878434E-09
15 SD, Nc=Ns=7	-2.49957723083909E-01	3.26829273854127E-07	-2.49999577237499E-01	3.26829273878434E-09
15 SD, Nc=Ns=8	-2.49957723083909E-01	3.26829273854127E-07	-2.49999577237499E-01	3.26829273878434E-09
15 SD, Nc=Ns=9	-2.49957723083909E-01	3.26829273854127E-07	-2.49999577237499E-01	3.26829273878434E-09
15 SD, Nc=Ns=10	-2.49957723083909E-01	3.26829273854127E-07	-2.49999577237499E-01	3.26829273878434E-09
15 SD, Nc=Ns=11	-2.49957723083909E-01	3.26829273854127E-07	-2.49999577237499E-01	3.26829273878434E-09
15 SD, Nc=Ns=12	-2.49957723083909E-01	3.26829273854127E-07	-2.49999577237499E-01	3.26829273878434E-09

APPENDIX E

Table E.4: Convergence of our algorithm for Case 40.

z′ =	5.000		4.500	
	REAL{F(r')}	IMAG{F(r')}	REAL{F(r')}	IMAG{F(r')}
15 SD, Nc=Ns=4	1.63265177430638E-03	4.94291929209383E-03	2.19197452706613E-04	5.83059487773860E-03
15 SD, Nc=Ns=5	1.63265177430639E-03	4.94291929209384E-03	2.19197452706570E-04	5.83059487773854E-03
15 SD, Nc=Ns=6	1.63265177430638E-03	4.94291929209383E-03	2.19197452706587E-04	5.83059487773856E-03
15 SD, Nc=Ns=7	1.63265177430638E-03	4.94291929209383E-03	2.19197452706583E-04	5.83059487773856E-03
15 SD, Nc=Ns=8	1.63265177430638E-03	4.94291929209383E-03	2.19197452706583E-04	5.83059487773856E-03
15 SD, Nc=Ns=9	1.63265177430638E-03	4.94291929209383E-03	2.19197452706583E-04	5.83059487773856E-03
15 SD, Nc=Ns=10	1.63265177430638E-03	4.94291929209383E-03	2.19197452706583E-04	5.83059487773856E-03
15 SD, Nc=Ns=11	1.63265177430638E-03	4.94291929209383E-03	2.19197452706583E-04	5.83059487773856E-03
15 SD, Nc=Ns=12	1.63265177430638E-03	4.94291929209383E-03	2.19197452706583E-04	5.83059487773856E-03

z′ =	1.000		0.010	
	REAL{F(r')}	IMAG{F(r')}	REAL{F(r')}	IMAG{F(r')}
15 SD, Nc=Ns=4	-3.75158019087497E-02	3.13776649155315E-03	-2.93455187094148E-02	3.26512413841501E-05
15 SD, Nc=Ns=5	-3.75158019087259E-02	3.13776649153445E-03	-2.93455187090839E-02	3.26512413098356E-05
15 SD, Nc=Ns=6	-3.75158019087259E-02	3.13776649153445E-03	-2.93455187090841E-02	3.26512413098946E-05
15 SD, Nc=Ns=7	-3.75158019087259E-02	3.13776649153445E-03	-2.93455187090841E-02	3.26512413098946E-05
15 SD, Nc=Ns=8	-3.75158019087259E-02	3.13776649153445E-03	-2.93455187090841E-02	3.26512413098946E-05
15 SD, Nc=Ns=9	-3.75158019087259E-02	3.13776649153445E-03	-2.93455187090841E-02	3.26512413098946E-05
15 SD, Nc=Ns=10	-3.75158019087259E-02	3.13776649153445E-03	-2.93455187090841E-02	3.26512413098946E-05
15 SD, Nc=Ns=11	-3.75158019087259E-02	3.13776649153445E-03	-2.93455187090841E-02	3.26512413098946E-05
15 SD, Nc=Ns=12	-3.75158019087259E-02	3.13776649153445E-03	-2.93455187090841E-02	3.26512413098946E-05

z′ =	0.0001		0.000001	
	REAL{F(r')}	IMAG{F(r')}	REAL{F(r')}	IMAG{F(r')}
15 SD, Nc=Ns=4	-2.98383298898281E-04	3.26513705511685E-07	-2.98383804959292E-06	3.26513705640839E-09
15 SD, Nc=Ns=5	-2.98383298895017E-04	3.26513704775711E-07	-2.98383804956028E-06	3.26513704904855E-09
15 SD, Nc=Ns=6	-2.98383298895019E-04	3.26513704776294E-07	-2.98383804956031E-06	3.26513704905455E-09
15 SD, Nc=Ns=7	-2.98383298895019E-04	3.26513704776294E-07	-2.98383804956031E-06	3.26513704905455E-09
15 SD, Nc=Ns=8	-2.98383298895019E-04	3.26513704776294E-07	-2.98383804956031E-06	3.26513704905455E-09
15 SD, Nc=Ns=9	-2.98383298895019E-04	3.26513704776294E-07	-2.98383804956031E-06	3.26513704905455E-09
15 SD, Nc=Ns=10	-2.98383298895019E-04	3.26513704776294E-07	-2.98383804956031E-06	3.26513704905455E-09
15 SD, Nc=Ns=11	-2.98383298895019E-04	3.26513704776294E-07	-2.98383804956031E-06	3.26513704905455E-09
15 SD, Nc=Ns=12	-2.98383298895019E-04	3.26513704776294E-07	-2.98383804956031E-06	3.26513704905455E-09

THIS PAGE INTENTIONALLY LEFT BLANK

APPENDIX F
CUBATURE COMPUTATION OF DOUBLE-LAYER POTENTIAL

We examine the calculation of the double-layer potential

$$F(\mathbf{r}') = -\frac{1}{4\pi} \int_T \frac{\partial}{\partial z}\left(\frac{e^{-ikR}}{R}\right) dS . \tag{F.1}$$

The expression as is presents problems due to the presence of the normal derivative. We re-write it in the form

$$F(\mathbf{r}') = -\frac{1}{4\pi} \int_T \frac{\partial}{\partial z}\left(\frac{e^{-ikR}-1}{R}\right) dS - \frac{1}{4\pi} \int_T \frac{\partial}{\partial z}\left(\frac{1}{R}\right) dS . \tag{F.2}$$

The second term on the right is related to the solid-angle integral and we have calculated that elsewhere. We write for the first term

$$-\frac{1}{4\pi} \int_T \frac{\partial}{\partial z}\left(\frac{e^{-ikR}-1}{R}\right) dS = -\frac{1}{4\pi} \int_T \frac{\partial}{\partial z}\left[\frac{\cos(kR)-1-i\sin(kR)}{R}\right] dS$$

$$= -\frac{1}{4\pi} \int_T \frac{\partial}{\partial z}\left[\frac{\cos(kR)-1}{R}\right] dS + \frac{i}{4\pi} \int_T \frac{\partial}{\partial z}\left[\frac{\sin(kR)}{R}\right] dS . \tag{F.3}$$

Performing the differentiations, we get

$$\frac{\partial}{\partial z}\left[\frac{\cos(kR)-1}{R}\right] = \frac{-kR\sin(kR)-\left[\cos(kR)-1\right]}{R^2}\cdot\frac{\partial R}{\partial z}\bigg|_{z=0}$$

$$= k^2 \frac{(kR)\sin(kR)+\left[\cos(kR)-1\right]}{(kR)^2}\left(\frac{z'}{R}\right) \tag{F.4}$$

and

$$\frac{\partial}{\partial z}\left[\frac{\sin(kR)}{R}\right] = \frac{(kR)\cos(kR)-\sin(kR)}{R^2}\cdot\frac{\partial R}{\partial z}\bigg|_{z=0} = -k^2 \frac{(kR)\cos(kR)-\sin(kR)}{(kR)^2}\left(\frac{z'}{R}\right). \tag{F.5}$$

In (F.4) we expand the trigonometric functions in power series and we keep enough terms to make the remainder smaller than a prescribed value

$$\frac{\partial}{\partial z}\left[\frac{\cos(kR)-1}{R}\right] = \left(\frac{z'}{R}\right)k^2\left\{\sum_{n=0}^{L-1}(-1)^n\frac{(kR)^{2n}}{(2n+1)!} + \sum_{n=1}^{M-1}(-1)^n\frac{(kR)^{2n-2}}{(2n)!}\right\}. \tag{F.6}$$

We let N be the greater of L and M, and write

$$\frac{\partial}{\partial z}\left[\frac{\cos(kR)-1}{R}\right]=\left(\frac{z'}{R}\right)k^2\left\{\sum_{n=0}^{N-1}(-1)^n\frac{(kR)^{2n}}{(2n+1)!}-\sum_{n=0}^{N-2}(-1)^n\frac{(kR)^{2n}}{(2n+2)!}\right\}$$

$$=\left(\frac{z'}{R}\right)k^2\left\{\sum_{n=0}^{N-2}(-1)^n(kR)^{2n}\left[\frac{1}{(2n+1)!}-\frac{1}{(2n+2)!}\right]-(-1)^N\frac{(kR)^{2(N-1)}}{(2N-1)!}\right\}$$

$$=\left(\frac{z'}{R}\right)k^2\left\{\sum_{n=0}^{N-2}(-1)^n\frac{(2n+1)(kR)^{2n}}{(2n+2)!}-(-1)^N\frac{(kR)^{2(N-1)}}{(2N-1)!}\right\}. \tag{F.7}$$

We repeat this process for (F.5)

$$\frac{\partial}{\partial z}\left[\frac{\sin(kR)}{R}\right]=-\left(\frac{z'}{R}\right)k^2\left\{\sum_{n=0}^{N-1}(-1)^n\frac{(kR)^{2n-1}}{(2n)!}-\sum_{n=0}^{N-1}(-1)^n\frac{(kR)^{2n-1}}{(2n+1)!}\right\}$$

$$=-2\left(\frac{z'}{R}\right)k^2\sum_{n=1}^{N-1}(-1)^n\frac{n(kR)^{2n-1}}{(2n+1)!}=2z'k^3\sum_{n=0}^{N-2}(-1)^n\frac{(n+1)(kR)^{2n}}{(2n+3)!}. \tag{F.8}$$

We note that this expression is well behaved for small kR; in fact, if we plot a normalized form of (F.5)

$$f(kR)=\frac{1}{k^3z'}\frac{\partial}{\partial z}\left[\frac{\sin(kR)}{R}\right]=-\frac{(kR)\cos(kR)-\sin(kR)}{(kR)^3} \tag{F.9}$$

we get a rather slowly varying graph, even around the origin (see Figure F.1). A low-order cubature should then work very well on this function.

This is no longer true for (F.7) when kR is small, as can be seen in Figure F.2 where we plot the function g

$$g(kR)=\frac{1}{k^3z'}\frac{\partial}{\partial z}\left[\frac{\cos(kR)-1}{R}\right]=\frac{(kR)\sin(kR)+\left[\cos(kR)-1\right]}{(kR)^3}. \tag{F.10}$$

We return to (F.4) and write

$$\frac{\partial}{\partial z}\left[\frac{\cos(kR)-1}{R}\right]=\frac{k^2}{2}\left(\frac{z'}{R}\right)+k^2\left\{\frac{(kR)\sin(kR)+\left[\cos(kR)-1\right]}{(kR)^2}-\frac{1}{2}\right\}\left(\frac{z'}{R}\right)$$

$$=\frac{k^2}{2}\left(\frac{z'}{R}\right)+k^2\left\{\frac{2(kR)\sin(kR)+2\left[\cos(kR)-1\right]-(kR)^2}{2(kR)^2}\right\}\left(\frac{z'}{R}\right). \tag{F.11}$$
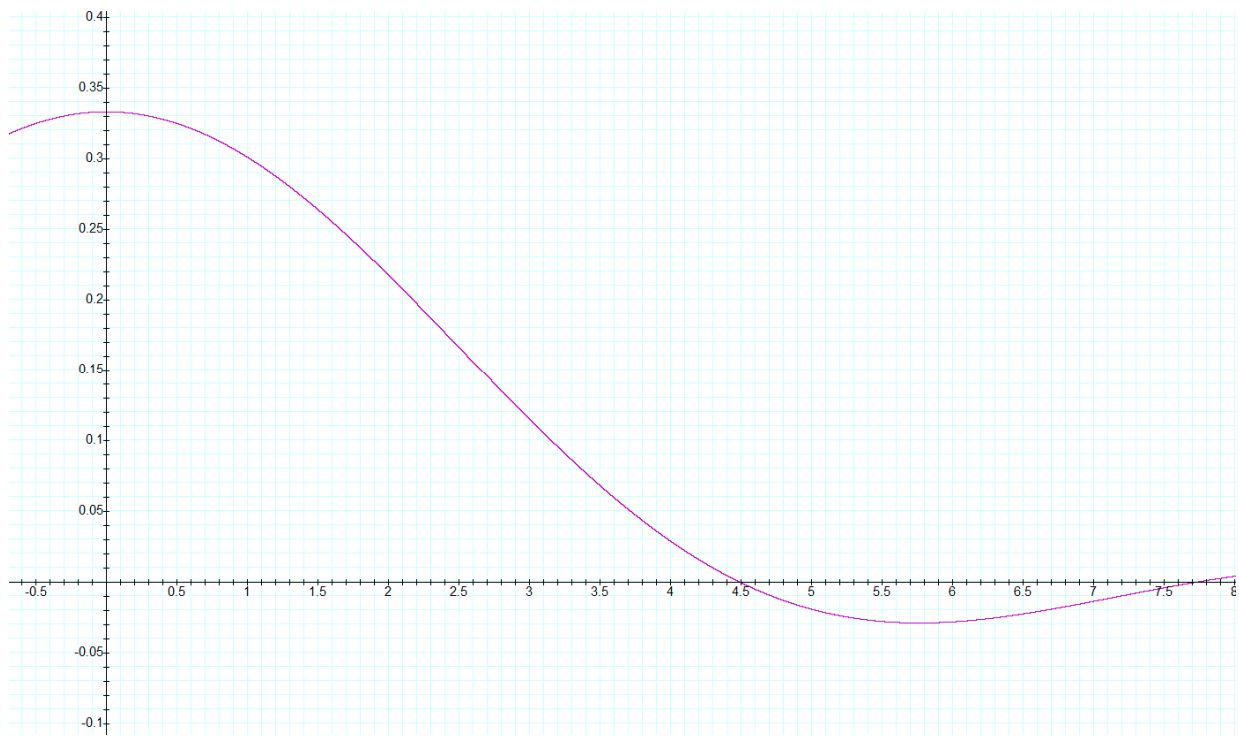
Figure F.1: The graph of the function *f* in (F.9).
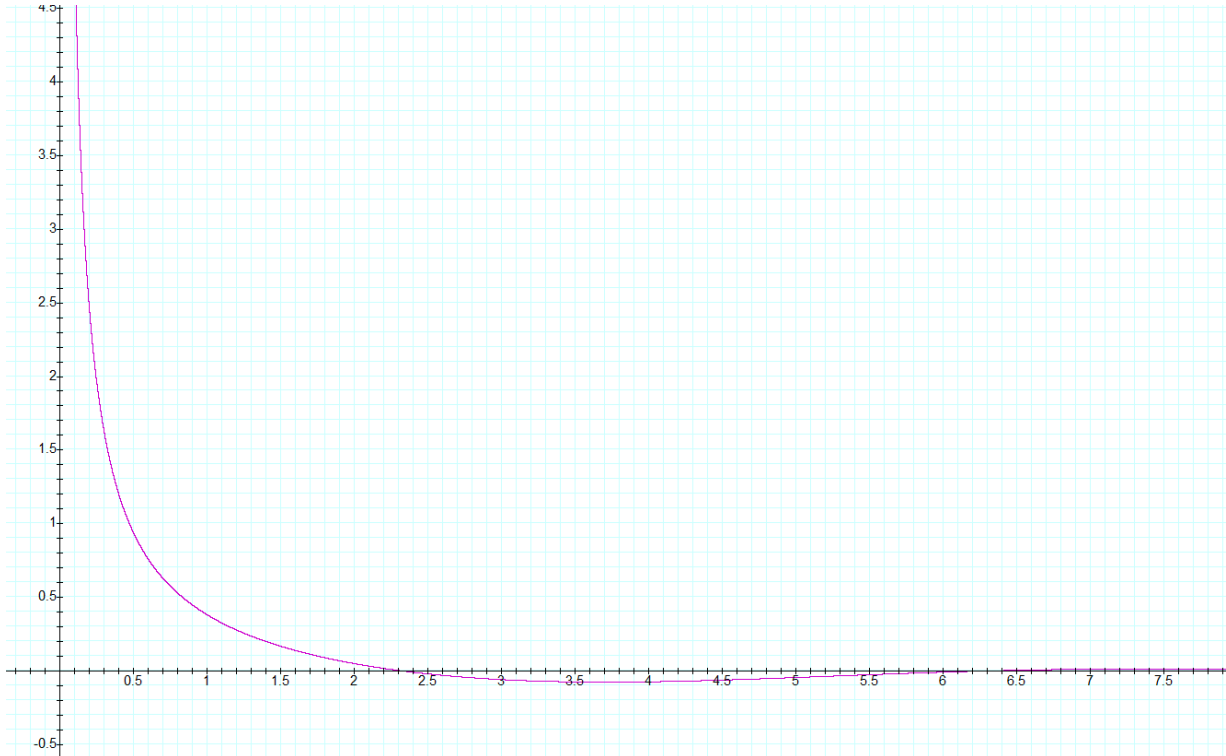
Figure F.2: The graph of the function *g* in (F.10).

APPENDIX F

If we employ (F.7) in (F.11), we get

$$\frac{\partial}{\partial z}\left[\frac{\cos(kR)-1}{R}\right]=\frac{k^2}{2}\left(\frac{z'}{R}\right)+\left(\frac{z'}{R}\right)k^2\left\{\sum_{n=1}^{N-2}(-1)^n\frac{(2n+1)(kR)^{2n}}{(2n+2)!}-(-1)^N\frac{(kR)^{2(N-1)}}{(2N-1)!}\right\}$$

$$=\frac{k^2}{2}\left(\frac{z'}{R}\right)-z'k^3\left\{\sum_{n=0}^{N-3}(-1)^n\frac{(2n+3)(kR)^{2n+1}}{(2n+4)!}+(-1)^N\frac{(kR)^{2N-3}}{(2N-1)!}\right\} \qquad \text{(F.12)}$$

which clearly shows that the expression in braces is well behaved for all kR. We can also demonstrate this by looking at the graph of the function

$$h(kR)=\frac{2(kR)\sin(kR)+2\left[\cos(kR)-1\right]-(kR)^2}{2(kR)^3} \qquad \text{(F.13)}$$

in Figure F.3.
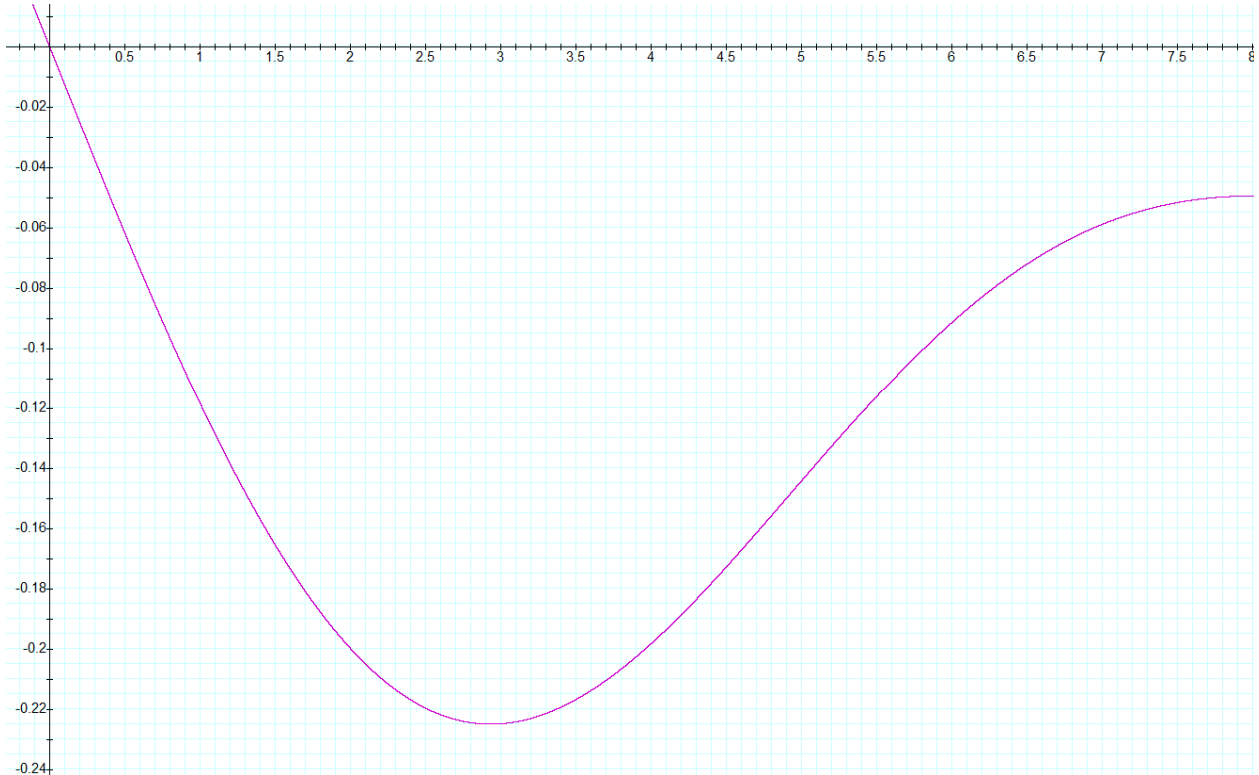
Figure F.3: The graph of the function h in (F.13).

We return to (F.3) and substitute (F.5) and (F.11) in it

$$-\frac{1}{4\pi}\int_T \frac{\partial}{\partial z}\left(\frac{e^{-ikR}-1}{R}\right)dS = -\frac{1}{4\pi}\int_T \frac{\partial}{\partial z}\left[\frac{\cos(kR)-1}{R}\right]dS + \frac{i}{4\pi}\int_T \frac{\partial}{\partial z}\left[\frac{\sin(kR)}{R}\right]dS$$

$$= -\frac{k^2 z'}{8\pi}\int_T \frac{1}{R}dS - \frac{k^3 z'}{8\pi}\int_T \frac{2(kR)\sin(kR)+2\left[\cos(kR)-1\right]-(kR)^2}{(kR)^3}dS$$

$$-\frac{ik^3 z'}{4\pi}\int_T \frac{(kR)\cos(kR)-\sin(kR)}{(kR)^3}dS \ . \tag{F.14}$$

The last two integrals on the right may be computed using cubatures. The first integral is identical to Q_0 in (2.4). It has been thoroughly studied in Section 2 of reference 1. The appropriate integral there is given by the second one in (1.21), p. 9, with n equal to zero. This is transformed to three line integrals in (2.1), p. 11. These line integrals are subsequently evaluated starting with Subsection 2.2, p. 17.

THIS PAGE INTENTIONALLY LEFT BLANK

APPENDIX G
CUBATURE RESULTS FOR THE CASES OF TABLE 6.14

In this Appendix, we complete the presentation of the data for the cubature calculations for the points of Table 6.14. The results for Case 36 are displayed in Table 6.17. Here, we use the same format to display the results for the rest of the cases. The conclusions are summarized in Figures 6.4 to 6.7.

Table G.1.a: Comparison of our results for the surface integral of Case 37 with those obtained through a Riemann sum and cubatures.

z′ =		5.0	4.5
15 SD, Nc=Ns=8			
MFIE METHOD	REAL{F(r')}	1.66229178654613E-03	2.67743268334125E-04
	IMAG{F(r')}	4.90079446997064E-03	5.78612816705257E-03
RIEMANN SUM	REAL{F(r')}	1.66229178673289E-03	2.67743268658897E-04
N = 10,000	IMAG{F(r')}	4.90079446948171E-03	5.78612816653607E-03
CUBATURE DIM	SD	RE{F(r')}	
21		1.66229178654563E-03	2.67743268333071E-04
28	15	1.66229178654613E-03	2.67743268334128E-04
36		1.66229178654613E-03	2.67743268334128E-04
45		1.66229178654614E-03	2.67743268334133E-04
46		1.66229178654613E-03	2.67743268334126E-04
54		1.66229178654613E-03	2.67743268334126E-04
55		1.66229178654613E-03	2.67743268334128E-04
66		1.66229178654613E-03	2.67743268334130E-04
78		1.66229178654613E-03	2.67743268334130E-04
85		1.66229178654613E-03	2.67743268334133E-04
91		1.66229178654613E-03	2.67743268334135E-04
105		1.66229178654613E-03	2.67743268334133E-04
120	14	1.66229178654613E-03	2.67743268334124E-04
126		1.66229178654612E-03	2.67743268334130E-04
CUBATURE DIM	SD	IM{F(r')}	
21	15, 15	4.90079446997064E-03	5.78612816705257E-03
28		4.90079446997064E-03	5.78612816705257E-03
36		4.90079446997063E-03	5.78612816705256E-03
45		4.90079446997065E-03	5.78612816705259E-03
46		4.90079446997063E-03	5.78612816705256E-03
54		4.90079446997063E-03	5.78612816705256E-03
55		4.90079446997064E-03	5.78612816705257E-03
66		4.90079446997063E-03	5.78612816705257E-03
78		4.90079446997063E-03	5.78612816705257E-03
85		4.90079446997063E-03	5.78612816705256E-03
91		4.90079446997063E-03	5.78612816705257E-03
105		4.90079446997063E-03	5.78612816705257E-03
120		4.90079446997064E-03	5.78612816705257E-03
126		4.90079446997063E-03	5.78612816705256E-03

Table G.1.b: Comparison of our results for the surface integral of Case 37 with those obtained through a Riemann sum and cubatures.

z′ =		1.0E+00	1.0E-02
15 SD, Nc=Ns=8			
MFIE METHOD	REAL{F(r')}	-3.30414650308277E-02	-1.23597765854119E-01
	IMAG{F(r')}	3.11999935001460E-03	3.24684604964614E-05
RIEMANN SUM	REAL{F(r')}	-3.30414650272966E-02	-1.23597765853978E-01
N = 10,000	IMAG{F(r')}	3.11999934980801E-03	3.24684604943186E-05
CUBATURE DIM	SD	RE{F(r')}	
21		-3.30414650438932E-02	-1.23597766234781E-01
28		-3.30414650318885E-02	-1.23597765889297E-01
36		-3.30414650308531E-02	-1.23597765930566E-01
45		-3.30414650308289E-02	-1.23597765825503E-01
46		-3.30414650308252E-02	-1.23597765902280E-01
54		-3.30414650308280E-02	-1.23597765892955E-01
55		-3.30414650308278E-02	-1.23597765841787E-01
66	15	-3.30414650308277E-02	-1.23597765854805E-01
78		-3.30414650308277E-02	-1.23597765862033E-01
85		-3.30414650308277E-02	-1.23597765862308E-01
91		-3.30414650308277E-02	-1.23597765848987E-01
105		-3.30414650308277E-02	-1.23597765857442E-01
120		-3.30414650308277E-02	-1.23597765854512E-01
126	12	-3.30414650308277E-02	-1.23597765854274E-01
CUBATURE DIM	SD	IM{F(r')}	
21		3.11999935001461E-03	3.24684604964487E-05
28		3.11999935001461E-03	3.24684604964487E-05
36	15	3.11999935001460E-03	3.24684604964486E-05
45	11	3.11999935001461E-03	3.24684604964489E-05
46		3.11999935001460E-03	3.24684604964486E-05
54		3.11999935001460E-03	3.24684604964487E-05
55		3.11999935001461E-03	3.24684604964487E-05
66		3.11999935001460E-03	3.24684604964488E-05
78		3.11999935001460E-03	3.24684604964487E-05
85		3.11999935001460E-03	3.24684604964487E-05
91		3.11999935001461E-03	3.24684604964488E-05
105		3.11999935001460E-03	3.24684604964487E-05
120		3.11999935001461E-03	3.24684604964486E-05
126		3.11999935001460E-03	3.24684604964487E-05

Table G.1.c: Comparison of our results for the surface integral of Case 37 with those obtained through a Riemann sum and cubatures.

z' =		1.0E-04	1.0E-06
15 SD, Nc=Ns=8			
MFIE METHOD	REAL{F(r')}	-1.24986000612199E-01	-1.24999860001488E-01
	IMAG{F(r')}	3.24685891484467E-07	3.24685891594534E-09
RIEMANN SUM	REAL{F(r')}	-1.24986000611931E-01	-1.24999860007953E-01
N = 10,000	IMAG{F(r')}	3.24685891454803E-07	3.24685891583276E-09
CUBATURE DIM	SD	RE{F(r')}	
21		-1.24986000615963E-01	-1.24999860001526E-01
28		-1.24986000612553E-01	-1.24999860001492E-01
36		-1.24986000612965E-01	-1.24999860001496E-01
45		-1.24986000612010E-01	-1.24999859883931E-01
46		-1.24986000612687E-01	-1.24999860001493E-01
54		-1.24986000612612E-01	-1.24999860001493E-01
55		-1.24986000612120E-01	-1.24999859923020E-01
66	12	-1.24986000612220E-01	-1.24999860001489E-01
78		-1.24986000612306E-01	-1.24999860001490E-01
85		-1.24986000612301E-01	-1.24999860001489E-01
91	15	-1.24986000612160E-01	-1.24999860001488E-01
105		-1.24986000612241E-01	-1.24999860001489E-01
120		-1.24986000612212E-01	-1.24999860001489E-01
126		-1.24986000612210E-01	-1.24999860001489E-01
CUBATURE DIM	SD	IM{F(r')}	
21		3.24685891476039E-07	3.24685891604692E-09
28		3.24685891476039E-07	3.24685891604691E-09
36		3.24685891476038E-07	3.24685891604691E-09
45		3.24685891486629E-07	3.24686002148726E-09
46		3.24685891476039E-07	3.24685891604692E-09
54	10	3.24685891476040E-07	3.24685891604690E-09
55	11	3.24685891483108E-07	3.24685965392274E-09
66		3.24685891476041E-07	3.24685891604691E-09
78		3.24685891476041E-07	3.24685891604691E-09
85		3.24685891476038E-07	3.24685891604691E-09
91		3.24685891476038E-07	3.24685891604691E-09
105		3.24685891476040E-07	3.24685891604691E-09
120		3.24685891476040E-07	3.24685891604690E-09
126		3.24685891476040E-07	3.24685891604690E-09

Table G.2.a: Comparison of our results for the surface integral of Case 38 with those obtained through a Riemann sum and cubatures.

z' =		5.0	4.5
15 SD, Nc=Ns=8			
MFIE METHOD	REAL{F(r')}	1.72890617968236E-03	3.77040226832734E-04
	IMAG{F(r')}	4.80316359879895E-03	5.68301993259889E-03
RIEMANN SUM	REAL{F(r')}	1.72890617951762E-03	3.77040226535453E-04
N = 10,000	IMAG{F(r')}	4.80316359927620E-03	5.68301993310194E-03
CUBATURE DIM	**SD**	**RE{F(r')}**	
21		1.72890617968219E-03	3.77040226832552E-04
28	15	1.72890617968236E-03	3.77040226832749E-04
36		1.72890617968236E-03	3.77040226832744E-04
45		1.72890617968236E-03	3.77040226832749E-04
46		1.72890617968236E-03	3.77040226832742E-04
54		1.72890617968235E-03	3.77040226832744E-04
55		1.72890617968235E-03	3.77040226832744E-04
66		1.72890617968236E-03	3.77040226832742E-04
78		1.72890617968236E-03	3.77040226832749E-04
85		1.72890617968236E-03	3.77040226832749E-04
91		1.72890617968236E-03	3.77040226832749E-04
105	13	1.72890617968235E-03	3.77040226832741E-04
120		1.72890617968236E-03	3.77040226832744E-04
126		1.72890617968235E-03	3.77040226832742E-04
CUBATURE DIM	**SD**	**IM{F(r')}**	
21	15, 15	4.80316359879895E-03	5.68301993259889E-03
28		4.80316359879895E-03	5.68301993259889E-03
36		4.80316359879895E-03	5.68301993259889E-03
45		4.80316359879896E-03	5.68301993259890E-03
46		4.80316359879895E-03	5.68301993259889E-03
54		4.80316359879895E-03	5.68301993259888E-03
55		4.80316359879892E-03	5.68301993259886E-03
66		4.80316359879895E-03	5.68301993259889E-03
78		4.80316359879895E-03	5.68301993259889E-03
85		4.80316359879895E-03	5.68301993259889E-03
91		4.80316359879895E-03	5.68301993259889E-03
105		4.80316359879895E-03	5.68301993259889E-03
120		4.80316359879896E-03	5.68301993259890E-03
126		4.80316359879895E-03	5.68301993259889E-03

Table G.2.b: Comparison of our results for the surface integral of Case 38 with those obtained through a Riemann sum and cubatures.

z′ =		1.0E+00	1.0E-02
15 SD, Nc=Ns=8			
MFIE METHOD	REAL{F(r')}	-2.61083307127456E-02	-6.20687168677050E-02
	IMAG{F(r')}	3.07874207413142E-03	3.20439982334867E-05
RIEMANN SUM	REAL{F(r')}	-2.61083307149989E-02	-6.20687168677565E-02
N = 10,000	IMAG{F(r')}	3.07874207433365E-03	3.20439982355682E-05
CUBATURE DIM	**SD**	RE{F(r')}	
21		-2.61083307217141E-02	-6.20687169957358E-02
28		-2.61083307132206E-02	-6.20687168032204E-02
36		-2.61083307127649E-02	-6.20687168915915E-02
45		-2.61083307127448E-02	-6.20687168431814E-02
46		-2.61083307127475E-02	-6.20687168821266E-02
54		-2.61083307127455E-02	-6.20687168767932E-02
55		-2.61083307127457E-02	-6.20687168541300E-02
66	15	-2.61083307127456E-02	-6.20687168688377E-02
78		-2.61083307127456E-02	-6.20687168704573E-02
85		-2.61083307127456E-02	-6.20687168707639E-02
91		-2.61083307127456E-02	-6.20687168662112E-02
105	10	-2.61083307127456E-02	-6.20687168684284E-02
120		-2.61083307127456E-02	-6.20687168685661E-02
126		-2.61083307127456E-02	-6.20687168684846E-02
CUBATURE DIM	**SD**	IM{F(r')}	
21	13	3.07874207413143E-03	3.20439982334859E-05
28	15	3.07874207413142E-03	3.20439982334858E-05
36		3.07874207413142E-03	3.20439982334859E-05
45		3.07874207413143E-03	3.20439982334858E-05
46		3.07874207413142E-03	3.20439982334859E-05
54		3.07874207413142E-03	3.20439982334858E-05
55		3.07874207413141E-03	3.20439982334857E-05
66		3.07874207413142E-03	3.20439982334858E-05
78		3.07874207413142E-03	3.20439982334858E-05
85		3.07874207413142E-03	3.20439982334859E-05
91		3.07874207413142E-03	3.20439982334859E-05
105		3.07874207413142E-03	3.20439982334858E-05
120		3.07874207413143E-03	3.20439982334859E-05
126		3.07874207413142E-03	3.20439982334858E-05

Table G.2.c: Comparison of our results for the surface integral of Case 38 with those obtained through a Riemann sum and cubatures.

z' =		1.0E-04	1.0E-06
15 SD, Nc=Ns=8			
MFIE METHOD	REAL{F(r')}	-6.24956990989627E-02	-6.24999569922107E-02
	IMAG{F(r')}	3.20441256830233E-07	3.20441257358174E-09
RIEMANN SUM	REAL{F(r')}	-6.24956990988243E-02	-6.24999569919056E-02
N = 10,000	IMAG{F(r')}	3.20441256846239E-07	3.20441256973727E-09
CUBATURE DIM	**SD**	**RE{F(r')}**	
21		-6.24956991001147E-02	-6.24999569922222E-02
28		-6.24956990982312E-02	-6.24999569922033E-02
36		-6.24956990991425E-02	-6.24999569922125E-02
45		-6.24956990988784E-02	-6.24999568746547E-02
46		-6.24956990990698E-02	-6.24999569922117E-02
54		-6.24956990990267E-02	-6.24999569922113E-02
55		-6.24956990988958E-02	-6.24999569235308E-02
66		-6.24956990989744E-02	-6.24999569922108E-02
78		-6.24956990989821E-02	-6.24999569922109E-02
85		-6.24956990989821E-02	-6.24999569922109E-02
91	13, 15	-6.24956990989635E-02	-6.24999569922107E-02
105		-6.24956990989641E-02	-6.24999569922107E-02
120		-6.24956990989685E-02	-6.24999569922107E-02
126		-6.24956990989677E-02	-6.24999569922107E-02
CUBATURE DIM	**SD**	**IM{F(r')}**	
21		3.20441256825502E-07	3.20441256952951E-09
28		3.20441256825502E-07	3.20441256952952E-09
36		3.20441256825502E-07	3.20441256952951E-09
45		3.20441256836092E-07	3.20441367496987E-09
46		3.20441256825502E-07	3.20441256952951E-09
54	10	3.20441256825503E-07	3.20441256952952E-09
55		3.20441256831688E-07	3.20441321536074E-09
66		3.20441256825502E-07	3.20441256952952E-09
78		3.20441256825503E-07	3.20441256952952E-09
85		3.20441256825503E-07	3.20441256952951E-09
91	8	3.20441256825502E-07	3.20441256952953E-09
105		3.20441256825502E-07	3.20441256952952E-09
120		3.20441256825503E-07	3.20441256952952E-09
126		3.20441256825503E-07	3.20441256952951E-09

NAWCADPAX/TR-2012/200

Table G.3.a: Comparison of our results for the surface integral of Case 39 with those obtained through a Riemann sum and cubatures.

z' =		5.0	4.5
15 SD, Nc=Ns=8			
MFIE METHOD	REAL{F(r')}	1.62745189256202E-03	2.10686757212199E-04
	IMAG{F(r')}	4.95019906577089E-03	5.83827756766797E-03
RIEMANN SUM	REAL{F(r')}	1.62745189236729E-03	2.10686756873228E-04
N = 10,000	IMAG{F(r')}	4.95019906626393E-03	5.83827756818758E-03
CUBATURE DIM	**SD**	**RE{F(r')}**	
21		1.62745189256148E-03	2.10686757211024E-04
28	15	1.62745189256202E-03	2.10686757212207E-04
36		1.62745189256202E-03	2.10686757212207E-04
45		1.62745189256203E-03	2.10686757212216E-04
46		1.62745189256202E-03	2.10686757212206E-04
54	12	1.62745189256202E-03	2.10686757212201E-04
55		1.62745189256202E-03	2.10686757212206E-04
66		1.62745189256202E-03	2.10686757212209E-04
78		1.62745189256202E-03	2.10686757212213E-04
85		1.62745189256203E-03	2.10686757212207E-04
91		1.62745189256203E-03	2.10686757212213E-04
105		1.62745189256202E-03	2.10686757212211E-04
120		1.62745189256202E-03	2.10686757212211E-04
126		1.62745189256202E-03	2.10686757212213E-04
CUBATURE DIM	**SD**	**IM{F(r')}**	
21	15	4.95019906577089E-03	5.83827756766798E-03
28	15	4.95019906577089E-03	5.83827756766797E-03
36		4.95019906577089E-03	5.83827756766797E-03
45		4.95019906577090E-03	5.83827756766798E-03
46		4.95019906577089E-03	5.83827756766797E-03
54		4.95019906577089E-03	5.83827756766797E-03
55		4.95019906577089E-03	5.83827756766797E-03
66		4.95019906577089E-03	5.83827756766797E-03
78		4.95019906577089E-03	5.83827756766797E-03
85		4.95019906577089E-03	5.83827756766797E-03
91		4.95019906577089E-03	5.83827756766798E-03
105		4.95019906577089E-03	5.83827756766797E-03
120		4.95019906577088E-03	5.83827756766796E-03
126		4.95019906577089E-03	5.83827756766797E-03

Table G.3.b: Comparison of our results for the surface integral of Case 39 with those obtained through a Riemann sum and cubatures.

z′ =		1.0E+00	1.0E-02
15 SD, Nc=Ns=8			
MFIE METHOD	REAL{F(r')}	-3.85251154819883E-02	-2.45768216011319E-01
	IMAG{F(r')}	3.14083404791340E-03	3.26827981281800E-05
RIEMANN SUM	REAL{F(r')}	-3.85251154867750E-02	-2.45768216011701E-01
N = 10,000	IMAG{F(r')}	3.14083404812180E-03	3.26827981303243E-05
CUBATURE DIM	**SD**	RE{F(r')}	
21		-3.85251155571443E-02	-2.45768238119501E-01
28		-3.85251154844081E-02	-2.45768223087241E-01
36		-3.85251154822801E-02	-2.45768222768720E-01
45		-3.85251154819970E-02	-2.45768218058558E-01
46		-3.85251154819630E-02	-2.45768211272347E-01
54		-3.85251154819900E-02	-2.45768216765815E-01
55	10	-3.85251154819879E-02	-2.45768216054808E-01
66	15	-3.85251154819883E-02	-2.45768214392943E-01
78		-3.85251154819883E-02	-2.45768217743930E-01
85		-3.85251154819883E-02	-2.45768216711269E-01
91		-3.85251154819883E-02	-2.45768214753590E-01
105		-3.85251154819883E-02	-2.45768215655422E-01
120		-3.85251154819883E-02	-2.45768217248556E-01
126		-3.85251154819883E-02	-2.45768216240576E-01
CUBATURE DIM	**SD**	IM{F(r')}	
21	15, 13	3.14083404791340E-03	3.26827981281858E-05
28		3.14083404791340E-03	3.26827981281880E-05
36		3.14083404791340E-03	3.26827981281867E-05
45		3.14083404791341E-03	3.26827981281870E-05
46		3.14083404791340E-03	3.26827981281865E-05
54		3.14083404791340E-03	3.26827981281866E-05
55		3.14083404791340E-03	3.26827981281868E-05
66		3.14083404791340E-03	3.26827981281865E-05
78		3.14083404791340E-03	3.26827981281874E-05
85		3.14083404791340E-03	3.26827981281861E-05
91		3.14083404791340E-03	3.26827981281866E-05
105		3.14083404791340E-03	3.26827981281858E-05
120		3.14083404791340E-03	3.26827981281866E-05
126		3.14083404791340E-03	3.26827981281862E-05

Table G.3.c: Comparison of our results for the surface integral of Case 39 with those obtained through a Riemann sum and cubatures.

z' =		1.0E-04	1.0E-06
15 SD, Nc=Ns=8			
MFIE METHOD	REAL{F(r')}	-2.49957723083909E-01	-2.49999577237499E-01
	IMAG{F(r')}	3.26829273854127E-07	3.26829273878434E-09
RIEMANN SUM	REAL{F(r')}	-2.49957723083307E-01	-2.49999577256479E-01
N = 10,000	IMAG{F(r')}	3.26829273871477E-07	3.26829274000744E-09
CUBATURE DIM	SD	RE{F(r')}	
21		-2.49957723309702E-01	-2.49999577239756E-01
28		-2.49957723158600E-01	-2.49999577238245E-01
36		-2.49957723152704E-01	-2.49999577238186E-01
45		-2.49957723106961E-01	-2.49999577237729E-01
46		-2.49957723035387E-01	-2.49999577237013E-01
54		-2.49957723091232E-01	-2.49999577237572E-01
55	11, 14	-2.49957723084043E-01	-2.49999577237500E-01
66		-2.49957723066964E-01	-2.49999577237329E-01
78		-2.49957723102660E-01	-2.49999577237686E-01
85		-2.49957723091748E-01	-2.49999577237577E-01
91		-2.49957723070645E-01	-2.49999577237366E-01
105		-2.49957723081466E-01	-2.49999577237474E-01
120		-2.49957723097360E-01	-2.49999577237633E-01
126		-2.49957723086500E-01	-2.49999577237524E-01
CUBATURE DIM	SD	IM{F(r')}	
21		3.26829273850200E-07	3.26829273979439E-09
28	11	3.26829273850206E-07	3.26829273979443E-09
36		3.26829273850184E-07	3.26829273979447E-09
45		3.26829273850196E-07	3.26829273979437E-09
46		3.26829273850186E-07	3.26829273979442E-09
54		3.26829273850187E-07	3.26829273979442E-09
55		3.26829273850185E-07	3.26829273979444E-09
66		3.26829273850186E-07	3.26829273979443E-09
78		3.26829273850185E-07	3.26829273979442E-09
85		3.26829273850265E-07	3.26829273979717E-09
91		3.26829273850184E-07	3.26829273979442E-09
105		3.26829273850156E-07	3.26829273979450E-09
120	9	3.26829273850185E-07	3.26829273979435E-09
126		3.26829273850184E-07	3.26829273979440E-09

Table G.4.a: Comparison of our results for the surface integral of Case 40 with those obtained through a Riemann sum and cubatures.

z' =		5.0	4.5
15 SD, Nc=Ns=8			
MFIE METHOD	REAL{F(r')}	1.63265177430638E-03	2.19197452706583E-04
	IMAG{F(r')}	4.94291929209383E-03	5.83059487773856E-03
RIEMANN SUM	REAL{F(r')}	1.63265177408649E-03	2.19197452322990E-04
N = 10,000	IMAG{F(r')}	4.94291929265363E-03	5.83059487832946E-03
CUBATURE DIM	SD	RE{F(r')}	
21		1.63265177430584E-03	2.19197452705390E-04
28	15	1.63265177430639E-03	2.19197452706573E-04
36		1.63265177430639E-03	2.19197452706573E-04
45		1.63265177430640E-03	2.19197452706578E-04
46		1.63265177430639E-03	2.19197452706571E-04
54		1.63265177430639E-03	2.19197452706573E-04
55		1.63265177430639E-03	2.19197452706573E-04
66		1.63265177430639E-03	2.19197452706569E-04
78		1.63265177430639E-03	2.19197452706575E-04
85		1.63265177430640E-03	2.19197452706578E-04
91	14	1.63265177430640E-03	2.19197452706580E-04
105		1.63265177430639E-03	2.19197452706569E-04
120		1.63265177430639E-03	2.19197452706573E-04
126		1.63265177430639E-03	2.19197452706561E-04
CUBATURE DIM	SD	IM{F(r')}	
21	15	4.94291929209384E-03	5.83059487773856E-03
28	15	4.94291929209383E-03	5.83059487773856E-03
36		4.94291929209383E-03	5.83059487773856E-03
45		4.94291929209384E-03	5.83059487773857E-03
46		4.94291929209383E-03	5.83059487773856E-03
54		4.94291929209383E-03	5.83059487773856E-03
55		4.94291929209383E-03	5.83059487773856E-03
66		4.94291929209383E-03	5.83059487773856E-03
78		4.94291929209383E-03	5.83059487773856E-03
85		4.94291929209383E-03	5.83059487773856E-03
91		4.94291929209383E-03	5.83059487773856E-03
105		4.94291929209383E-03	5.83059487773856E-03
120		4.94291929209382E-03	5.83059487773854E-03
126		4.94291929209383E-03	5.83059487773856E-03

Table G.4.b: Comparison of our results for the surface integral of Case 40 with those obtained through a Riemann sum and cubatures.

z' =		1.0E+00	1.0E-02
15 SD, Nc=Ns=8			
MFIE METHOD	REAL{F(r')}	-3.75158019087259E-02	-2.93455187090841E-02
	IMAG{F(r')}	3.13776649153445E-03	3.26512413098946E-05
RIEMANN SUM	REAL{F(r')}	-3.75158019140408E-02	-2.93455187120835E-02
N = 10,000	IMAG{F(r')}	3.13776649177036E-03	3.26512413123283E-05
CUBATURE DIM	SD	RE{F(r')}	
21		-3.75158019812679E-02	-2.93455303684519E-02
28		-3.75158019110651E-02	-2.93455223333366E-02
36		-3.75158019090099E-02	-2.93455218856173E-02
45		-3.75158019087327E-02	-2.93455194872424E-02
46		-3.75158019087016E-02	-2.93455165345567E-02
54		-3.75158019087273E-02	-2.93455186197702E-02
55		-3.75158019087256E-02	-2.93455184475968E-02
66	15	-3.75158019087259E-02	-2.93455180058965E-02
78		-3.75158019087259E-02	-2.93455191161826E-02
85		-3.75158019087259E-02	-2.93455188876310E-02
91		-3.75158019087259E-02	-2.93455182707200E-02
105		-3.75158019087259E-02	-2.93455186095185E-02
120		-3.75158019087259E-02	-2.93455189809726E-02
126	12	-3.75158019087259E-02	-2.93455187119994E-02
CUBATURE DIM	SD	IM{F(r')}	
21		3.13776649153446E-03	3.26512413098932E-05
28		3.13776649153446E-03	3.26512413098933E-05
36	15, 13	3.13776649153445E-03	3.26512413098934E-05
45		3.13776649153446E-03	3.26512413098934E-05
46		3.13776649153445E-03	3.26512413098932E-05
54		3.13776649153446E-03	3.26512413098933E-05
55		3.13776649153446E-03	3.26512413098933E-05
66		3.13776649153446E-03	3.26512413098934E-05
78		3.13776649153446E-03	3.26512413098934E-05
85		3.13776649153446E-03	3.26512413098933E-05
91		3.13776649153446E-03	3.26512413098933E-05
105		3.13776649153445E-03	3.26512413098933E-05
120		3.13776649153445E-03	3.26512413098932E-05
126		3.13776649153445E-03	3.26512413098933E-05

Table G.4.c: Comparison of our results for the surface integral of Case 40 with those obtained through a Riemann sum and cubatures.

z' =		1.0E-04	1.0E-06
15 SD, Nc=Ns=8			
MFIE METHOD	REAL{F(r')}	-2.98383298895019E-04	-2.98383804956031E-06
	IMAG{F(r')}	3.26513704776294E-07	3.26513704905455E-09
RIEMANN SUM	REAL{F(r')}	-2.98383298926211E-04	-2.98383804987222E-06
N = 10,000	IMAG{F(r')}	3.26513704800458E-07	3.26513704929694E-09
CUBATURE DIM	SD	RE{F(r')}	
21		-2.98383416437008E-04	-2.98383922498115E-06
28		-2.98383335647856E-04	-2.98383841708918E-06
36		-2.98383331021954E-04	-2.98383837083002E-06
45		-2.98383306868899E-04	-2.98383812929930E-06
46		-2.98383276881133E-04	-2.98383782942117E-06
54		-2.98383297940533E-04	-2.98383804001537E-06
55		-2.98383296208764E-04	-2.98383802269768E-06
66		-2.98383291728056E-04	-2.98383797789053E-06
78		-2.98383303054725E-04	-2.98383809115745E-06
85		-2.98383300707697E-04	-2.98383806768710E-06
91		-2.98383294414452E-04	-2.98383800475453E-06
105		-2.98383297902541E-04	-2.98383803963552E-06
120		-2.98383301680386E-04	-2.98383807741404E-06
126	9, 10	-2.98383298924706E-04	-2.98383804985717E-06
CUBATURE DIM	SD	IM{F(r')}	
21	13	3.26513704776282E-07	3.26513704905445E-09
28	13	3.26513704776278E-07	3.26513704905448E-09
36		3.26513704776280E-07	3.26513704905446E-09
45		3.26513704776280E-07	3.26513704905448E-09
46		3.26513704776279E-07	3.26513704905447E-09
54		3.26513704776278E-07	3.26513704905447E-09
55		3.26513704776279E-07	3.26513704905446E-09
66		3.26513704776279E-07	3.26513704905446E-09
78		3.26513704776279E-07	3.26513704905447E-09
85		3.26513704776279E-07	3.26513704905446E-09
91		3.26513704776279E-07	3.26513704905447E-09
105		3.26513704776278E-07	3.26513704905447E-09
120		3.26513704776278E-07	3.26513704905446E-09
126		3.26513704776279E-07	3.26513704905446E-09

THIS PAGE INTENTIONALLY LEFT BLANK

APPENDIX H
LINE INTEGRAL RESULTS FOR REST OF CASES OF TABLE 6.14

In this Appendix, we present the rest of the line integral results for the points of Table 6.14. The first result, Case 38, was presented in Table 6.19.

Table H.1: The line integral of (6.3) for an OP above the interior point (-7/30, -7/30) of the triangle. The minimum distance of this point to a side is 10 mλ. Despite the small distance, the G-K quadrature remains stable in the approach to this point and agrees with our method to at least 14 SD.

Case	36	PRESENT METHOD		MATLAB G-K QUADRATURE	
z'	Side	RE{INTG_1}	IM{INTG_1}	RE{INTG_1}	IM{INTG_1}
5.0	S 1	-2.79991492725852E-01	8.51159900317967E-03	-2.79991492725852E-01	8.51159900317923E-03
	S 2	-1.98953683726784E-01	3.13739353010368E-03	-1.98953683726784E-01	3.13739353010371E-03
	S 3	-1.98953683726784E-01	3.13739353010368E-03	-1.98953683726784E-01	3.13739353010371E-03
1.0	S 1	8.40496217754253E-01	-8.04197056952424E-01	8.40496217754254E-01	-8.04197056952425E-01
	S 2	6.93958697338809E-01	-5.77816790212706E-01	6.93958697338809E-01	-5.77816790212707E-01
	S 3	6.93958697338809E-01	-5.77816790212706E-01	6.93958697338809E-01	-5.77816790212707E-01
0.01	S 1	1.90555978762984E+00	-8.60414763093154E-01	1.90555978762985E+00	-8.60414763093154E-01
	S 2	3.68186409929430E+00	-6.17941085308805E-01	3.68186409929431E+00	-6.17941085308805E-01
	S 3	3.68186409929430E+00	-6.17941085308805E-01	3.68186409929431E+00	-6.17941085308805E-01
1.E-04	S 1	1.90582347488829E+00	-8.60420497617676E-01	1.90582347488830E+00	-8.60420497617676E-01
	S 2	3.69035822004681E+00	-6.17945177996947E-01	3.69035822004681E+00	-6.17945177996947E-01
	S 3	3.69035822004681E+00	-6.17945177996947E-01	3.69035822004681E+00	-6.17945177996947E-01
1.E-06	S 1	1.90582350126170E+00	-8.60420498191129E-01	1.90582350126170E+00	-8.60420498191130E-01
	S 2	3.69035907413992E+00	-6.17945178406217E-01	3.69035907413992E+00	-6.17945178406217E-01
	S 3	3.69035907413992E+00	-6.17945178406217E-01	3.69035907413992E+00	-6.17945178406217E-01

Table H.2: The line integral of (6.3) for an OP above the 90-deg corner of the triangle. As the OP approaches this point, the G-K quadrature begins to lose SD over Sides 2 and 3, the two sides that have this corner in common. As expected, the loss occurs in the real part of the integral and its maximum is 3 SD.

Case	37	PRESENT METHOD		MATLAB G-K QUADRATURE	
z'	Side	RE{INTG_1}	IM{INTG_1}	RE{INTG_1}	IM{INTG_1}
5.0	S 1	-2.78895727915674E-01	1.16009605809162E-02	-2.78895727915675E-01	1.16009605809165E-02
	S 2	-1.98613359322592E-01	4.11400306068684E-03	-1.98613359322592E-01	4.11400306068682E-03
	S 3	-1.98613359322592E-01	4.11400306068684E-03	-1.98613359322592E-01	4.11400306068682E-03
1.0	S 1	7.57961656479037E-01	-7.94313693101739E-01	7.57961656479037E-01	-7.94313693101740E-01
	S 2	6.64800195907522E-01	-5.74698696029768E-01	6.64800195907522E-01	-5.74698696029768E-01
	S 3	6.64800195907522E-01	-5.74698696029768E-01	6.64800195907522E-01	-5.74698696029768E-01
0.01	S 1	1.54106739353266E+00	-8.50128426276417E-01	1.54106739353267E+00	-8.50128426276417E-01
	S 2	5.20119889335351E+00	-6.14696002448062E-01	5.20119889335352E+00	-6.14696002448062E-01
	S 3	5.20119889335351E+00	-6.14696002448062E-01	5.20119889335352E+00	-6.14696002448062E-01
1.E-04	S 1	1.54122507689600E+00	-8.50134119929503E-01	1.54122507689600E+00	-8.50134119929504E-01
	S 2	9.80640081789547E+00	-6.14700082256520E-01	9.80640081789577E+00	-6.14700082256521E-01
	S 3	9.80640081789547E+00	-6.14700082256520E-01	9.80640081789577E+00	-6.14700082256521E-01
1.E-06	S 1	1.54122509266618E+00	-8.50134120498870E-01	1.54122509266618E+00	-8.50134120498870E-01
	S 2	1.44115710116019E+01	-6.14700082664501E-01	1.44115710116314E+01	-6.14700082664502E-01
	S 3	1.44115710116019E+01	-6.14700082664501E-01	1.44115710116314E+01	-6.14700082664502E-01

Table H.3: The line integral of (6.3) for an OP above the midpoint of the triangle's hypotenuse. As the OP approaches this point, the G-K quadrature begins to lose SD over Side 1, the side that contains this point. As expected, the loss occurs in the real part of the integral and its maximum is 3 SD.

Case	39	PRESENT METHOD		MATLAB G-K QUADRATURE	
z'	Side	RE{INTG_1}	IM{INTG_1}	RE{INTG_1}	IM{INTG_1}
5.0	S 1	-2.81880767906103E-01	2.93537294387515E-03	-2.81880767906104E-01	2.93537294387527E-03
	S 2	-1.98635108609686E-01	4.14499167474095E-03	-1.98635108609687E-01	4.14499167474129E-03
	S 3	-1.98635108609686E-01	4.14499167474095E-03	-1.98635108609687E-01	4.14499167474129E-03
1.0	S 1	1.02749414262907E+00	-8.21944754365135E-01	1.02749414262907E+00	-8.21944754365135E-01
	S 2	6.49008525848461E-01	-5.74633334885979E-01	6.49008525848462E-01	-5.74633334885979E-01
	S 3	6.49008525848461E-01	-5.74633334885979E-01	6.49008525848462E-01	-5.74633334885979E-01
0.01	S 1	9.80559256320577E+00	-8.78883957009733E-01	9.80559256320577E+00	-8.78883957009734E-01
	S 2	1.65043165737456E+00	-6.14628761354497E-01	1.65043165737457E+00	-6.14628761354498E-01
	S 3	1.65043165737456E+00	-6.14628761354497E-01	1.65043165737457E+00	-6.14628761354498E-01
1.E-04	S 1	1.90159400618196E+01	-8.78889764710227E-01	1.90159400618196E+01	-8.78889764710228E-01
	S 2	1.65073124075261E+00	-6.14632840972885E-01	1.65073124075262E+00	-6.14632840972886E-01
	S 3	1.65073124075261E+00	-6.14632840972885E-01	1.65073124075262E+00	-6.14632840972886E-01
1.E-06	S 1	2.82262804435970E+01	-8.78889765290998E-01	2.82262805735581E+01	-8.78889765290999E-01
	S 2	1.65073127071816E+00	-6.14632841380848E-01	1.65073127071817E+00	-6.14632841380848E-01
	S 3	1.65073127071816E+00	-6.14632841380848E-01	1.65073127071817E+00	-6.14632841380848E-01

Table H.4: The line integral of (6.3) for an OP above the exterior point 1/5, 1/5) of the triangle. The minimum distance of this point to the hypotenuse is 4.71 mλ. Despite the small distance, the G-K quadrature remains stable in the approach to this point and agrees with our method to 15 SD.

Case	40	PRESENT METHOD		MATLAB G-K QUADRATURE	
z'	Side	RE{INTG_1}	IM{INTG_1}	RE{INTG_1}	IM{INTG_1}
5.0	S 1	-2.81867912873243E-01	2.97446971612503E-03	-2.81867912873244E-01	2.97446971612546E-03
	S 2	-1.98486089338058E-01	4.58230465634543E-03	-1.98486089338059E-01	4.58230465634484E-03
	S 3	-1.98486089338058E-01	4.58230465634543E-03	-1.98486089338059E-01	4.58230465634484E-03
1.0	S 1	1.02595651253827E+00	-8.21820720358887E-01	1.02595651253827E+00	-8.21820720358887E-01
	S 2	6.35056002113453E-01	-5.73240619963098E-01	6.35056002113454E-01	-5.73240619963099E-01
	S 3	6.35056002113453E-01	-5.73240619963098E-01	6.35056002113454E-01	-5.73240619963099E-01
0.01	S 1	6.66104112899468E+00	-8.78754890018984E-01	6.66104112899468E+00	-8.78754890018985E-01
	S 2	1.55348859766489E+00	-6.13179408371834E-01	1.55348859766489E+00	-6.13179408371834E-01
	S 3	1.55348859766489E+00	-6.13179408371834E-01	1.55348859766489E+00	-6.13179408371834E-01
1.E-04	S 1	6.70502030483591E+00	-8.78760697209028E-01	6.70502030483591E+00	-8.78760697209028E-01
	S 2	1.55374448005436E+00	-6.13183482245833E-01	1.55374448005436E+00	-6.13183482245833E-01
	S 3	1.55374448005436E+00	-6.13183482245833E-01	1.55374448005436E+00	-6.13183482245833E-01
1.E-06	S 1	6.70502480107593E+00	-8.78760697789748E-01	6.70502480107593E+00	-8.78760697789748E-01
	S 2	1.55374450564806E+00	-6.13183482653221E-01	1.55374450564806E+00	-6.13183482653221E-01
	S 3	1.55374450564806E+00	-6.13183482653221E-01	1.55374450564806E+00	-6.13183482653221E-01

DISTRIBUTION:

NAVAIRSYSCOM (AIR-4.5.5/Douglas McLaughlin), Bldg. 2187, Room 3215   (1)
    48110 Shaw Road, Patuxent River, MD 20670-1906
University of Mississippi (Attn: Prof. Allen W. Glisson), 302 Anderson Hall   (1)
    P.O. Box 1848, University, MS 38677-1848
Ohio State University (Attn: Prof. John L. Volakis), Electroscience Lab   (1)
    1320 Kinnear Road, Columbus, OH 43212
University of Houston (Attn: Prof. Donald R. Wilton), E.E. Dept.   (1)
    N 308 Engineering Building 1, Houston, TX 77204-4005
NAVAIRSYSCOM (AIR-5.1), Bldg. 304, Room 100   (1)
    22541 Millstone Road, Patuxent River, MD 20670-1606
NAVAIRWARCENACDIV (4.12.6.2), Bldg. 407, Room 116   (1)
    22269 Cedar Point Road, Patuxent River, MD 20670-1120
DTIC   (1)
    Suite 0944, 8725 John J. Kingman Road, Ft. Belvoir, VA 22060-6218